UFL/COEL-89/011

FLOW-FINE SEDIMENT HYSTERESIS IN SEDIMENT-STRATIFIED COASTAL WATERS

by

Rui C.F. Gameiro da Costa

Sponsor:

U.S. Army Engineer
Waterways Experiment Station
P.O. Box 631
Vicksburg, MS 39180

August, 1989

REPORT DOCUMENTATION PAGE

1. Report No.	2.	3. Recipient's Accession No.

4. Title and Subtitle	5. Report Date
FLOW-FINE SEDIMENT HYSTERESIS IN SEDIMENT-STRATIFIED COASTAL WATERS	August, 1989
	6.

7. Author(s)	8. Performing Organization Report No.
Rui C.F. Gameiro da Costa	UFL/COEL-89/011

9. Performing Organization Name and Address	10. Project/Task/Work Unit No.
Coastal and Oceanographic Engineering Dept. University of Florida 336 Weil Hall Gainesville, FL 32611	11. Contract or Grant No. DACW 39-87-K-0023
12. Sponsoring Organization Name and Address	13. Type of Report
U.S. Army Engineer Waterways Experiment Station P.O. Box 631 Vicksburg, MS 39180	Final
	14.

15. Supplementary Notes

16. Abstract

An examination of the causes for generation and dynamics of turbidity maxima in estuaries reveals the critical role of sediment tidal pumping phenomenon and, to a lesser extent, of the well-known effect of residual gravitational circulation due to salt water penetration. Both phenomena depend on the vertical sediment concentration profile and, consequently, on the magnitude of the vertical mass transport fluxes. Where high concentration suspensions occur regularly, the erosion/deposition fluxes can be drastically modified by sediment stratification, consequently influencing suspended sediment response to currents and wave action. This influence is inherent in flow-sediment hysteresis, which therefore reflects the role of vertical mass transport in the estuarine and coastal suspended fine sediment regime.

A vertical transport numerical model was used to investigate the influence of several key parameters describing sediment settling, bed properties and stabilized diffusion on the concentration profile. The model was also applied to simulate the influence of the same parameters on the time-lagged sediment response to flow variations, reflected in the characteristics of flow-sediment hysteresis loops.

Field data obtained in Hangzhou Bay (People's Republic of China), a high concentration environment, showed typical features of flow-sediment hysteresis and confirmed the importance of the vertical mass fluxes in contributing to sediment transport in the bay. A qualitative simulation provided by the numerical model,

- Continued -

17. Originator's Key Words	18. Availability Statement
Coastal bays Coastal sediments Fine-grained sediment Mud erosion Sediment resuspension	

19. U. S. Security Classif. of the Report	20. U. S. Security Classif. of This Page	21. No. of Pages	22. Price
Unclassified	Unclassified	172	

using settling parameters corresponding to local sediment, while confirming the importance of the hysteresis phenomenon, also revealed the critical need to use algorithms describing adequately stabilized diffusion and bed fluxes.

Additional evidence of hysteresis was obtained through analysis of microscale variables, such as the Reynolds stresses and the variances of the velocity components resulting from combined effects of wave action and turbulence. Spectral analysis of the measured random variations did not support the commonly accepted hypothesis of similarity between the responses to turbulent flow of sediment concentration and temperature. The normalized turbulent intensities for all the measured velocity components showed their highest values during the period of lowest sediment concentration; this result is consistent with the hypothesis of turbulent intensity damping by suspended sediment.

UFL/COEL-89/011

FLOW-FINE SEDIMENT HYSTERESIS IN SEDIMENT- STRATIFIED COASTAL WATERS

by

Rui C.F. Gameiro da Costa

Coastal and Oceanographic Engineering Department
University of Florida
336 Weil Hall
Gainesville, FL 32611

Sponsor:

U.S. Army Engineer
Waterways Experiment Station
P.O. Box 631
Vicksburg, MS 39180

August, 1989

ACKNOWLEDGEMENTS

The author would like to express his sincere gratitude to Dr. Ashish J. Mehta, Professor of Coastal Engineering, for his guidance, advice and support during the author's study period at the University of Florida. The author's appreciation is extended to Dr. Hsiang Wang, Dr. D. M. Sheppard, and and Dr. Robert G. Dean for their helpful comments.

The author is indebted to Dr. Mark A. Ross, who developed the numerical transport model used in the present study, for his assistance in using the model and for his helpful advice. The author would also like to thank Dr. Yixin Yan and Sidney Schofield who participated in the field experiment, Subarna Malakar for his assistance in some aspects of data processing, Jiang Feng who did the laboratory tests at the Hohai University and Dr. Robert Kirby who calibrated the turbidity sensors and provided most of the material included in Appendix A. Special thanks are due to Helen Twedell of the Coastal Engineering Archives, Shannon Smyth and Barry Underwood of the Engineering Publications Services.

Support for this study was made possible by contract N° DACW 39-87-K-0023, "Investigation of Cohesive Bed and Fluid Mud Response to Current and Waves," from the U. S. Army Engineer Waterways Experiment Station (WES), Vicksburg,

MS. Thanks are due to Ms. Tamsen Dozier who was the project manager. The field study in Hangzhou Bay, People's Republic of China, was conducted in cooperation with Dr. Hsiang Wang, as a part of his WES supported study (contract N° DACW 39-86-K-009) "A Joint Research with People's Republic of China on Muddy Coast Dynamics."

TABLE OF CONTENTS

LIST OF FIGURES

LIST OF TABLES

LIST OF SYMBOLS

a	Cross-sectional area; erosion parameter
A	Tidal variation of the cross-sectional area
	(the same convention applies to other variables)
$A_{i\cdot}$	Partial area in row i of the cross-section
$A_{\cdot j}$	Partial area in column j of the cross- section
$\overline{A}$	Tidal mean of the cross-sectional area
	(an overbar denotes time averaging, except when otherwise noted)
A'	Turbulent fluctuation of the cross-sectional area
	(primed variables have a similar meaning, except when otherwise noted)
ΔA_{ij}	Partial area corresponding to position ij
c	Concentration (of generic constituent or of suspended sediment)
c_{dt}	Transverse deviation of the concentration
	(similar subscripts apply to other variables)
c_{dv}	Vertical deviation of the concentration
	(similar subscripts apply to other variables)
c_v	Vertical deviation of concentration
	(a similar subscript applies to other variables)
c_A	Cross-sectional average of the concentration
	(a similar subscript applies to other variables)
c_T	Celerity of the tidal wave
C_{ab}	Complex cross-spectrum of variables a and b
C_f	Residual concentration

C_D	Drag coefficient
$\overline{C}_D$	Integral of the vertical concentration profile from the surface to a level D
C_0	Upper limit of the flocculation settling range; initial concentration
$\overline{C}$, C	Time average concentration of sediment
	(the overbar may be omitted for convenience)
d	Average depth of the pressure gage during a measurement period
D	Molecular diffusion coefficient; dispersion coefficient;
	sediment grain diameter
D_b	Mass of sediment accumulated at the bottom per unit area
e	Generic measured variable
e_t	Tidal trend in a generic measured variable
e_1	Generic variable including wave induced and turbulent effects
$\overline{e}$	Time-average part of a generic measured variable
$\overline{e}_n$	Average of n points of a record of a generic measured variable
$\tilde{e}$	Wave coherent part of a generic measured variable
e'	Turbulent part of a generic measured variable
E	Momentum eddy diffusivity
E_b	Mass of sediment eroded per unit bed area
E_n	Momentum eddy diffusivity for non stratified conditions
	(the same subscript applies to turbulent mass diffusivity)
E_s	Momentum eddy diffusivity for stratified conditions
	(the same subscript applies to turbulent mass diffusivity)
f	Sediment flux; frequency
$\overline{f}$	Cutoff frequency
F	Sediment flux
F_d	Diffusive flux of sediment
F_e	Erosional flux of sediment

F_p	Depositional flux of sediment
F_s	Settling flux of sediment
g	Acceleration of gravity
h	Water depth; mean water depth
H_F	Frequency response function of a filter
H_s	Significant wave height
k	Inverse of the volume of a given suspension sample; wavenumber
k_1, k_2	Settling velocity parameters
$\vec{k}$	Vertical unit vector
K	Turbulent mass diffusivity
K_l	Longitudinal mass dispersion coefficient
l	Prandtl's mixing length
L	Monin-Obukov length; complex transfer function
L_0	Wavelength
M	Mass transport; erosion rate constant
M_T	Total mass of a suspension sample
M_W	Mass of a suspension sample volume of salt water
n	Manning resistance coefficient; number of runs in stationarity test
n_1, n_2	Settling velocity parameters
N	Net sediment flux
p	Probability of sediment deposition; pressure
Q	Transport of water; salt flux
$\vec{q}$	Fluid velocity vector
R	River discharge; hydraulic radius
Re	Reynolds number
Ri	Richardson number

s	Salinity
s_d	Deviation of salinity
s_D	Depth average of s
	(the same subscript applies to other variables)
s_{ij}	Measured salinity at position ij
	(the same subscripts apply to other variables)
$s'_{i\cdot}$	Deviation of the lateral mean of the salinity
	(the same subscripts apply to other variables)
$s'_{\cdot j}$	Deviation of the vertical mean of the salinity
	(the same subscripts apply to other variables)
s_0	Time averaged salinity
S	Water surface slope
S_a	Power spectrum of variable a
S_{ij}	Interaction constant the salinity at position ij
	(the same notation applies to other variables)
S_t	Schmidt number
$s_{\cdot\cdot}$	Cross sectional average salinity
	(the same subscripts apply to other variables)
t	Time
T	Tidal period; finite time interval
T_m	Modal period
u	Velocity in the x direction
u_*	Friction velocity
$\overline{u}_D$	River cross-sectional mean velocity
v	Velocity in the y direction
V_e	Erosion velocity
V_t	Transport velocity

w	Velocity in the z direction
W_s	Settling velocity of the sediment particles
$\overline{W}_{s0}$, W_{s0}	Peak settling velocity, modified peak settling velocity
x	Longitudinal cartesian coordinate; generic random process
$\overline{x}$	Filtered time series of a generic random process
X	Fourier transform of a generic random process x
y	Transverse cartesian coordinate
z	Vertical cartesian coordinate; distance from a solid boundary
z_0	Roughness length
$\overline{z}$	Mean height of sediment suspension
α, α'	Stabilized diffusion empirical constants
α_i	Erosion resistance defining parameter
$\overline{\alpha}$	Stratification parameter
β, β'	Stabilized diffusion empirical constants
δ	Boundary layer thickness
ϵ	Erosion rate; spectrum bandwidth parameter
η	Tidal elevation relative to a given datum
κ	Von Karman universal constant
λ	Wavelength
μ	Dynamic viscosity
ν	Kinematic viscosity
ρ	Density of the fluid
ρ_s	Grain density
ρ_w	Water density
τ	Shear stress
τ_b	Bottom shear stress

τ_{cd}, τ_{ci}	Critical shear stresses for deposition
τ_0	Shear stress at the wall
τ_s	Bed shear strength

CHAPTER 1
INTRODUCTION

1.1 Problem Significance

Estuaries and coastal bays have traditionally offered multiple advantages for the development of urban and industrial centers on their banks due to, among other reasons, the existence of sheltered harbors and waste disposal sites and to the possibility of inland navigation. The rapid development of many of those centers has led to intensive use of estuarine and coastal waters and, as a consequence of competing demands and negative environmental effects, to technical and ecologic problems.

Of the problems resulting from human impact in estuarine and coastal areas, some of the most important ones, both in economical and practical terms, are directly related to sediment dynamics. Such aspects include:

1. Dredging of navigation channels and deepening of natural waterways;
2. Changes in natural topography and land reclamation;
3. Water quality problems due to transport of sorbed nutrients and contaminants by fine sediment particles or to turbidity increases;
4. Shoaling or scouring of natural bottoms due to hydrodynamic changes;
5. Changes in the position of the zones of maximum turbidity and, in general, in the patterns of sediment circulation within the estuary or bay.

This last aspect is particularly relevant, since one of the most generalized features in estuarine environments is the existence of a turbidity maximum, a zone of high

suspended sediment concentration through which sediment is continuously circulated.

The understanding of the physical mechanisms contributing to sediment transport in estuaries is, consequently, fundamental in predicting any effects of anthropogenic activities. The nature and relative importance of estuarine transport processes has been investigated by several researchers through the analysis of velocity, salinity and suspended sediment data. Although several procedures have been applied to a variety of estuaries showing different geometries and stratification conditions, two transport mechanisms, tidal pumping and vertical shear, have been generally found to be dominant.

Tidal pumping results from phase differences between cross-sectional area variations and average cross-sectional velocities and concentrations of salt or sediment. Transport by vertical shear effect is caused by the residual gravitational circulation due to salt water penetration. Both transport mechanisms depend strongly on the vertical concentration profile and, in the case of sediment, are related to erosion/deposition phenomena at the bed and to settling and diffusion in the water column or, in more general terms, to the vertical sediment fluxes. Such fluxes reflect the time lagged response of sediment to flow variations which is globally expressed by the well known flow-sediment hysteresis phenomenon. Moreover, the differences between salt and suspended sediment behavior (resulting from negative buoyancy and erosion/deposition) suggest the importance of the study of sediment-stratified flows and of their differences relative to salt-stratified flows; this approach, which is supported by recent field results contradicts the assumption, implicit in some early studies, that the dominant physical mechanisms transporting salt and sediment landward in an estuary or coastal bay should be the same. A description of sediment dynamics in the vertical direction as a function of sediment stabilized turbulent flow characteristics and of bed and sediment settling properties is, conse-

quently, of fundamental importance.

1.2 Objective and Methodology

The main purpose of the present investigation was to study the effect of different physical processes in the evolution of the vertical concentration profile in a sediment-stratified coastal environment. In particular, the influence of the sediment settling properties, stabilized diffusion parameters and bed properties on the general features of the profile and their effects on the corresponding lag phenomena contributing to flow-sediment hysteresis were investigated. A vertical transport numerical model was used to generate concentration profiles and to study the effect caused by the variation of settling velocities, and of stabilized diffusion and erosion/deposition parameters. Measured field data of pressure, velocities and suspended sediment concentrations were obtained in a high-concentration coastal environment (Hangzhou Bay, People's Republic of China). Laboratory tests of local sediment allowed the evaluation of the pertinent physical parameters. The field data were used to test the importance of fine sediment lagged response to flow changes in a sediment- stratified environment and compared with the model's results.

1.3 Outline of Upcoming Chapters

A summary of the different transport processes acting in estuaries and coastal bays is presented in Chapter 2. An overview and comparison of the methods and results obtained by several researchers, leading to the identification of the dominant transport mechanisms acting to transport salt and sediment landward is also included in the chapter. In Chapter 3 a review of the physical processes described by the vertical transport model is presented, together with the general mathematical and numerical formulation of the problem. Some possible limitations of the model's approach when dealing with high concentration environments are also discussed.

The field experiment carried out in Hangzhou Bay and the laboratory experiments leading to the definition of the local sediment's settling and erosional properties, the experiments' methodologies and data pre-processing methods are described in Chapter 4. The results and discussion of model simulations and field data interpretation are presented in Chapter 5. Finally, Chapter 6 includes a summary and the conclusions derived from the study.

CHAPTER 2
TRANSPORT PROCESSES IN ESTUARIES AND COASTAL BAYS

2.1 The Turbidity Maximum

2.1.1 General Aspects

One of the most generalized features in estuarine environments is the turbidity maximum; in this zone, usually located at the limit of the salt intrusion and, generally, containing more sediment than the annual estuarine supply, the concentrations of suspended sediment are 10 to 100 times higher than landward (fluvial zone) or seaward. Under the turbidity maximum, but more limited in size, another feature, the mud reach, a place of continuous shoaling of fine particles in the channel, can occur. Wellershaus (1981) presents a summary of the characteristics of 20 estuaries, in different areas of the world, which shows the existence of a turbidity maximum near the tip of the salt wedge in, at least, 15 of them, with a significant group also showing a mud shoal.

The turbidity maximum can be understood as an indication of fine sediment transport potential in an estuary; despite the opposing effects of flushing river currents, mixing and dilution phenomena it contains a high percentage of the available mobile fine sediment, corresponding to a narrow band of diameters with low settling velocities. Moreover, its importance is fundamental in the circulation of sediment within the estuary (since sediment is continuously circulated, in successive cycles of deposition and reentrainment, through it) and in controlling its flow from the river to the sea.

In a very general way, the existence of a turbidity maximum can be predicted

as a consequence of both net estuarine hydrodynamics and the properties of fine sediment suspensions. Officer (1981) divides fine sediment transport in estuaries into two forms: suspended sediment transport (with higher velocities and lower concentrations) and near bed sediment transport (with higher concentrations but lower velocities); fluid mud, a high concentration suspension, commonly found close to the bed in many estuaries is included in the latter.

From the net hydrodynamics viewpoint, an estuarine gravitational circulation pattern is commonly observed, with net flow seaward in the upper layers and landward in the lower layers; it follows that sediment, suspended due to mixing, and flowing seaward, in the upper layer, in the middle to lower reaches of an estuary will, in more quiescent areas, settle towards the bottom and be carried back landward, to form a zone of maximum concentration. This mechanism can also explain the narrow band of sediment diameters found in the turbidity maximum: the coarser particles will deposit in the lower reaches of the estuary and will move only as bedload; among the finer ones, some hardly deposit and are carried to the sea by the mean flow, while the remaining settle down and are carried landward to form the turbidity maximum.

The flow patterns close to the bottom can, additionally, contribute to the formation of this feature, since the net flow in the upper (fluvial) reaches is seaward, while in the lower areas (due to gravitational circulation) is landward. As a consequence, the near bed sediment will be transported to a null point close to the tip of the saline intrusion.

2.1.2 The Variability of the Turbidity Maximum

The previously mentioned processes may largely explain the existence of a turbidity maximum in microtidal (tidal range $< 2\,m$) and mesotidal (tidal range between 2 and 4 m) estuaries. Some of its features, especially in macrotidal estuaries

(tidal range $> 4\,m$), cannot, however, be explained exclusively in terms of the net transport. The peak concentration, for example, can vary by as much as one order of magnitude, typical values being 100-200 mg/l in low tidal range estuaries and 1000-10000 mg/l in high tidal range estuaries (Dyer, 1989). This variability can be measured during the tidal cycle, in spring-neap cycles and due to seasonal variations in river flow and is, consequently, associated with the erosion and deposition of sediment.

Studies in the Gironde estuary (Allen et al., 1980, cited by Nichols and Biggs, 1985) show that the core of the turbidity maximum moves during the tidal cycle 10 to 30 km, while concentrations grow and decrease during the same period. As expected, the turbidity maximum occupies its most landward position at high water and its most seaward position at low water. At slack water the low flow velocities allow deposition to occur and the dimensions of the turbidity maximum decay. Fully developed ebb and flow currents cause erosion and transport and the growth of the maximum; however, due to the asymmetry of the tidal currents (higher flood than ebb currents), the net effect, after a number of tidal cycles, will be landward transport of sediment, consequently supporting the existence of a turbidity maximum.

The fortnightly transition from spring to neap tides also affects the turbidity maximum, since decreasing peak currents and increasing slack durations allow increasing sedimentation and the decrease of the turbidity maximum; during spring tides the turbidity maximum will be at its most landward position. The transition from neap to spring tide will cause the opposite effect. However, some of the sediment settled during the neap tides will have consolidated and will not be resuspended, thus causing net shoaling (Allen et al., 1977 and Allen et al., 1980, cited by Nichols and Biggs, 1985).

The effect of variations in river flow is apparent in the position of the turbidity maximum, higher flows pushing it towards the mouth of the estuary. Low flow situations allow the salt intrusion limit to migrate landward; the turbidity maximum corresponding to this case will be located upstream of its normal position.

2.1.3 Transport Mechanisms in Estuaries

Several physical processes of conflicting effects can be identified in an estuary, contributing to salt and sediment transport. Among such mechanisms can be included, according to Officer (1981), the following:

1. Gravitational, nontidal (net) circulation, and near bottom residual circulation, together with the tidal average sediment concentration.

   As mentioned before, the characteristic estuarine type of circulation consists, within the area of saline penetration, of a seaward net flow in the upper layers of the water column and a net landward flow in the lower layers. In the fluvial zone, landward of the saline intrusion, the net transport is seaward in the whole water column. If this pattern is combined with a tidal average sediment concentration a net seaward sediment transport can be expected upstream of the limit of the saline propagation; downstream, the transport can be expected to be seaward in the upper layers and landward in the lower layers. This combination of residual circulation and average sediment concentration can, consequently, explain the dependence of the turbidity maximum on the limit of the saline penetration, this limit being related to variations in tidal range and runoff.

2. Flood and ebb tide variations in vertical concentrations of sediment in conjunction with a symmetric tidal current.

The variations in vertical sediment concentrations can be explained by the directions of the vertical velocities associated with a standing tidal wave (the dominating tidal effect in many estuaries) which are upwards during the flood and downwards during the ebb period. The resulting net effect of this superposition should cause landward transport.

3. Lag effects between the vertical sediment distribution and the governing tidal cycle in conjunction with an asymmetric tidal current.

This effect was described by Postma (1967) and can be explained, with some initial simplifications by considering the following assumptions:

(a) Uniform velocities in the cross sections of the tidal channel.

(b) Symmetry of the tidal curve (sine curve) at all points.

(c) Simultaneous high and low tide along the tidal channel (standing wave).

(d) Linear decrease, from the sea to the head, of the average tidal current velocity.

(e) Constant tidal range.

If a plot of velocity versus position is made for various water masses (fig. 2.1) it is apparent that, although the tide is symmetrical, the curves are asymmetrical. The tangent P to the curves represents the maximum current velocity at each point and corresponds, in each curve, to a point attained by the water mass at half tide. Two lag phenomena are related to these curves:

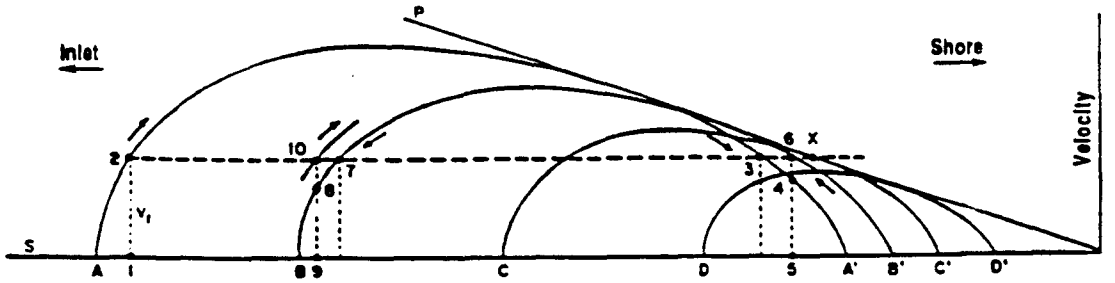

Figure 2.1: Velocities with which different water masses move with the tides, illustrating the effects of settling lag and scour lag. From Postma, 1967.

(a) The settling lag, corresponding to the delay between the time when the particle starts to settle and that when it reaches the bed; during that time the particle is carried along some distance.

(b) The scour lag, which is the time delay between the occurrence of the transportation velocity V_t and the erosion velocity V_e, the latter being higher.

If only the settling lag is considered, and using figure 2.1, it can be seen that a particle at rest in point 1 and requiring a velocity V_1 to be suspended will be entrained in the flood flow by the water mass coming from A; at point 3 the current has decreased below the lowest transportation velocity and the particle begins to settle, while still being carried landward. The particle will reach the bottom at point 5 and the water mass will come to rest at A' before returning in the following ebb tide. The water mass coming from A' reaches point 5

with a velocity lower than V_1 and cannot, consequently, resuspend the particle which is only removed by water mass BB'. Following the particle during the ebb tide, it follows that it will begin to settle at point 7 and will reach the bottom at point 9. Consequently, a net landward movement of the particle from points 1 to 9 happens during a tidal cycle.

Alternatively, if only the scour lag is considered, again from figure 2.1 ($V_e > V_t$), and considering $V_1 = V_e$, the particle eroded in 1 will deposit at point 4 (V_t) and will settle to 5 instantaneously (no settling lag). Again, only water mass BB' will be able to erode the particle which will be carried and will begin to settle at point 8, reaching the bottom at 9. As a consequence, a landward transport from point 1 to point 9 will have occurred.

If both the settling lag and the scour lag act simultaneously, it is obvious that the landward movement of a particle during the tidal cycle will be greater. Furthermore, the effect of the time-velocity asymmetry has to be considered, since for equal flood and ebb discharges the velocities have to be higher around low water, when the cross sectional area is smaller. The slack water period is, then, longer around high tide than around low tide, consequently allowing deposition of some of the sediment carried landward during the flood; it should also be mentioned that, in general, the estuarine cross sections change, from wide shapes close to high tide to confined channels close to low tide: the average depth is, accordingly, lower at high tide and more suspended sediment will deposit. The cumulative effect is, then, a landward shift of particles during the tidal cycle.

4. Different ebb and flood durations and consequent net transport effects related to the differing flood and ebb current magnitudes.

   Another cause of asymmetry in velocity-time plots is the asymmetry of the tidal (height-time) curve itself. In estuaries, where the water depth is of comparable magnitude to the tidal amplitude (and much lower than the wavelength), the tidal wave propagates as a shallow water wave with celerity

$$c_T = \sqrt{g(h+\eta)} \tag{2.1}$$

   where h is the mean water depth, η the local tidal elevation relative to the mean water level and g the acceleration of gravity. As a consequence the tidal crest (high water) travels faster than the the trough (low water) and the tidal wave deforms while propagating landward, the flood period decreasing while the ebb duration increases. Flood velocities are, then, higher than ebb velocities and produce greater erosion and higher sediment concentrations around high water. This phenomenon, combined with the previously mentioned longer duration of the slack period around high water, will cause a landward net transport.

5. Hydrodynamic tidal mixing exchanges in the direction of the longitudinal concentration gradient.

   This Fickian transport process can be described by the negative of the product of a longitudinal dispersion (tidal mixing) coefficient by the longitudinal average concentration gradient, in the form

$$-K_l \frac{\partial \overline{C}}{\partial x} \tag{2.2}$$

and can include, besides some of the above mentioned effects, turbulent transport contributions and those related to topographical irregularities, such as tidal trapping.

The most evident transport mechanism in estuaries is, however, that associated with seaward advection caused by the non-tidal drift $\bar{u}_A$ (mean flow); this flow can be explained by the superposition of the river flow and of flows that compensate the landward transport associated with the partial progressive wave nature of the tide in estuaries.

2.2 Salt and Sediment Fluxes and Mass Transports in Estuaries and Coastal Bays

2.2.1 General Aspects

The variability of the turbidity maximum, as noted before, can be related to several aspects of the estuarine hydrodynamics and sediment properties. Those physical processes and their effects can be better understood by considering the decomposition of the cross sectional, tidally averaged, fluxes (or mass transports) of sediment and salt, occurring in different cross sections of an estuary. Different types of flux and mass transport decompositions have been used by several authors, initially with the purpose of determining salt fluxes (and dispersion coefficients) and, later, for the calculation of suspended sediment fluxes. In the following subsections a brief summary of the different methods will be presented.

2.2.2 Bowden (1963)

Bowden was the first author to decompose the mass transport into different contributions; he examined the effect of vertical shear by assuming an estuary without lateral variations. The instantaneous mass transport of salt through a unit width

area, perpendicular to the flow is

$$M = \int_0^h us\, dz = h(us)_D \tag{2.3}$$

where h is the depth and the subscript D indicates depth averaging. Considering that, at any depth,

$$u = u_0 + u' \tag{2.4}$$

$$s = s_0 + s' \tag{2.5}$$

(where u_0 (s_0) are values averaged over a time interval of several minutes and u' (s') are turbulent fluctuations) and further decomposing u_0 and s_0 into depth average values u_D, s_D and vertical deviations u_{dv}, s_{dv}:

$$u = u_D + u_{dv} + u' \tag{2.6}$$

$$s = s_D + s_{dv} + s' \tag{2.7}$$

Furthermore, u_D and s_D can be decomposed into tidal averages $\bar{u}_D$, $\bar{s}_D$ and tidal deviations U, S; consequently

$$u = \bar{u}_D + U + u_{dv} + u' \tag{2.8}$$

$$s = \bar{s}_D + S + s_{dv} + s' \tag{2.9}$$

Averaging the salt mass transport over a tidal cycle and over the depth

$$\begin{aligned} \overline{M} &= \frac{1}{T}\int_0^T h(us)_D\, dt = \\ &= \overline{h(us)_D} = \\ &= \bar{h}\bar{u}_D\bar{s}_D + \overline{hUS} + \overline{h(u_{dv}s_{dv})_D} + \overline{h(u's')_D} = \\ &= \overline{M}_1 + \overline{M}_2 + \overline{M}_3 + \overline{M}_4 \end{aligned} \tag{2.10}$$

where terms $\bar{u}_D\overline{hS}$, $\overline{hU}\bar{s}_D$ have been omitted by the author and the overbar denotes tidal averaging. The partial mass transports have the following meaning:

$\overline{M}_1$ - Contribution of the mean values of depth, velocity and salinity (or, in Bowden's definition, the contribution due to advection by the mean flow corresponding to the river discharge);

$\overline{M}_2$ - Third order correlation of tidal deviations in depth and mean velocity and salinity;

$\overline{M}_3$ - Contribution of the correlation of depth deviations of velocity and salinity (this term is associated with the vertical gravitational circulation);

$\overline{M}_4$ - Turbulent mass transport of salt.

Bowden calculated the values of $\overline{M}_1$, $\overline{M}_2$ and $\overline{M}_3$ for the Mersey Narrows on four occasions; $\overline{M}_4$ was not computed due to the nature of the available data but it was assumed to be small. From the computed mass transport terms, $\overline{M}_1$ was downstream and compensated by the upstream effect of $\overline{M}_2$ and $\overline{M}_3$, the former being dominant. The computation of $(\overline{M}_1 + \overline{M}_2 + \overline{M}_3)/\bar{h}$ showed a net upstream salt transport which could be explained by:

1. Short period horizontal diffusion due to turbulence (term $\overline{M}_4$).

2. Non stationarity of the mean salinity.

3. Lateral effects in the transport.

Bowden and Sharaf el Din (1966) cited by Dyer (1973) confirmed, by analyzing three stations in a cross section, the existence of lateral variations in $(\overline{M}_1 + \overline{M}_2 + \overline{M}_3)/\bar{h}$; the net transport was, then, seaward. An additional difficulty was related to the fact that $\overline{M}_1$ was computed using $\bar{u}_D = R/\overline{A}$ where R is the river discharge and $\overline{A}$ the mean fluvial cross sectional area; the value found by the authors for $\bar{u}_D$ over the estuarine cross section was one order of magnitude higher than the value calculated using the river discharge, due, possibly to undetected variations in the velocity or measurement imprecisions or, more likely, to compensation flows due to the partial

progressive nature of the tidal wave.

2.2.3 Hansen (1965)

Hansen considered the instantaneous velocity at any point of the cross section (u) as composed by a cross sectional average (u_A) and a deviation (u_d):

$$u = u_A + u_d \tag{2.11}$$

A similar decomposition was applied to the salinity:

$$s = s_A + s_d \tag{2.12}$$

The instantaneous mass transport of salt through the cross section is, consequently:

$$M(t) = \int_a us\, da = a[u_A s_A + (u_d s_d)_A] \tag{2.13}$$

In this equation $u_A s_A$ corresponds to the salt flux due to the sectional means of both the current and the salinity and has the direction of the mean current; the second term is known as "shear effect" and accounts for the correlation between deviations of velocity and salinity from their sectional mean values. This "shear effect" is a consequence of density currents and shear induced currents, combined with vertical and lateral salinity deviations. The mean longitudinal salt transport over a tidal cycle is then

$$\overline{M} = \overline{a u_A s_A} + \overline{a(u_d s_d)_A} \tag{2.14}$$

(the overbar denoting tidal cycle averaging).

Hansen further divided the average components of the velocity, u_A, and of the salinity, s_A, into a tidal mean (denoted with an overbar), a tidal oscillation and a turbulent fluctuation (denoted with a prime):

$$u_A = \overline{u}_A + U_A + u'_A \tag{2.15}$$

$$s_A = \overline{s}_A + S_A + s'_A \tag{2.16}$$

and applied a similar subdivision to the cross sectional area:

$$a = \overline{A} + A + A' \tag{2.17}$$

and to the deviation term of the instantaneous salt flux:

$$(u_d s_d)_A = \overline{(u_d s_d)}_A + (U_d S_d)_A + (u_d s_d)'_A \tag{2.18}$$

Expanding $\overline{M}$:

$$\begin{aligned} \overline{M} &= \overline{(\overline{A} + A + A')(\overline{u}_A + U_A + u'_A)(\overline{s}_A + S_A + s'_A)} + \\ &+ \overline{(\overline{A} + A + A')[(u_d s_d)_A + (U_d S_d)_A + (u_d s_d)'_A]} \end{aligned} \tag{2.19}$$

and eliminating terms with uncorrelated or weakly correlated variables, the following result is obtained:

$$\begin{aligned} \overline{M} &= \overline{A}\overline{u}_A\overline{s}_A + \overline{A}\overline{U}_A\overline{s}_A + \overline{A'u'}_A\overline{s}_A + \overline{A}\,\overline{U_A S_A} + \\ &+ \overline{A}\,\overline{u'_A s'_A} + \overline{u}_A\overline{A S}_A + \overline{A U_A S}_A + \overline{u}_A\overline{A' s'}_A + \\ &+ \overline{A' u'_A s'}_A + \overline{A}\overline{(u_d s_d)}_A + \overline{A(U_d S_d)}_A + \overline{A'(u_d s_d)'}_A \end{aligned} \tag{2.20}$$

where it should be noted that terms $\overline{A(U_d S_d)}_A$ and $\overline{A(u_d s_d)'}_A$ were not retained. If, furthermore, the first three terms are grouped, by noticing that $\overline{M}_W = \overline{A}\overline{u}_A + \overline{A}\overline{U}_A + \overline{A'u'}_A$ is the mean transport of water through the section during the tidal cycle, and the remaining terms corresponding to turbulent fluctuations are also included in a term $\overline{M'}$:

$$\begin{aligned} \overline{M} &= \overline{M}_W\overline{s}_A + \overline{A}\,\overline{U_A S_A} + \overline{u}_A\overline{A S}_A + \overline{A U_A S_A} + \\ &+ \overline{A}\,\overline{(u_d s_d)}_A + \overline{A(U_d S_d)}_A + \overline{M'} = \\ &= \overline{M}_1 + \ldots + \overline{M}_7 \end{aligned} \tag{2.21}$$

The previous terms correspond to the mass transports associated with

$\overline{M}_1$ - The mean river flow and salinity;

$\overline{M}_2$ - Correlation of tidal period variations of the sectional mean salinity

and current;

$\overline{M}_3$ - Correlation of tidal period variations of cross section and mean salinity;

$\overline{M}_4$ - Third order correlation of tidal period variations in cross section and mean salinity and velocity;

$\overline{M}_5$ - Mean shear effect;

$\overline{M}_6$ - Covariance of shear effect and cross section;

$\overline{M}_7$ - Correlation between shorter period fluctuations of the various quantities.

Hansen applied his decomposition scheme to data from a cross section of the Columbia River Estuary, assuming small changes in salt storage up-estuary of the section, and concluded that:

1. Only 70% of the measured non-tidal drift $\overline{u}_A$ corresponded to freshwater discharge; the remaining 30% were a compensation current for the inward Stokes transport by the tidal wave $\overline{AU_A}$, the turbulent flux being assumed negligible (this confirms the difference between Bowden's derived and computed $\overline{M}_1$ term);

2. Of the salt advected seaward with the mean river discharge, about 40% was balanced by covariance between fluctuations of tidal periodicity (term 2), and about 45% was balanced by shear effects (term 5). The remaining 15% were attributed to short period fluctuations (term 7);

3. Terms 3,4 and 6 were small and of the order of magnitude of the uncertainty in the evaluation of the major transport terms;

4. The importance of term 5 may be explained by the large vertical salinity gradient coupled with systematic, even if small, density induced variations in the velocity profile.

Dyer (1973) also points out that the large values obtained for $\overline{AU}_A$ and $\overline{A}\,\overline{U_A S_A}$ show that U_A and S_A are not 90° out of phase. However, since $\overline{AU_A S_A}$ is small, the progressive component of the tidal wave (reflected in the cross sectional variation) cancels out the effect produced by U_A and S_A. It should also be noted that, since the deviation terms were not decomposed into vertical and lateral contributions, the relative importance of these contributions cannot be evaluated.

2.2.4 Fischer (1972)

Fischer studied the Mersey estuary, in an attempt to clarify the relative importance of the mechanisms transporting dissolved constituents in partially mixed and vertically homogeneous estuaries of the coastal plain type. The author decomposed the observed velocity into an average value and a deviation, as before,

$$u = u_A + u_d \tag{2.22}$$

and considered also a separation into a tidal mean and the corresponding deviation:

$$u_A = \overline{u}_A + U_A \tag{2.23}$$

$$u_d = \overline{u}_d + U_d \tag{2.24}$$

By considering a three-dimensional profile, both $\overline{u}_d$ and U_d were explicitly separated into variations in the vertical and transverse directions:

$$\overline{u}_d = \overline{u}_{dt} + \overline{u}_{dv} \tag{2.25}$$

$$U_d = U_{dt} + U_{dv} \tag{2.26}$$

$\overline{u}_{dt}$ and U_{dt} are transverse velocity profiles, respectively the depth means of $\overline{u}_d$ and U_d; $\overline{u}_{dv}$ and U_{dv} are vertical variations from the local vertical mean.

Then

$$u = \overline{u}_A + U_A + \overline{u}_{dt} + U_{dt} + \overline{u}_{dv} + U_{dv} \tag{2.27}$$

and, similarly, for the concentration

$$c = \overline{c}_A + C_A + \overline{c}_{dt} + C_{dt} + \overline{c}_{dv} + C_{dv} \tag{2.28}$$

It should be noted that the turbulent fluctuations were neglected. A graphical representation of the velocity decomposition is presented in figures 2.2 and 2.3. The tidal cycle average of the longitudinal mass transport is

$$\overline{M} = \frac{1}{T}\int_0^T \int_a uc\, da\, dt \tag{2.29}$$

Fischer assumed that, in the area decomposition $a = \overline{A} + A$ (tidal average and deviation), A is small and, consequently, $a \simeq \overline{A}$. Accordingly, using Hansen's result and neglecting the turbulent term:

$$\begin{aligned} \overline{M} &= \overline{M}_W \overline{c}_A + \overline{A}\,\overline{U_A C_A} + \overline{u}_A \overline{A C_A} + \overline{A U_A C_A} + \overline{a(u_d c_d)_A} = \\ &= \overline{M}_1 + \ldots + \overline{M}_5 \end{aligned} \tag{2.30}$$

In this equation the last term corresponds to terms 5 and 6 of Hansen's result; if, as noted before, $a \simeq \overline{A}$ and terms 3 and 4 are neglected due to Hansen's calculations then

$$\overline{M} = \overline{M}_W \overline{c}_A + \overline{A}\,\overline{U_A C_A} + \overline{A}(\overline{u_d c_d})_A \tag{2.31}$$

Using the previous decomposition of u_d and c_d:

$$\begin{aligned} \overline{M} &= \overline{M}_W \overline{c}_A + \overline{A}\,\overline{U_A C_A} + \\ &\quad + \overline{A}[(\overline{u}_{dt}\overline{c}_{dt})_A + (\overline{u}_{dv}\overline{c}_{dv})_A + \overline{(U_{dt}C_{dt})}_A + \overline{(U_{dv}C_{dv})}_A] = \\ &= \overline{M'}_1 + \ldots + \overline{M'}_6 \end{aligned} \tag{2.32}$$

The transport terms represent the following processes :

$\overline{M'}_1$ - Mean flow of the river discharge;

$\overline{M'}_2$ - Correlations of tidal variations of sectional mean velocity and

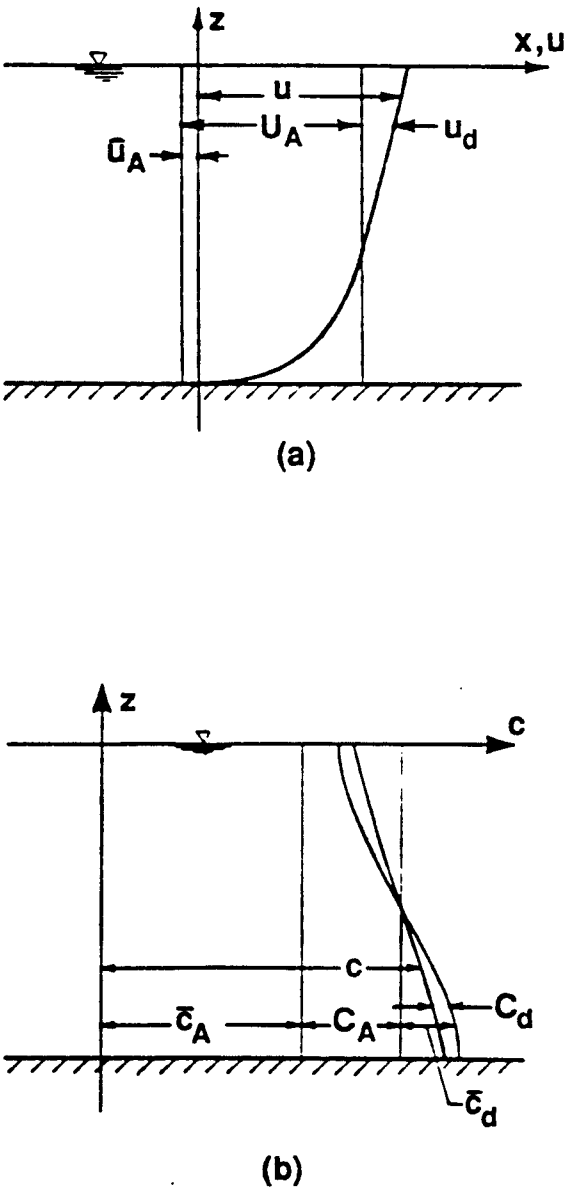

Figure 2.2: Decomposition of two-dimensional profiles into components: a) velocity; b) concentration. Adapted from Fischer, 1972.

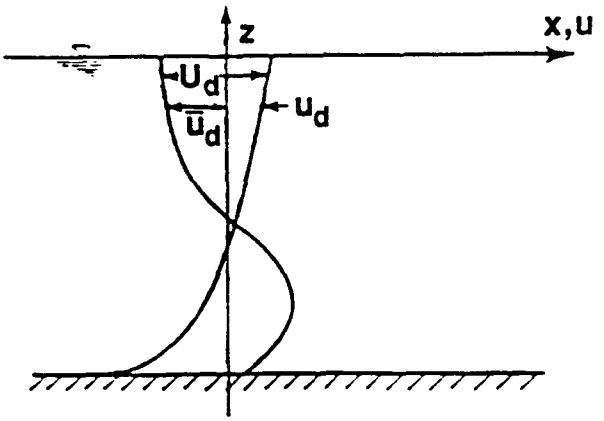

(a)

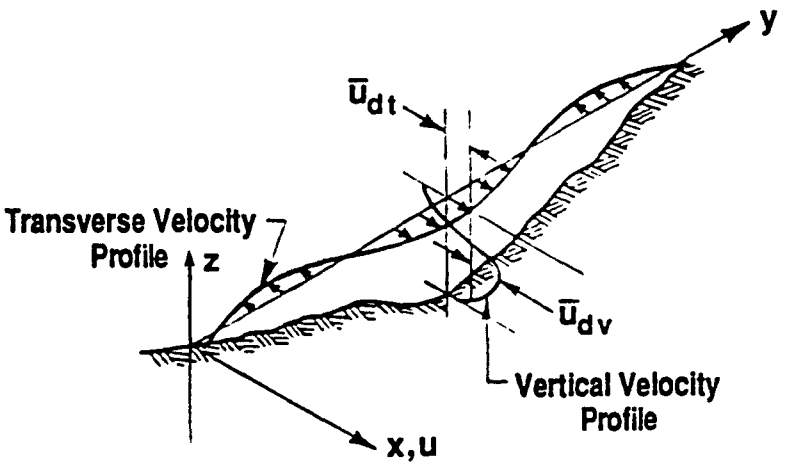

(b)

Figure 2.3: Decomposition of velocity components: a) u_d into steady and fluctuating parts; b) $\overline{u}_d$ into transverse and vertical profiles. Adapted from Fischer, 1972.

concentration;

$\overline{M'_3}$ - Net transverse circulation;

$\overline{M'_4}$ - Net vertical circulation;

$\overline{M'_5}$ - Transverse oscillatory shear;

$\overline{M'_6}$ - Vertical oscillatory shear.

Fischer considered salinity equilibrium ($\overline{M} = 0$) and neglected the second term (tidal pumping); through theoretical and empirical results applied to data from the Mersey estuary he evaluated the contribution of the last four terms (i.e. the bracketed expression in 2.32) to a dispersion coefficient defined as

$$D = \frac{\overline{u_d c_d}}{\frac{d\bar{c}}{dx}} \tag{2.33}$$

by dividing them by $d\bar{c}/dx$.

$$\begin{aligned} D &= \frac{1}{d\bar{c}/dx}[(\overline{u}_{dt}\overline{c}_{dt})_A + (\overline{u}_{dv}\overline{c}_{dv})_A + (U_{dt}C_{dt})_A + (U_{dv}C_{dv})_A] = \\ &= D_1 + D_2 + D_3 + D_4 \end{aligned} \tag{2.34}$$

These partial dispersion coefficients had the values:

$D_1 = 430\,m^2/sec$ (transverse (net) gravitational circulation, probably overestimated, according to the author).

$D_3 = 6\,m^2/sec$ (transverse oscillatory shear).

$D_2 = 32\,m^2/sec$ (vertical (net) gravitational circulation).

$D_4 = 23\,m^2/sec$ (vertical oscillatory shear).

Fischer concluded from these values (although resulting from certain hypotheses) that the vertical gravitational circulation (D_2) is not, necessarily, the most important transport mechanism in estuaries. The author mentioned that the exclusion of the transverse gravitational circulation from previous analyses might, indeed, mean that the most important part of the estuarine circulation was omitted. The transverse gravitational circulation was, actually, in this case, one order of magnitude

higher than the combined vertical effects.

2.2.5 Dyer (1973)

Dyer extended the previous analyses by including a tidally fluctuating cross section in the calculation of the mass transport and by considering a turbulent fluctuation in the several variables:

$$a = \overline{A} + A + A' \tag{2.35}$$

$$u_A = \overline{u}_A + U_A + u'_A \tag{2.36}$$

$$s_A = \overline{s}_A + S_A + s'_A \tag{2.37}$$

$$u_d = \overline{u}_d + U_d + u'_d \tag{2.38}$$

$$s_d = \overline{s}_d + S_d + s'_d \tag{2.39}$$

$$\overline{u}_d = \overline{u}_{dt} + \overline{u}_{dv} \tag{2.40}$$

$$\overline{s}_d = \overline{s}_{dt} + \overline{s}_{dv} \tag{2.41}$$

$$U_d = U_{dt} + U_{dv} \tag{2.42}$$

$$S_d = S_{dt} + S_{dv} \tag{2.43}$$

$$u'_d = u'_{dt} + u'_{dv} \tag{2.44}$$

$$s'_d = s'_{dt} + s'_{dv} \tag{2.45}$$

where the symbols have the previous meanings but the deviations are more intuitively defined as

$\overline{u}_{dt}$: mean deviation of the depth mean at any position from the cross sectional mean.

$\overline{u}_{dv}$: mean deviation of the mean value at any depth from the depth mean value.

U_{dt} : tidal fluctuation of the depth mean deviation at any position.

U_{dv} : tidal fluctuation of the vertical deviation at any depth.

u'_{dt} : turbulent transverse deviation.

u'_{dv} : turbulent vertical deviation.

The mass transport becomes, by neglecting some terms:

$$\begin{aligned}
\overline{M} &= \overline{a(us)_A} = \\
&= \overline{A}\overline{u}_A\overline{s}_A + \overline{AU_A}\overline{s}_A + \overline{AS_A}\overline{u}_A + \overline{A}\,\overline{U_AS_A} + \\
&\quad + \overline{AU_AS_A} + \overline{A}(\overline{u}_{dt}\overline{s}_{dt})_A + \overline{A}(\overline{u}_{dv}\overline{s}_{dv})_A + \overline{A}\,(\overline{U_{dt}S_{dt}})_A + \qquad (2.46)\\
&\quad + \overline{A}\,(\overline{U_{dv}S_{dv}})_A + \overline{A(U_{dt}S_{dt})}_A + \overline{A(U_{dv}S_{dv})}_A + \overline{A}\,(\overline{u'_{dt}s'_{dt}})_A + \overline{A}\,(\overline{u'_{dv}s'_{dv}})_A = \\
&= \overline{M}_1 + \ldots + \overline{M}_{13}
\end{aligned}$$

Dyer considers

$$\overline{M'} = \overline{A}(\overline{u'_{dt}s'_{dt}})_A + \overline{A}(\overline{u'_{dv}s'_{dv}})_A = \overline{M}_{12} + \overline{M}_{13} \qquad (2.47)$$

and neglects such terms as $\overline{A}\,(\overline{u'_As'_A})_A$, $\overline{u}_A(\overline{A's'_A})_A$, $\overline{s}_A(\overline{A'u'_A})_A$, $A'(\overline{u'_As'_A})_A$, $A'(\overline{u'_{dt}s'_{dt}})_A$ and $A'(\overline{u'_{dv}s'_{dv}})_A$.

Also neglected were terms of similar nature and probably small such as

$$(\overline{u}_{dt}(\overline{AS_{dt}}))_A, (\overline{u}_{dv}(\overline{AS_{dv}}))_A$$

$$(\overline{s}_{dt}(\overline{U_{dt}A}))_A, (\overline{s}_{dv}(\overline{U_{dv}A}))_A$$

$$(\overline{s}_{dt}(\overline{u'_{dt}A'}))_A, (\overline{s}_{dv}(\overline{u'_{dv}A'}))_A$$

$$(\overline{u}_{dt}(\overline{s'_{dt}A'}))_A, (\overline{u}_{dv}(\overline{s'_{dv}A'}))_A$$

This decomposition scheme was not applied to any specific case, due, probably, to practical difficulties that the evaluation of some terms would present.

2.2.6 Dyer (1974)

Dyer used a simplified version of his previous mass transport decomposition by considering :

$$a = \overline{A} + A \qquad (2.48)$$

$$u = \overline{u}_A + U_A + \overline{u}_{dt} + U_{dt} + \overline{u}_{dv} + U_{dv} \tag{2.49}$$

$$s = \overline{s}_A + S_A + \overline{s}_{dt} + S_{dt} + \overline{s}_{dv} + S_{dv} \tag{2.50}$$

The mean mass transport during a tidal cycle is then

$$\begin{aligned}
\overline{M} &= \overline{a(us)}_A = \\
&= \overline{u}_A\overline{A}\overline{s}_A + \overline{AU_A}\overline{s}_A + \overline{AS_A}\overline{u}_A + \overline{A}\,\overline{U_AS_A} + \\
&\quad + \overline{AU_AS_A} + \overline{A}(\overline{u}_{dt}\overline{s}_{dt})_A + \overline{A}(\overline{u}_{dv}\overline{s}_{dv})_A + \\
&\quad + \overline{A}\,\overline{(U_{dt}S_{dt})}_A + \overline{A}\,\overline{(U_{dv}S_{dv})}_A + \overline{A(U_{dt}S_{dt})}_A + \overline{A(U_{dv}S_{dv})}_A = \\
&= \overline{M}_1 + \ldots + \overline{M}_{11}
\end{aligned} \tag{2.51}$$

In this expression terms $(\overline{u}_{dv}(\overline{AS_{dv}}))_A, (\overline{u}_{dt}(\overline{AS_{dt}}))_A, ((\overline{U_{dv}A})\overline{s}_{dv})_A, ((\overline{U_{dt}A})\overline{s}_{dt})_A$ are neglected. Again, terms 1 and 2 correspond to the effects of the mean flow and salinity, and terms 3 to 5 are correlations of tidal period fluctuations. Terms 6 to 9 correspond to the last four terms in Fischer's expression 2.32 or to terms 5 and 6 in Hansen's analysis.

Dyer applied several decomposition schemes to compute the salt transport in the Vellar estuary (salt wedge/partially mixed), in Southampton Water (partially mixed) and in the Mersey (partially mixed with lateral variations of salinity and velocity).

A first computation was made with Southampton Water data, using Bowden's decomposition; if a mean velocity $\overline{u} = R/A$ (where R is the river discharge) is considered, the results show large downstream salt fluxes which are difficult to explain without a decreasing salt content in the upper part of the estuary. If, however, the measured $\overline{u}_D$ values are used, term $\overline{M}_1$ (in Bowden's decomposition) becomes much larger than the remaining ones but shows considerable lateral variation in the cross section. This confirmed the need for a complete cross sectional analysis.

The application of Hansen's scheme to the three estuaries was considered from an order of magnitude viewpoint due to errors in the evaluation of $\overline{u}_A$. In most

cases the salt balance was maintained by terms (in Hansen's notation) 2 and 5, while term 3 was small; terms 3 and 4 were within the probable error range, term 6 and the additional $\overline{A}(\overline{U_d S_d})_A$ were assumed negligible and term 7 was not considered (assumed small).

Dyer's scheme was applied to the additional terms (6 to 9) resulting from the decomposition of terms 5 and 6 in Hansen's equation, with good agreement between the results of the different procedures. In the Vellar the largest term was term 7 with a smaller contribution from term 9, the lateral terms being smaller. In Southampton Water terms 6 and 7 were of the same order of magnitude, with terms 8 and 9 one order of magnitude less. In the Mersey, all terms, 6 to 9 were of the same order of magnitude, terms 8 and 9 being one order of magnitude higher than in the previous case; these results are, as noted by Dyer, of different importance to that anticipated by Fischer (1972), since, even in the case of the two partially mixed estuaries, lateral shear terms never dominated.

Dyer concluded that the proportion of the salt balance effected by the lateral circulation is greater in partially mixed than in salt wedge estuaries; furthermore, with decreasing stratification and the development of a vertically homogeneous estuary, lateral effects should predominate.

2.2.7 Murray and Siripong (1978)

Murray and Siripong examined the salt flux in a shallow estuary under intense tidal mixing in conditions of low runoff, with the purpose of showing that, in a fairly straight channel, the lateral effect is larger than the gravitational vertical component. Their decomposition scheme was applied to data from the Rio Guayas in Ecuador, a shallow well mixed estuary.

The diurnal inequalities of the several measured parameters (tidal height, salinity, speed) were negligible and enabled the use of data collected in three successive

tidal cycles; a quasi- steady-state salinity distribution was also assumed. Murray and Siripong called their measured flux "advective salt flux" and the remaining, non measurable part, the "dispersive salt flux" (turbulent and high frequency fluxes).

In their decomposition scheme vertical (column) and lateral (row) effects are characterized by the deviations of the vertical and lateral means from the cross sectional mean; those are defined as

$$u_{i\cdot} = \frac{1}{m}\sum_{j}^{m} u_{ij} \tag{2.52}$$

(lateral means, m columns)

$$u_{\cdot j} = \frac{1}{n}\sum_{i}^{n} u_{ij} \tag{2.53}$$

(vertical means, n rows)

$$u_A = \frac{1}{n}\sum_{i}^{n} u_{i\cdot} = \frac{1}{m}\sum_{j}^{m} u_{\cdot j} = \frac{1}{mn}\sum_{i}^{n}\sum_{j}^{m} u_{ij} \tag{2.54}$$

(cross sectional mean).

The deviations of each mean from the cross sectional mean are denoted by a prime:

$$u'_{i\cdot} = u_{i\cdot} - u_A \tag{2.55}$$

(deviation of each lateral mean)

$$u'_{\cdot j} = u_{\cdot j} - u_A \tag{2.56}$$

(deviation of each vertical mean).

The sums of both sets of deviations are zero. The observed velocities, u_{ij}, are written as the sum of the cross sectional mean, lateral and vertical deviations and an interaction constant U_{ij}.

$$u_{ij} = u_A + u'_{i\cdot} + u'_{\cdot j} + U_{ij} \tag{2.57}$$

the interaction constant being defined as

$$U_{ij} = u_{ij} - (u_A + u'_{i.} + u'_{.j}) \tag{2.58}$$

and having non-zero values only when a non-linear trend exists in either the vertical or lateral values of u_{ij}. The sum of the interaction constants is zero along lateral and vertical lines and in the cross section. The salinity values are decomposed similarly:

$$s_{ij} = s_A + s'_{i.} + s'_{.j} + S_{ij} \tag{2.59}$$

Expanding $u_{ij}s_{ij}$, averaging over time, and over the cross section, excluding trivial terms, the advective salt flux becomes

$$\begin{aligned} \overline{Q}_{sa} &= \overline{u_A s_A} + (\overline{u'_{i.}s'_{i.}})_A + (\overline{u'_{i.}s'_{.j}})_A + (\overline{u'_{i.}S_{ij}})_A + \\ &\quad + (\overline{u'_{.j}s'_{i.}})_A + (\overline{u'_{.j}s'_{.j}})_A + (\overline{u'_{.j}S_{ij}})_A + \\ &\quad + (\overline{U_{ij}s'_{i.}})_A + (\overline{U_{ij}s'_{.j}})_A + (\overline{U_{ij}S_{ij}})_A = \\ &= \overline{Q}_1 + \ldots + \overline{Q}_{10} \end{aligned} \tag{2.60}$$

where the cross sectional average, denoted by the subscript A, corresponds to

$$\Phi_A = \frac{1}{A}\sum_{ij} \Phi_{ij}\Delta A_{ij} \tag{2.61}$$

The authors expected only terms 1, 2 and 6 to be important, corresponding, respectively, to salt flux by mean current, to gravitational circulation and to flux by lateral variations in salt and velocity.

The computed values for the time averaged mass transports, i.e. $\overline{\sum_{ij} \Phi_{ij}\Delta A_{ij}}$ showed that:

1. The terms corresponding to downstream transport were 1,3,7,8 and 10; term 1 accounted for 93% of the transport, the remaining terms being negligible;

2. Terms 2,4,5,6 and 9 produced upstream transport; from those, term 2 (gravitational circulation) accounted for 35.5%, term 6 (lateral variations) accounted

for 53.1% and term 5 for 10.1%; the authors considered this last term to, eventually, result from spurious correlations;

3. All terms containing interaction constants were negligible.

The authors support the idea that their scheme is better than Fischer's since it evaluates both vertical and lateral effects from a single vertical and lateral profile; nevertheless they claim that for the data used both methods produced almost the same results.

From the above results it can be seen that the lateral gradient transport was 1.5 times higher than the one produced by gravitational circulation, confirming Fischer's hypothesis. However, there was also a lack of balance between downstream and upstream fluxes, the ratio being of 4 to 1; if the steady state hypothesis is accepted this would imply that about 75% of the upstream transport was carried out by the non-measured "dispersive component". Consequently, the most important upstream transport process would be the one associated with turbulence and high frequency advective fluxes rather than the ones corresponding to lateral variations or gravitational circulation.

2.2.8 Dyer (1978)

With the purpose of studying salt and sediment mass transports, Dyer applied a simplified version of his decomposition scheme to data from the Gironde (well-mixed) and Thames (partially-mixed) estuaries; both estuaries show a turbidity maximum. The following equation was used:

$$\begin{aligned} \overline{M} &= \overline{A}\overline{u}_A\overline{c}_A + \overline{AU}_A\overline{c}_A + \overline{AC}_A\overline{u}_A + \overline{A}\,\overline{U_AC_A} + \\ &\quad + \overline{AU_AC_A} + \overline{A}\,(\overline{u}_{dt}\overline{c}_{dt})_A + \\ &\quad + \overline{A}\,(\overline{u}_{dv}\overline{c}_{dv})_A + \overline{A}(\overline{U_{dt}C_{dt}})_A + \overline{A}(\overline{U_{dv}C_{dv}})_A = \\ &= \overline{M}_1 + \ldots + \overline{M}_9 \end{aligned} \tag{2.62}$$

where the overbars denote tidal cycle averaging and the subscript A denotes averaging over the cross section; c corresponds to a generic concentration of salt or sediment.

Terms 1 and 2 are related to the river flow R, since

$$R = \overline{A}\overline{u}_A + \overline{AU_A} \tag{2.63}$$

where $\overline{u}_A$ is the non tidal drift and $\overline{AU_A}$ (negative) corresponds to the landward transport due to the partially progressive nature of the tidal wave (Stokes drift). Terms 3,4 and 5 are correlations between tidal oscillations of concentration, cross sectional area and velocity, commonly called the tidal pumping terms. Terms 6 and 7 are due to the net transverse and vertical (gravitational) circulations, while terms 8 and 9 represent the corresponding tidal effects. By defining a dispersion coefficient as

$$D = \frac{R\overline{c}_A}{A\frac{d\overline{c}_A}{dx}} \tag{2.64}$$

it can be seen that terms 1 and 2 are advective terms, while terms 3 to 9 correspond to dispersive processes. Dyer's main purpose was to extend the previous applications of the method to the case of well mixed estuaries. In these, a well developed turbidity maximum exists near the head of the salt intrusion, suggesting that the mechanisms that drive salt upstream should also be effective in transporting suspended sediment.

The calculations made for three sections of the Gironde estuary showed in all of them a total landward dispersion of salt; the total dispersion of sediment was seaward in the two upper sections and landward but small in the third. For the Thames a total landward dispersion was found both of salt and sediment.

In the Gironde term 4 was consistently the largest, being partly compensated by opposite contributions from terms 3 and 5. In the case of salt transport, term 7 was the largest of the shear terms at the upper section but term 8 became dominant

towards the mouth; for sediment transport, terms 7 and 9 were the largest at the upper sections but terms 6 and 8 increased in importance towards the mouth.

In the case of the Thames the largest shear contribution to salt transport was due to the vertical mean circulation (term 7) although the transverse effects were large as happens with other partially mixed estuaries. The tidal terms (tidal pumping) were of comparable magnitude to the total shear transport. The suspended sediment transport showed a large seaward contribution from term 9, with an opposite contribution of term 4 of, approximately, twice its magnitude.

Dyer, assuming that the results of the Gironde are typical of well mixed estuaries in low river discharge, steady state conditions, concluded that the normal situation would correspond to landward dispersion of suspended sediment; at the mouth the dominant mechanism should be tidal dispersion, while upstream the importance of the shear effects should increase.

Summarizing, and relative to partially mixed estuaries, Dyer concluded that, by analogy with the salt transport mechanisms, the shear terms would be dominant, with the turbidity maximum maintained by the gravitational circulation. However, and due to lags in sediment movement, the sediment distribution may respond more slowly than the salt distribution estuarine dynamics.

2.2.9 Rattray and Dworsky (1980)

In an attempt to assess the validity of previous results, Rattray and Dworsky examined the effects of three sampling procedures (cross-section decomposition into sub-areas) for determining flux terms. In their analysis only the transport mechanisms associated with time-means of velocity and salinity were considered.

The three sampling designs are shown in figure 2.4 and have the following characteristics:

Design i) : uniform vertical spacing, proportional transverse spacing;

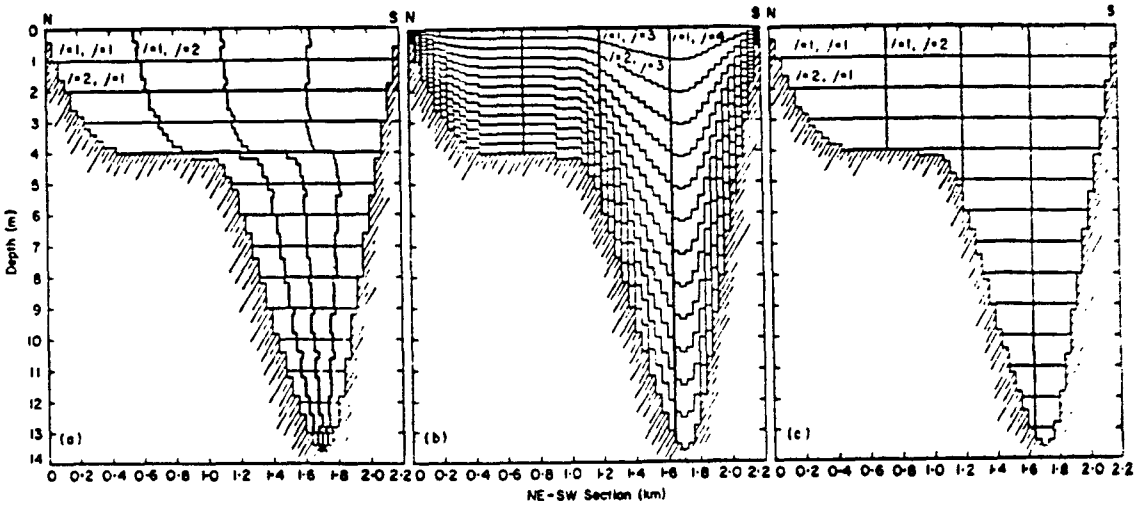

Figure 2.4: Cross-sectional area decompositions: a) Design i); b) Design ii); c) Design iii). From Rattray and Dworsky, 1980.

Design ii) : proportional vertical spacing, uniform horizontal spacing;

Design iii) : uniform vertical spacing, uniform horizontal spacing.

Denoting the average values of salinity and velocity in each sub- area, ΔA_{ij} as s_{ij} and u_{ij} (i denoting the row and j the column), the averages of the rows and columns are defined as

$$s_{.j} = \frac{1}{A_{.j}} \sum_i s_{ij} \Delta A_{ij} \tag{2.65}$$

(average salinity in the column)

$$s_{i.} = \frac{1}{A_{i.}} \sum_j s_{ij} \Delta A_{ij} \tag{2.66}$$

(average salinity in the row)

$$s_{..} = s_A = \frac{1}{A} \sum_i \sum_j s_{ij} \Delta A_{ij} = \frac{1}{A} \sum_i s_{i.} A_{i.} = \frac{1}{A} \sum_j s_{.j} A_{.j} \tag{2.67}$$

(average salinity in the area) where

$$A_{\cdot j} = \sum_i \Delta A_{ij} \tag{2.68}$$

$$A_{i\cdot} = \sum_j \Delta A_{ij} \tag{2.69}$$

$$A = \sum_i \sum_j \Delta A_{ij} = \sum_i A_{i\cdot} = \sum_j A_{\cdot j} \tag{2.70}$$

Several deviations are also defined:

$$s_{dvi} = s_{i\cdot} - s_{\cdot\cdot} \tag{2.71}$$

(primary vertical deviation)

$$s_{dtj} = s_{\cdot j} - s_{\cdot\cdot} \tag{2.72}$$

(primary transverse deviation)

$$S_{dvij} = s_{ij} - s_{dtj} - s_{\cdot\cdot} = s_{ij} - s_{\cdot j} \tag{2.73}$$

(secondary vertical deviation)

$$S_{dtij} = s_{ij} - s_{dvi} - s_{\cdot\cdot} = s_{ij} - s_{i\cdot} \tag{2.74}$$

(secondary transverse deviation)

$$\begin{aligned} S_{ij} &= s_{ij} - s_{i\cdot} - s_{\cdot j} + s_{\cdot\cdot} = \\ &= s_{ij} - s_{dvi} - s_{dtj} - s_{\cdot\cdot} \end{aligned} \tag{2.75}$$

(vertical-transverse interaction).

The authors used two-way analysis of variance techniques to test three hypotheses regarding the dominant pattern of variation:

a) The primary variation is transverse;

$$s_{ij} = s_{\cdot\cdot} + s_{dtj} + S_{dvij} \tag{2.76}$$

b) Both variations (vertical and transverse) are of comparable importance and their effects are essentially additive;

$$s_{ij} = s_{..} + s_{dvi} + s_{dtj} + S_{ij} \tag{2.77}$$

c) The primary variation is vertical.

$$s_{ij} = s_{..} + s_{dvi} + S_{dtij} \tag{2.78}$$

Neglecting Design iii), hypothesis b) due to limited utility, the contributions to the net advective salt flux due to spatial correlations over the cross section between velocity and salinity components can be identified for each hypothesis as

Hypothesis a)

$$(us)_{..} = u_{..}s_{..} + \frac{1}{A}\sum_{j} u_{dtj}s_{dtj}A_{.j} + \frac{1}{A}\sum_{i}\sum_{j} U_{dvij}S_{dvij}\Delta A_{ij} \tag{2.79}$$

Hypothesis b)

$$(us)_{..} = u_{..}s_{..} + \frac{1}{A}\sum_{i} u_{dvi}s_{dvi}A_{i.} + \frac{1}{A}\sum_{j} u_{dtj}s_{dtj}A_{.j} + \frac{1}{A}\sum_{i}\sum_{j} U_{ij}S_{ij}\Delta A_{ij} \tag{2.80}$$

Hypothesis c)

$$(us)_{..} = u_{..}s_{..} + \frac{1}{A}\sum_{i} u_{dvi}s_{dvi}A_{i.} + \frac{1}{A}\sum_{i}\sum_{j} U_{dtij}S_{dtij}\Delta A_{ij} \tag{2.81}$$

Data from a cross section in Southampton Water was used to test the three designs which, combined with the three hypotheses a), b), c) produced nine (eight, by neglecting iii-b)) distinct determinations of advective salt flux components. This estuary was chosen due to the existence of marked lateral variation in its depth, suitable for generating a transverse circulation as discussed by Fischer (1972); previous computations by Dyer (1974, 1978) had reported comparable contributions of the vertical and transverse circulations to the mean salt flux at the cross section.

For design i) all three hypotheses led to the conclusion that the advective flux was mainly due to the vertical contribution. In the case of design ii) all the hypotheses showed comparable contributions from the vertical and transverse components.

Design iii) showed comparable vertical and transverse contributions under hypothesis a) (predominance of transverse effect), consequently denying the assumption, but predominance of the vertical circulation contribution with hypothesis c), which is consistent with the basic assumption.

The authors concluded that different methods of data treatment produce different interpretations regarding the dominating transport processes, requiring additional criteria to be applied.

By comparing the assumed dominant patterns with the obtained results, especially in case iii) in which the transverse component never dominates, even in case a), Rattray and Dworsky concluded that the most important contribution arises from the vertical effects; this interpretation is reinforced by physical reasoning indicating that salinity and velocity (due to longitudinal salinity gradients) should be vertically stratified. Accordingly, a strong dependence of both variables upon vertical position should lead to a dominant contribution from gravitational effects; this contribution is implicit in designs i) and iii) but partly neglected in design ii) by attributing part of the vertical effects to a transverse contribution (the horizontal sub-areas are not at the same levels). Another reason for the small contribution of the transverse effects to the advective flux is the low correlation between transverse fluctuations of u and s, while their vertical deviations are physically related.

2.2.10 Uncles, Elliot and Weston (1984)

Uncles et al. (1984) investigated the transverse variations in water, salt and sediment transports in the upper reaches of the Tamar estuary which is a partially mixed estuary; data were collected for three cross sections, each during spring and neap tidal cycles.

The transport of water per unit width is

$$Q_D = hu_D \tag{2.82}$$

where h is the tidal depth and u_D the velocity (the subscript D denotes depth averaging). The residual water transport is

$$\overline{Q}_D = \overline{hu_D} = \overline{Q_E} + \overline{Q_S} = \overline{Q_L} \tag{2.83}$$

in which the overbar denotes a tidal average and where:

$$\overline{Q_E} = \overline{h}\,\overline{u}_D \tag{2.84}$$

(Eulerian residual transport per unit width)

$$\overline{Q}_S = \overline{HU} \tag{2.85}$$

(residual transport associated with the tidal wave, equivalent to the Stokes transport for 1-D flows), with $U = u_D - \overline{u}_D$ and $H = h - \overline{h}$.

$\overline{Q}_L$ is the residual transport of water per unit width.

Considering

$$u = \overline{u}_D + U + u_v \tag{2.86}$$

$$s = \overline{s}_D + S + s_v \tag{2.87}$$

(where u_v and s_v are the vertical deviations from the depth averages), the residual, depth averaged rate of transport of salt per unit width is

$$\begin{aligned}
\overline{M} &= \overline{h(us)_D} = \\
&= \overline{h}\,\overline{u}_D\overline{s}_D + \overline{h}(\overline{US}) + \overline{u}_D(\overline{HS}) + \overline{s}_D(\overline{HU}) + \\
&\quad + \overline{HUS} + \overline{h}(\overline{u_v s_v})_D + \overline{H(u_v s_v)_D} = \\
&= \overline{Q}_E\overline{s}_D + \overline{Q}_S\overline{s}_D + \overline{QS} + \overline{h}(\overline{u_v s_v})_D + \overline{H(u_v s_v)_D} = \\
&= \overline{M}_L + \overline{M}_{TP} + \overline{M}_v
\end{aligned} \tag{2.88}$$

the three contributions corresponding, respectively, to the residual flow of water, to tidal pumping and to vertical shear. Similarly, defining the instantaneous suspended sediment concentration $c = \overline{c}_D + C + c_v$, the depth averaged sediment transport is

$$\overline{M'} = \overline{h(uc)_D} = \overline{M'}_L + \overline{M'}_{TP} + \overline{M'}_v \tag{2.89}$$

where

$$\overline{M'_L} = \overline{Q}_L \overline{c}_D \tag{2.90}$$

$$\overline{M'_{TP}} = \overline{QC} \tag{2.91}$$

$$\overline{M'_v} = \overline{h(u_v c_v)} + \overline{H(u_v c_v)_D} \tag{2.92}$$

The measured data generally confirmed some well known features of the estuarine hydrodynamics, such as higher currents during spring tides relative to neaps and tidal asymmetry (higher flood currents over shorter duration). During spring tides this last feature produced more local resuspension and higher sediment concentrations during the flood stages than during the ebb stages, in the two upper sections under study.

The obtained results showed higher values of the Stokes water transport in spring tides than in neap tides; this transport was directed up-estuary in the deeper parts of the cross sections and was small and down-estuary in the inter-tidal areas. The Eulerian transport was always directed down-estuary; the total residual transport tended to be down-estuary in the shallower parts of the cross sections and smaller (up or down estuary) in the deeper areas.

Data for salt transport showed vertical shear transport to be always up estuary and larger in the deeper parts of the cross sections, where gravitational circulation is more developed. Tidal pumping transport was directed up-estuary in the deeper parts of the cross sections and, in some cases, reversed direction in the shallower areas; the advective salt transport followed the pattern of the residual flow of water. The total residual transport of salt was up-estuary in the deeper parts of the cross sections and down-estuary in the shallower.

The sediment transport due to vertical shear was negligible while the advective transport of sediment due to the residual flow of water followed the latter. Transport during spring tides was between one and two orders of magnitude larger, relative to neap tides, due to strong local resuspension in higher currents. Tidal pumping

of sediment, due to increased sediment resuspension and up-estuary transport by flood currents was, as expected, larger during spring tides and was the dominant pattern in the two upper sections. However some down-estuary pumping occurred in the deepest part of the middle section, where sediment was, probably, more difficult to erode: the authors concluded that, in the absence of local resuspension, tidal pumping of sediment acts in the opposite way to the tidal pumping of salt. At the most downstream section, the slight asymmetry of tidal currents allowed down-estuary sediment pumping.

2.2.11 Uncles, Elliot and Weston (1985a)

Uncles, Elliot and Weston extended their previous analysis to seven stations in the Tamar estuary, including the central stations of the three cross sections previously studied by the authors (Uncles et al., 1984), which were located in the upper part of the estuary.

The decomposition scheme used by the authors was similar to the one used in their 1984 study, the variables being normalized by $\overline{h}$, the tidal average depth. Consequently:

$$\overline{Q}_D = \overline{hu_D} = \overline{h}(u_{DE} + u_{DS}) = \overline{h}u_{DL} \tag{2.93}$$

where

$$u_{DE} = \overline{u}_D \tag{2.94}$$

$$u_{DS} = \overline{HU}/\overline{h} \tag{2.95}$$

$$u_{DL} = \overline{Q}_D/\overline{h} \tag{2.96}$$

A freshwater induced residual current u_{DF} was also defined by considering $\overline{A}$, the tidally averaged area of a cross section, and $\overline{Q}_{DF}$ the tidally averaged rate of input of freshwater volume up estuary of the section

$$u_{DF} = \overline{Q}_{DF}/\overline{A} \tag{2.97}$$

The residual transport of salt was similarly defined as

$$\overline{M} = \overline{M}_L + \overline{M}_{TP} + \overline{M}_v \tag{2.98}$$

where

$$\overline{M} = (\overline{h(us)_D})/\overline{h} \tag{2.99}$$

$$\overline{M}_L = \overline{u}_{DL}\overline{s}_D \tag{2.100}$$

$$\overline{M}_{TP} = \overline{QS}/\overline{h} \tag{2.101}$$

$$\overline{M}_v = \overline{h(u_v s_v)_D}/\overline{h} \tag{2.102}$$

The residual transport of sediment per unit width of the column is also:

$$\overline{M'} = \overline{M'}_L + \overline{M'}_{TP} + \overline{M'}_v \tag{2.103}$$

with corresponding definitions.

Uncles, Elliot and Weston completed the results obtained for the previously studied three sections (the first two of which, stations 1 and 2, were located up-estuary) with a study of four new stations, one located between stations 2 and 3 and the remaining located down-estuary of station 3.

The authors were able to confirm the spring-neap variability of suspended sediment concentration and local resuspension of sediment in the upper reaches of the estuary. A turbidity maximum was detected in the region of the lower salinities. In the lower reaches of the estuary bed sediment resuspension did not occur and suspended sediment concentrations were low.

The residual flux of salt per unit width during spring tides was directed up estuary, with tidal pumping generally dominating. In the absence of cross sectional data, enabling the evaluation of transverse shear effect, equilibrium conditions could only be assumed. The data for neap tide conditions showed a less systematic behavior; tidal pumping was still up-estuary but negligible in the deeper down estuary sections where vertical shear dominated.

The residual flux of suspended sediment during spring tides was dominated by tidal pumping, directed up estuary in the two upper sections (due to tidal asymmetry) and down estuary elsewhere. This down estuary nature of the tidal pumping was partly due to high freshwater inputs which caused higher ebb than flood currents. In the upper sections, where resuspension from the bed occurred and concentrations increased from bed to surface, the vertical shear flux was up estuary while the opposite happened in the down estuary stations where resuspension did not occur.

During neap tides the observed fluxes of sediment were either negligible or directed down estuary.

2.2.12 Uncles, Elliot and Weston (1985b)

The authors completed their previous study (Uncles et al., 1984) of three cross sections of the Tamar estuary by further investigating the transverse contributions to salt and sediment transport. Murray and Siripong's 1978 decomposition scheme was used, in which the instantaneous rate of transport of salt through a section is given by:

$$M = a(u_{ij}s_{ij})_A \tag{2.104}$$

Expanding:

$$M = au_A s_A + a(u'_{i.}s'_{i.})_A + a(u'_{.j}s'_{.j})_A + M^* \tag{2.105}$$

where

$$\begin{aligned} M^* \;=\; & a[(u'_{i.}s'_{.j})_A + (u'_{i.}S_{ij})_A + (u'_{.j}s'_{i.})_A + (u'_{.j}S_{ij})_A + \\ & +(U_{ij}s'_{i.})_A + (U_{ij}s'_{.j})_A + (U_{ij}S_{ij})_A] \end{aligned} \tag{2.106}$$

Decomposing the variables into a tidal mean and a tidal oscillation

$$q = \overline{q} + Q \tag{2.107}$$

$$s = \overline{s} + S \tag{2.108}$$

and averaging over a tidal cycle

$$\overline{M} = \overline{M}_L + \overline{M}_{TP} + \overline{M}_{sv} + \overline{M}_{st} + \overline{M^*}_s \tag{2.109}$$

where

$$\overline{M}_L = \overline{q}\,\overline{s}_A \tag{2.110}$$

$$\overline{M}_{TP} = \overline{QS} \tag{2.111}$$

$$\overline{M}_{sv} = \overline{a(u'_i.s'_i.)_A} \tag{2.112}$$

$$\overline{M}_{st} = \overline{a(u'_{.j}s'_{.j})_A} \tag{2.113}$$

In these, $\overline{M}_L$ is the rate of transport due to the residual flow of water over the section, $\overline{M}_{TP}$ is the rate of transport due to tidal pumping, $\overline{M}_{sv}$ and $\overline{M}_{st}$ are due, respectively, to vertical and transverse shear dispersion and $\overline{M^*}_s$ corresponds to interactions between vertical and transverse deviations.

Similar expressions are found for sediment, by substituting M' for M and c for s:

$$\overline{M'} = \overline{M'}_L + \overline{M'}_{TP} + \overline{M'}_{sv} + \overline{M'}_{st} + \overline{M'^*}_s \tag{2.114}$$

For the computation of the residual transport of salt the authors considered a sum of the deviation terms, corresponding to the shear processes over the cross section:

$$\overline{M}_s = \overline{M}_{sv} + \overline{M}_{st} + \overline{M^*}_s \tag{2.115}$$

which was found to be comparable or much larger than the tidal pumping term. The dominant component in $\overline{M}_s$ was $\overline{M}_{sv}$; from the remaining two, only $\overline{M}_{st}$ had some importance in the wider section. The authors concluded that transverse shear dispersion becomes more important with increased width.

Similarly, in the computation of the residual transport of suspended sediment a global shear term $\overline{M'}_s$ was defined. The residual transport during spring tides

was between one and two orders of magnitude higher than during neaps, due to sediment resuspension. The residual rate of sediment transport due to the residual discharge of water was always directed down estuary. Tidal pumping was the dominant mechanism at spring tides. $\overline{M'_s}$ (and its terms) were very small in all cases.

The author's conclusions stress the importance of the vertical gravitational circulation in the transport of salt which was, commonly, dominant relative to transverse shear and allows bidimensional (depth, axis) models to be used in partly mixed estuaries; those models, due to the importance of the tidal pumping terms cannot have steady state characteristics.

2.2.13 Dyer (1989)

Dyer used a condensed version of his 1978 decomposition, in the form:

$$\begin{aligned}\overline{M} &= (\overline{usa})_A = \\ &= \overline{u}_A\overline{s}_A\overline{A} + \overline{A\overline{U}_A}\overline{s}_A + \overline{A\overline{S}_A}\overline{u}_A + \overline{A}\,\overline{\overline{U}_A\overline{S}_A} + \\ &\quad + \overline{A\overline{U}_A\overline{S}_A} + \overline{A}(\overline{u}_d\overline{s}_d)_A + \overline{A}(\overline{U_dS_d})_A \qquad (2.116)\end{aligned}$$

Term 1 is the Eulerian flow and term 2 corresponds to inward transport due to the Stokes effect. Terms 3 to 5 are tidal pumping terms, while terms 6 and 7 correspond to vertical and transverse oscillatory shears.

Dyer complemented his 1978 data relative to the Gironde and Thames estuaries with Schubel's data from the Susquehana estuary, corresponding to two stations occupied in different conditions of river flow and stratification; one of the stations was landward of the turbidity maximum while the second was seaward. Despite the differences in stratification conditions, the flux terms corresponding to terms 6 $(\overline{u}_d\overline{s}_d)_A$ and 7 $(\overline{U_dS_d})_A$ were comparable and small, while tidal pumping $(\overline{U_AS_A})$ had higher values.

Dyer summarizes his results by considering that tidal pumping is the dominant process supporting the turbidity maximum in several estuaries. This mechanism balances the net outflow of sediment due to the combination of river flow and compensation flows for the Stokes drift.

2.2.14 Summary

In estuarine environments a long term quasi-equilibrium between seaward and landward mass transport of dissolved and suspended constituents is generally found. Tidally-averaged salinity and suspended sediment concentration at a given point, for example, usually show slow variations over time scales of days or even weeks. This quasi-stationarity over time scales higher than a tidal period and the existence of turbidity maxima have led to the investigation of the physical mechanisms that, within the tidal cycle, transport salt and sediment landward, balancing the flushing effect of the mean flow.

The basic tool used by several authors to investigate the relative importance of tidally averaged longitudinal mass transport phenomena in estuaries has been the decomposition of the relevant variables (velocity, concentration, cross-sectional area) into different components, either in terms of average values or values related to spatial or time variations. Through tidal cycle and cross-sectional averaging procedures and elimination of uncorrelated terms, the different processes contributing to transport salt or sediment are identified and evaluated through field measurements. Moreover, the hypothesis that the physical processes transporting salt and sediment are of similar importance has often been implicitly assumed.

A source of error in early studies proved to be the difference between the cross-sectional and tidally averaged velocity and the velocity that results from dividing the fresh water flow discharge by the cross-sectional area. The former velocity, in fact, accounts not only for the latter but also for seaward flows compensating the

landward Stokes effect (Hansen, 1965). A second source of uncertainty derives from the fact that the turbulent components of the mass transports were never evaluated; this, for example, makes an assessment of the results obtained by Bowden (1963) and Murray and Siripong (1978) difficult. A third source of uncertainty results from the fact that most authors do not explicitly describe their sampling procedure in the cross-section, which, if not correctly done, as shown by Rattray and Dworsky (1980), can lead to the overestimation of certain components. Finally, the fact that some terms are omitted in some of the mass transport expansions, without explicit evaluation of their magnitudes, provides an additional source of uncertainty.

The early results by Bowden (1963) showed the importance of the vertical gravitational circulation and tidal pumping terms, while confirming the existence of cross-sectional variations.

Hansen's study (Hansen, 1965) confirmed the dominance of tidal pumping and of the mean shear effect, although the latter was not decomposed into its lateral and vertical contributions.

Fischer (1972) used Hansen's decomposition scheme and through the use of theoretical and empirical results previously obtained by other authors concluded that the net transverse circulation might be the most important transport mechanism in estuaries. It should be noted, however, that the tidal pumping term was neglected in this analysis.

Dyer (1974) applied several of the previous decomposition schemes to three estuaries, confirming the dominance of tidal pumping and shear effect terms. Decomposition of the shear terms into vertical and transversal components showed vertical shear to prevail in the case of a salt wedge/partially mixed estuary and similar magnitudes for transverse and vertical shear in the case of partially mixed estuaries. Contrary to what had been anticipated by Fischer, lateral shear terms did not dominate. It should also be noted that Dyer's decomposition scheme cor-

responds to the hypothesis that the primary deviation is transverse (Rattray and Dworsky, 1980); information on the cross-sectional area decomposition should, consequently, allow a better assessment of the results.

Murray and Siripong (1978) applied a different decomposition scheme (assuming vertical and transverse variations of similar magnitude) to a shallow, well mixed estuary. This scheme did not allow for an explicit evaluation of tidal pumping. The obtained results showed the transverse shear and the vertical gravitational circulation to be of the same order of magnitude, the former being higher. The lack of balance between the measured landward and seaward transports, however, makes the significance of these results difficult to assess.

Dyer (1978) confirmed the dominance of tidal pumping and vertical shear terms in salt and sediment transport, although complete equivalence between the relative magnitudes of the transport processes in the cases of salt and sediment was not observed. A similar analysis by Dyer (1989) showed dominance of tidal pumping over shear terms in the case of sediment transport.

Rattray and Dworsky (1980) evaluated the effects produced by different methods of data treatment if either the transverse or the vertical deviations of the velocity and concentration are assumed to dominate and in case both variations are of comparable importance. The investigators concluded that the way in which the cross-section is divided may lead to overestimation of certain physical processes; in fact, a part of the transverse shear terms evaluated in previous studies might correspond to vertical effects.

Uncles et al. (1984, 1985a, 1985b) confirmed the importance of tidal pumping and vertical shear in the transport of salt and sediment. The dominant processes were not, however, entirely coincident; tidal pumping and vertical shear were dominant in the cases of sediment and salt, respectively. The difference between the relative importance of the main transport mechanisms in the cases of salt and sedi-

ment contradicts the assumption by previous investigators (Dyer, 1978, for example) of complete analogy between the causes for landward transport of both constituents. A further result obtained by Uncles et al. (1984, 1985a) relates the magnitude and direction of the sediment tidal pumping term to the erodability of the bed at the cross-sections.

The main transport processes acting to transport sediment landward seem, consequently, to be related to tidal pumping effects and, probably to a lesser degree, to the vertical gravitational circulation. Tidal pumping is a consequence of phase differences between tidal variations of the cross-sectional area and average cross-sectional velocity and sediment concentration. Such phase differences between the flow and the sediment concentrations are due to lags in sediment response to hydrodynamic changes and can be related to erosion-resuspension and settling-deposition phenomena during the tidal cycle. Sediment transport due to the vertical gravitational circulation is also strongly dependent on settling, diffusion and bottom conditions since these define the vertical concentration profile. A description of the physical phenomena contributing to sediment dynamics in the vertical direction is presented in Chapter 3.

CHAPTER 3
SOME ASPECTS OF FINE SEDIMENT DYNAMICS

3.1 The Transport Equation

Suspended sediment dynamics in a water body are described by the advection-diffusion equation which is a particular case of a mass conservation equation. The equation can be derived, in cartesian coordinates (x longitudinal, y lateral and z vertical, positive upwards from the water surface) by considering a differential control volume and equating the time rate of sediment accumulation inside the volume to the net flux of sediment through its boundaries. This continuity principle is a consequence of the assumption that, despite the continuous process of sediment floc formation and destruction within the control volume, the overall sediment size distribution remains constant and there is no net generation or destruction of the flocs of any particular size (Mehta, 1973). As a result, no production or decay terms need to be added to the equation and suspended sediment can be assumed to be conservative. The equation is then

$$\frac{\partial C}{\partial t} = -\nabla \cdot \vec{N} \tag{3.1}$$

where C is the instantaneous sediment concentration (mass of sediment/volume of suspension) and $\vec{N}$ is the net sediment flux vector. This vector can be decomposed into an advective component ($\vec{N_A}$), a molecular diffusion component ($\vec{N_D}$), and a settling component ($\vec{N_S}$), since the sediment is not neutrally buoyant

$$\vec{N_A} = \vec{q}C \tag{3.2}$$

$$\vec{N_D} = -D_m \nabla C \tag{3.3}$$

$$\vec{N_S} = -W_s C \vec{k} \tag{3.4}$$

where $\vec{q}$ is the fluid velocity vector, D_m the Fickian molecular diffusion coefficient (assumed isotropic), W_s the terminal settling velocity of the sediment particles or flocs and $\vec{k}$ the vertical unit vector (since several sediment sizes are present, the settling flux should be interpreted as the sum of the partial fluxes corresponding to the different sizes). This leads to

$$\frac{\partial C}{\partial t} = -\nabla \cdot (\vec{q}C - D_m \nabla C - W_s C\vec{k}) \tag{3.5}$$

Due to the turbulent characteristics of natural flows and the impossibility of tracking individual particle movements, flow velocity components and concentrations are usually decomposed into time averaged parts (over a longer period than the turbulent time scales involved), denoted by an overbar, and fluctuating components, denoted by a prime; for example

$$u = \overline{u} + u' \tag{3.6}$$

$$C = \overline{C} + C' \tag{3.7}$$

where u is the x component of the velocity vector in the cartesian coordinate system. Inserting these terms into equation 3.5, expanding, averaging over time (using the same time scale as before) and using the fluid continuity equation, the following equation is obtained:

$$\frac{\partial \overline{C}}{\partial t} + \overline{\vec{q}} \cdot \nabla \overline{C} = D_m \nabla^2 \overline{C} + \nabla \cdot (W_s \overline{C}\vec{k}) + \nabla \cdot (-\overline{\vec{q}'C'}) \tag{3.8}$$

which can also be written as

$$\begin{aligned} \frac{\partial \overline{C}}{\partial t} + \overline{u}\frac{\partial \overline{C}}{\partial x} + \overline{v}\frac{\partial \overline{C}}{\partial y} + \overline{w}\frac{\partial \overline{C}}{\partial z} &= D_m\left(\frac{\partial^2 \overline{C}}{\partial x^2} + \frac{\partial^2 \overline{C}}{\partial y^2} + \frac{\partial^2 \overline{C}}{\partial z^2}\right) + \frac{\partial}{\partial z}(W_s \overline{C}) - \\ &- \frac{\partial}{\partial x}(\overline{u'C'}) - \frac{\partial}{\partial y}(\overline{v'C'}) - \frac{\partial}{\partial z}(\overline{w'C'}) \end{aligned} \tag{3.9}$$

The last three terms in equation 3.9 correspond to gradients of turbulent diffusion fluxes and are commonly modeled, by analogy with the molecular diffusion case as

$$-\frac{\partial}{\partial x}(\overline{u'C'}) = -\frac{\partial}{\partial x}\left(-K_x \frac{\partial \overline{C}}{\partial x}\right) \tag{3.10}$$

$$-\frac{\partial}{\partial y}(\overline{v'C'}) = -\frac{\partial}{\partial y}(-K_y\frac{\partial \overline{C}}{\partial y}) \tag{3.11}$$

$$-\frac{\partial}{\partial z}(\overline{w'C'}) = -\frac{\partial}{\partial z}(-K_z\frac{\partial \overline{C}}{\partial z}) \tag{3.12}$$

where K_x, K_y and K_z are the turbulent mass diffusivities in the x, y, z directions, respectively. Turbulent diffusion coefficients are, however, much larger than the molecular diffusivities and the terms corresponding to the latter phenomenon can be neglected in equation 3.9 (Harleman, 1988). In order to investigate the vertical structure of sediment concentration a scaling analysis of the remaining terms in equation 3.9 is required. Ross (1988) shows that for estuarine flows, in which the advective vertical velocity w is negligibly small and the advective travel time trough the estuary is greater than the characteristic time for sediment settling, equation 3.9 reduces to

$$\frac{\partial C}{\partial t} = \frac{\partial}{\partial z}(W_s C + K_z\frac{\partial C}{\partial z}) \tag{3.13}$$

where the overbars (denoting time average values) have been omitted. The scaling analysis has, consequently, allowed horizontal and vertical advective fluxes to be neglected relative to vertical settling and diffusive fluxes. Equation 3.13 is valid in the water column (between the bed and the water surface) and requires appropriate boundary conditions. These are (Ross, 1988):

1. Bed Boundary Condition

   At the bed, $z = Z_b$, a bed flux term, F_b, (mass of sediment per unit bed area per unit time) must be defined, corresponding to a source or sink for the suspended sediment in conditions, respectively, of erosion or deposition. Consequently, in the z direction, and at the bed:

$$N(Z_b, t) = F_b = F_e - F_p \tag{3.14}$$

   where F_e and F_p are the erosion and deposition fluxes, respectively.

2. Surface boundary condition

   At the water surface, $z = 0$, a no flux condition is necessary, corresponding to a zero total flux, the diffusion flux always balancing the settling flux. Consequently:

$$N(0,t) = W_s C|_0 + K_z \frac{\partial C}{\partial z}|_0 = 0 \qquad (3.15)$$

In the water column, away from the boundaries, equation 3.13 applies; Ross (1988), solved this equation numerically, with the above boundary conditions, using a finite difference scheme. In the following paragraphs some of the physical phenomena described by the model will be presented.

3.2 Settling

3.2.1 General Aspects

The settling flux of cohesive sediment in turbulent flows is strongly dependent on the sediment concentration; this is due to the fact that the settling velocity itself depends on the concentration for a wide range of values. Moreover, the settling velocity of cohesive materials is a function of the suspension and not exclusively of the sediment (Mehta, 1988). This aspect can be understood if the causes for aggregation of cohesive particles are considered.

Aggregation occurs as a consequence of net attractive forces between particles, brought close enough by Brownian motion, differential settling and current shear. Although the relative importance of collision frequency due to the above mechanisms depends on the particle diameter, current shear seems to be the most important factor contributing to aggregation, with the exception of slack water periods when differential settling becomes dominant (Mehta, 1988). Aggregates or flocs are formed of individual particles and can, themselves, form aggregates of higher orders. They differ from primary particles in four main aspects:

1. their size is larger than that of individual particles;

2. their density is less than that of the particles due to interstitial water;

3. their shape is more spherical than the plate-like shape of the primary particles, which corresponds to reduced drag;

4. they are extremely weak, tending to break up.

From the above factors, the increase in fall diameter and the reduction of the drag are more significant than the decrease in density and the settling velocities of the flocs are higher than those of individual particles. The magnitude of the aggregate diameter and settling velocity are, moreover, only slightly dependent on the primary particle diameter. The dependence of the settling velocity of cohesive sediment particles (primary particles or flocs) on the concentration, neglecting secondary effects such as those of temperature and salinity falls within three cases (figure 3.1).

3.2.2 Free Settling

Free settling occurs for low concentrations, typically lower than 100 to 300 mg/l (Mehta, 1988). In this range the particles settle freely, without mutual interference; their terminal settling velocity is a result of the force balance between drag and net negative buoyancy. In the viscous range ($Re_s < 1$) the drag coefficient is

$$C_D = \frac{24}{Re_s} \tag{3.16}$$

(where $Re_s = WsD/\nu$) and the terminal settling velocity is (Vanoni, 1975)

$$W_s = \frac{D^2}{18}(\frac{\rho_s - \rho_w}{\mu})g \tag{3.17}$$

where D is the grain diameter, ρ_s and ρ_w are the grain and fluid densities, g is the acceleration of gravity and μ the fluid dynamic viscosity. Fine estuarial sediment in dispersed or quiescent conditions typically falls within these conditions although

the shape of the particles requires the use of an effective particle diameter (Ross, 1988).

3.2.3 Flocculation Settling

When the suspension concentration becomes higher than the free settling limit, increased concentration and inter-particle collision frequency cause an increase in aggregation and higher settling velocities. The general expression for the settling velocities in the flocculation range is

$$W_s = k_1 C^{n_1} \tag{3.18}$$

The coefficients in equation 3.18 may be determined in laboratory settling columns or in field tests; values determined by the latter procedure have been found to be higher by as much as an order of magnitude than those corresponding to the former, using the same sediment (Owen, 1971). This is due to the effect of local flow shearing rate on k_1.

3.2.4 Hindered Settling

For concentrations higher than a value C_0 of about 2 to 5 g/l the settling velocity decreases with the concentration. This is the result of hindered settling, a phenomenon in which aggregates become so closely packed that the fluid is forced to flow between them, through increasingly smaller pores. The general expression for the settling velocity in the hindered settling range is

$$\begin{aligned} W_s &= \overline{W}_{s0}[1 - \overline{k}_2(C - C_0)]^{n_2} \\ &= W_{s0}(1 - k_2 C)^{n_2} \end{aligned} \tag{3.19}$$

where $\overline{W}_{s0}$ is the settling velocity that corresponds to C_0, i.e., the maximum velocity of the flocculation range.

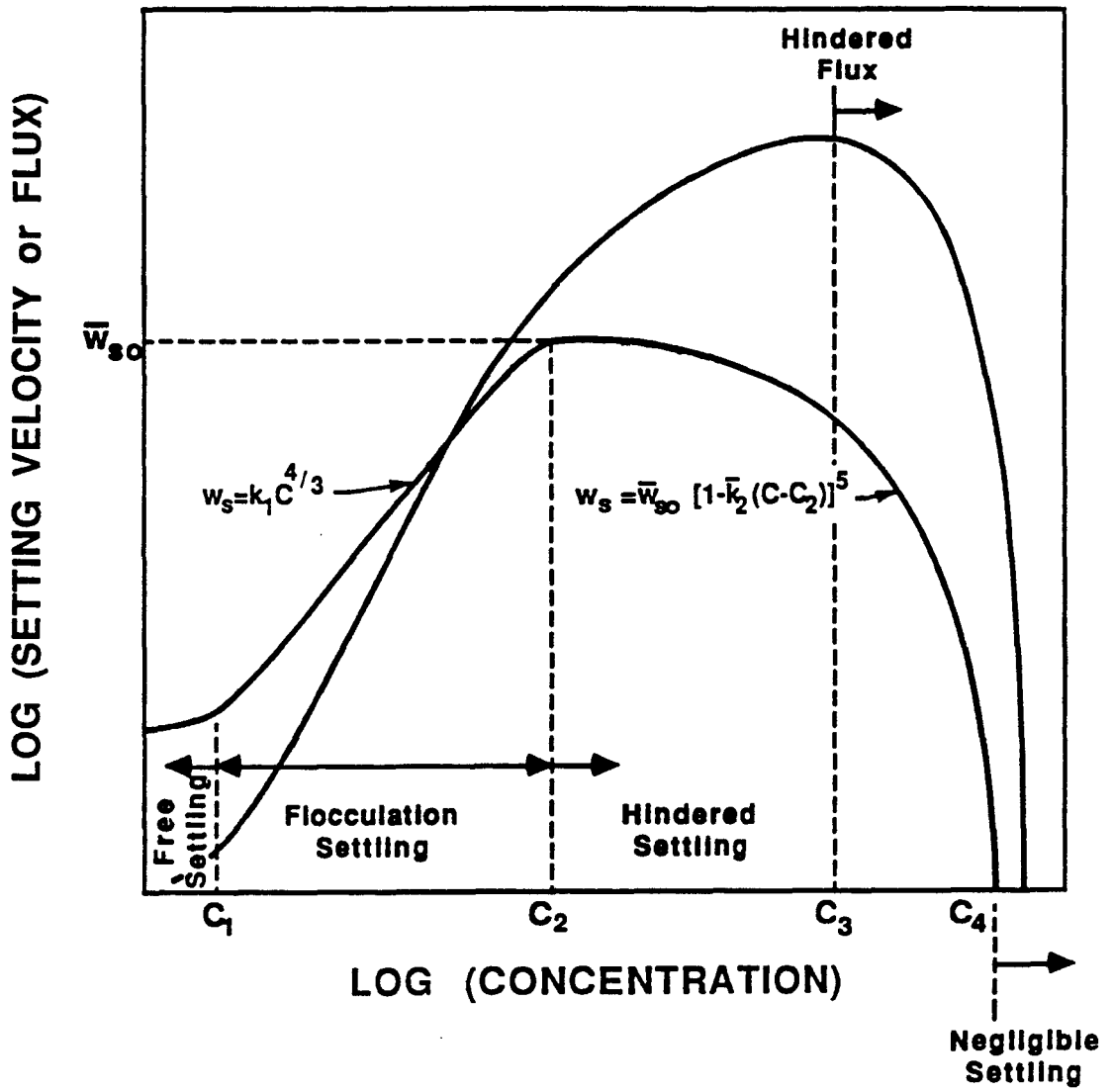

Figure 3.1: A general description of settling velocity and settling flux variation with suspension concentration of fine grained sediment ($n_1 = 1.33$, $n_2 = 5.0$).

3.2.5 Settling Flux

The behavior of the settling flux, itself, can be seen in figure 3.1 .The settling flux grows with the concentration within the flocculation settling range and for the lower concentrations of the hindered settling range. However, within the hindered settling zone the settling flux reaches a maximum, and decreases for higher concentrations. This is known as hindered flux and requires special consideration in the definition of numerical modeling schemes. The settling flux shows, consequently, a non-linear dependence on the concentration.

3.3 Diffusion

3.3.1 General Aspects

The vertical turbulent flux, expressed in equation 3.12 by the product of the vertical velocity and concentration deviations is the counterbalancing effect in the water column of the gravitational settling flux. It can be expressed by means of the Fickian analogy, as in equation 3.13 or by the use of more complex closure models. Similarly, turbulent fluxes of momentum can be defined, using the Fickian analogy by

$$\overline{u_i u_j} = -E_{ij}\frac{\partial \overline{u_i}}{\partial x_j} \tag{3.20}$$

where E_{ij} are the components of an eddy viscosity tensor; if turbulence is assumed to be isotropic $E_{ij} = E$. The ratio of the turbulent diffusion coefficients for momentum and mass (in the same direction) is called the Schmidt number (Harleman, 1988)

$$S_t = \frac{E}{K} \tag{3.21}$$

and can be taken as unity for particles in the Stokes range of settling, corresponding to sediment smaller than about 100 microns (Teeter, 1986), which includes typical cohesive sediment sizes. This fact allows the use of results, obtained theoretically for the vertical distribution of momentum diffusivity in the determination of mass

diffusivities in the water column, under conditions of non-stratified flow. For this purpose a description of the velocity profile in natural flows is necessary.

It is known that close to a wall or flow bed the flow velocity is reduced due to friction between the flowing water and the solid boundary. The layer in which velocity reduction, relative to the free stream velocity occurs is called the boundary layer, and, in the case of shallow water flows, can fill the whole water depth (Dyer,1986). Within the boundary layer, of thickness δ , two main zones can be defined (Dyer, 1986):

1. An inner zone, close to the wall, with thickness 0.1 to 0.2δ in which the shear stress can be assumed to be constant and the flow is not affected by external conditions; this zone can extend to the bed, if a rough bed exists, but can also be limited below by a buffer layer that separates it from a viscous sublayer (contiguous to the solid boundary) in the case of a smooth bed.

2. An outer layer which includes the remaining 80 to 90 per cent of the boundary layer and in which the flow is affected by external conditions, particularly by the free stream velocity.

Furthermore, in order to define velocity profiles which are adequate to describe turbulent flows, several differences have to be considered relative to viscous flows. Contrary to what happens in the case of molecular diffusion, the turbulent diffusivities are a function of the flow characteristics rather than of the fluid. Defining the turbulent shear stress in an unidirectional flow in the x direction as

$$\tau = \rho E \frac{d\bar{u}}{dz} \tag{3.22}$$

and noting that viscous forces in turbulent flow are approximately proportional to the square of the mean velocity rather than to its first power, as happens in the case of laminar flow (Schlichtling, 1979), it follows that E should be proportional to the mean velocity. Prandtl introduced the concept of a mixing length which is

a local function of the flow, measuring the length scale of turbulence. This length can be used as an indicator of the eddy size or of the average distance traveled by fluid parcels in their random movements, a similar concept to that of the "mean free path" in the kinetic theory of gases (Henderson, 1966). The eddy diffusivity is then defined through theoretical reasoning and experimental evidence as

$$E = l^2 \left|\frac{d\overline{u}}{dz}\right| \tag{3.23}$$

(since the sign of τ must change with $d\overline{u}/dz$) and the shear stress as

$$\tau = \rho l^2 \left|\frac{d\overline{u}}{dz}\right| \frac{d\overline{u}}{dz} \tag{3.24}$$

In the vicinity of a solid boundary it was assumed by Prandtl that the mixing length is directly proportional to the distance from the boundary, z

$$l = kz \tag{3.25}$$

where the constant of proportionality k is, in fact, the Von Karman universal constant κ , equal to 0.4 for homogeneous clear fluids (κ has been reported to decrease with increasing suspended solids concentration (Vanoni, 1975)); if, furthermore, it is assumed that in the same neighborhood the shear stress is constant (equal to the shear stress at the wall τ_0)

$$\tau_0 = \rho \kappa^2 z^2 \left(\frac{d\overline{u}}{dz}\right)^2 \tag{3.26}$$

and a friction velocity is defined as

$$u_* = \sqrt{\frac{\tau_0}{\rho}} \tag{3.27}$$

it is found that

$$\frac{d\overline{u}}{dz} = \frac{u_*}{\kappa z} \tag{3.28}$$

Integration of equation 3.28 produces a logarithmic velocity distribution law, of the form

$$\overline{u} = \frac{u_*}{\kappa} \ln z + const \tag{3.29}$$

This velocity law, applied to the inner zone of the boundary layer is known as the Prandtl law (Dyer, 1986)

$$\frac{\overline{u}}{u_*} = \frac{1}{\kappa}\ln(\frac{z}{z_0}) \tag{3.30}$$

where z_0 is the roughness length, a distance from the bottom at which the mean velocity becomes zero. In the outer layer equation 3.29 can tentatively be used, despite the fact that it was derived for a narrow zone, close to the solid boundary, of constant shear stress. Given that, at the surface $z = H$ and $\overline{u} = \overline{u}_{max}$, integration produces an universal velocity-defect law (Schlichtling, 1979)

$$\frac{\overline{u} - \overline{u}_{max}}{u_*} = \frac{1}{\kappa}\ln(\frac{z}{H}) \tag{3.31}$$

which describes the velocity distribution very accurately, even at substantial distances from the boundary where τ is different from τ_0 (Henderson, 1966). Since in both cases equation 3.28 applies, as noted before, assuming a linear shear stress variation in the water column, in the form

$$\tau = \tau_0(\frac{H - z}{H}) \tag{3.32}$$

and using equation 3.26, an expression for the momentum diffusivity is obtained as

$$E = \kappa u_*(H - z)\frac{z}{H} \tag{3.33}$$

This expression can also be used for the mass diffusivity, since $S_t = 1$ was assumed.

3.3.2 Stabilized Diffusion

In the presence of density stratification which can be caused by salinity, temperature or suspended sediment, the vertical diffusion of mass and momentum is affected, since a stable density gradient will tend to damp turbulence, strongly inhibiting mixing; in the limit, a large density gradient could lead to the formation of a stable interface with little turbulent exchange taking place across it. Furthermore,

mass and momentum diffusivities are not affected in the same manner, the latter having larger values (Oduyemi, 1986). A measure of the relative importance of the stabilizing gravitational forces to the destabilizing shear induced turbulence forces is the gradient Richardson number

$$Ri = -\frac{\frac{g}{\rho}\frac{d\rho}{dz}}{\left(\frac{du}{dz}\right)^2} \tag{3.34}$$

which takes positive values in the case of stable stratification and is negative in unstable stratification cases; neutral conditions have been found to occur for $0 < Ri < 0.03$. If the stratification becomes significant ($Ri > 0.25$) turbulence is damped out and the flow becomes essentially laminar (Dyer, 1986).

Density gradients also affect the velocity profile. Stratification changes the turbulent mixing length which becomes dependent not only on the distance from the wall but also on the length scale associated with stratification, L, known as the Monin-Obukov length. The gradient of the average velocity becomes

$$\frac{d\overline{u}}{dz} = \frac{u_*}{\kappa z}\Phi \tag{3.35}$$

where Φ is a function of z/L and

$$L = \frac{u_*^3\overline{\rho}}{\kappa g\overline{w'\rho'}} \tag{3.36}$$

($\overline{\rho}$ is the depth averaged density, w' and ρ' are the fluctuating parts of the vertical velocity and of the density, respectively, and $\overline{w'\rho'}$ is the time-average value of their product). The ratio z/L depends on Ri, being zero for $Ri = 0$ and increasing rapidly as Ri approaches 0.25. The function Φ is defined as (Dyer, 1986)

$$\Phi = (1 + \frac{\overline{\alpha}z}{L}) \tag{3.37}$$

which, substituting in equation 3.35 and for small z_0 leads to

$$\frac{\overline{u}}{u_*} = \frac{1}{\kappa}(\ln\frac{z}{z_0} + \overline{\alpha}\frac{z}{L}) \tag{3.38}$$

where $\overline{\alpha}$ has a value in the range from 4.7 to 5.2 (Dyer, 1986). Equation 3.38 is valid over small values of Ri and is similar to the Prandtl equation for the neutral case with an added correction term. Since z/L depends on Ri, Φ is often written as

$$\Phi = (1 + \beta' Ri)^{-\alpha'} \tag{3.39}$$

where α' , β' are empirical positive constants and, consequently

$$\frac{d\overline{u}}{dz} = \frac{u_*}{\kappa z}(1 + \beta' Ri)^{-\alpha'} \tag{3.40}$$

If equations 3.26 and 3.32 are again used, an expression for the momentum diffusivity in stratified conditions is obtained as

$$E_s = \frac{\kappa u_* (H - z)\frac{z}{H}}{(1 + \beta' Ri)^{\alpha'}} \tag{3.41}$$

or

$$\frac{E_s}{E_n} = (1 + \beta' Ri)^{-\alpha'} \tag{3.42}$$

where the subscripts s and n indicate, respectively, a stratified and a neutral situation. Since the Schmidt number is no longer unity (Oduyemi, 1986) a similar relationship for the mass diffusivity will require different empirical constants α and β:

$$\frac{K_s}{K_n} = (1 + \beta Ri)^{-\alpha} \tag{3.43}$$

The previous equations follow the general Munk and Anderson (1948) expression, relating diffusivities in stratified and neutral conditions; the empirical coefficients in equations 3.42 and 3.43, however, show a certain degree of variation, as reported in different studies (Ross, 1988).

3.3.3 Diffusion Flux

Another important effect of gravitational stabilization is the non-linearity between the diffusive flux, F_d, and the vertical concentration gradient $\partial C/\partial z$. This

is a result of the inverse dependence of the diffusion coefficient on a power α of the Richardson number, itself dependent on $\partial\rho/\partial z$ and consequently on $\partial C/\partial z$, while the diffusive flux is also directly dependent on $\partial C/\partial z$. A plot of F_d vs. $\partial C/\partial z$ (Ross, 88) is presented in figure 3.2 . It can be seen that $|F_d|$ reaches a maximum for a given value of $|\partial C/\partial z|$, say $\overline{C_z}$. For low gravitational stability $|\partial C/\partial z| < \overline{C_z}$, perturbations of the concentration profile are smoothed by diffusion, since the diffusive flux increases with $|\partial C/\partial z|$; the opposite effect occurs when $|\partial C/\partial z| > \overline{C_z}$ (high gravitational stability), since $|F_d|$ decreases with increasing $|\partial C/\partial z|$, mass accumulates and perturbations increase. However, for very high values of $|\partial C/\partial z|$, the gradient of $|F_d|$ with it tends to zero and perturbations will stabilize, forming step-like structures known as lutoclines. Consequently, an effect of the non-linearity between F_d and $\partial C/\partial z$ is the promotion of growth and stability of lutoclines, layers in which (analogously to what happens in the case of haloclines and thermoclines) steep concentration gradients and local minima in mixing and vertical diffusion occur. Further properties of such pycnocline layers include significant shear production and interfacial instability.

The above analysis, based on the hypothesis of similarity between lutocline phenomena and other pycnoclines should, however, be reviewed in the light of a fundamental difference: sediment is negatively buoyant, relatively to the surrounding fluid and the effects of settling should be added to the purely diffusive type of analysis. In this case, consequently, a settling flux counteracting the effect of diffusion in the water column, will contribute to enhance lutocline stability relatively to other types of pycnoclines; the net vertical flux (positive upwards) will still show minimum values at the levels of the lutoclines.

Examples of lutocline features (several of which may happen in a water column) are shown in figure 3.3 which shows a typical concentration profile, as observed in high sediment load environments. This figure shows the suspension layers which

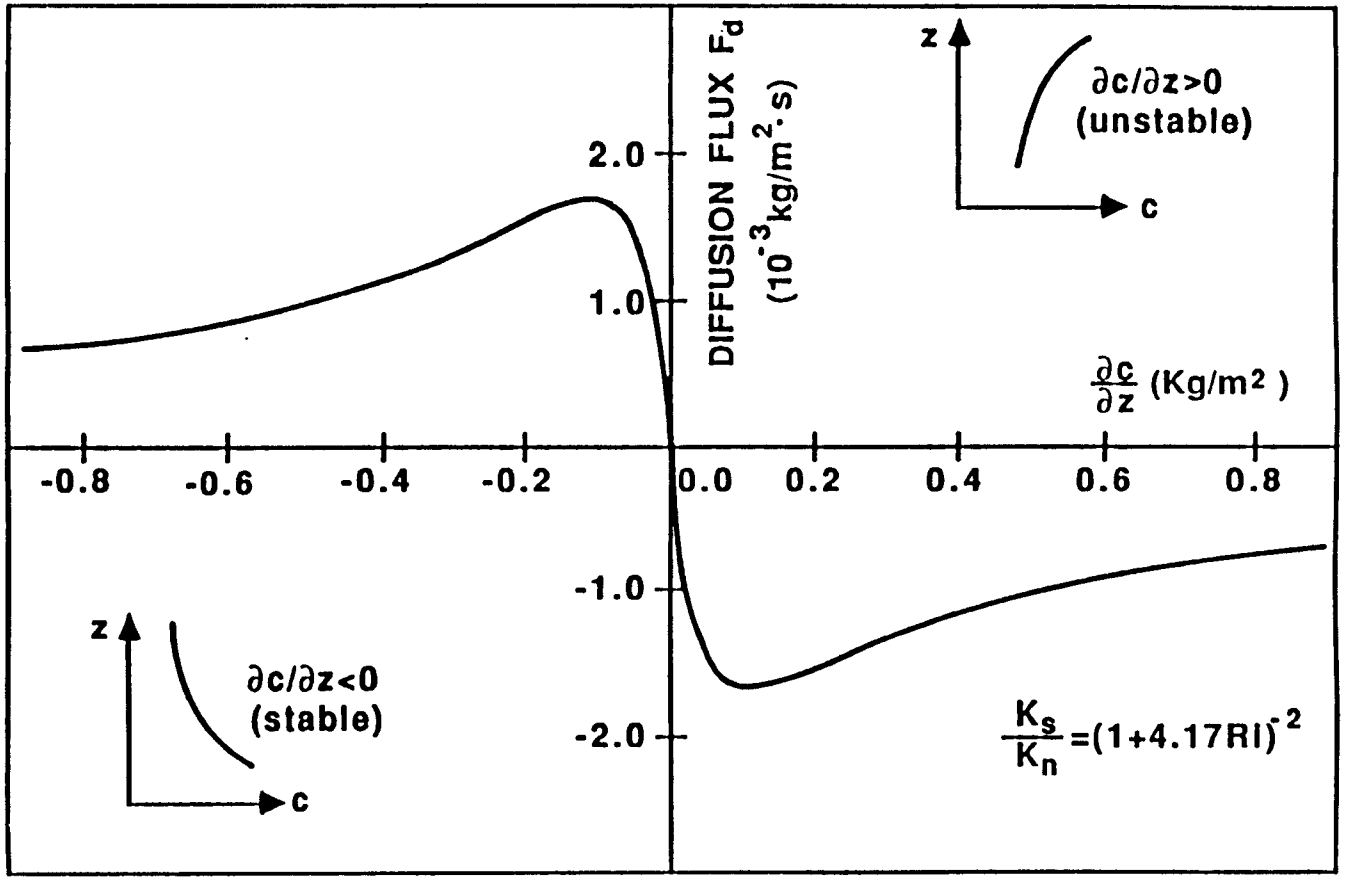

Figure 3.2: Diffusion flux as a function of $\partial C/\partial z$ for $\beta = 4.17$ and $\alpha = 2.0$. Adapted from Ross, 1988.

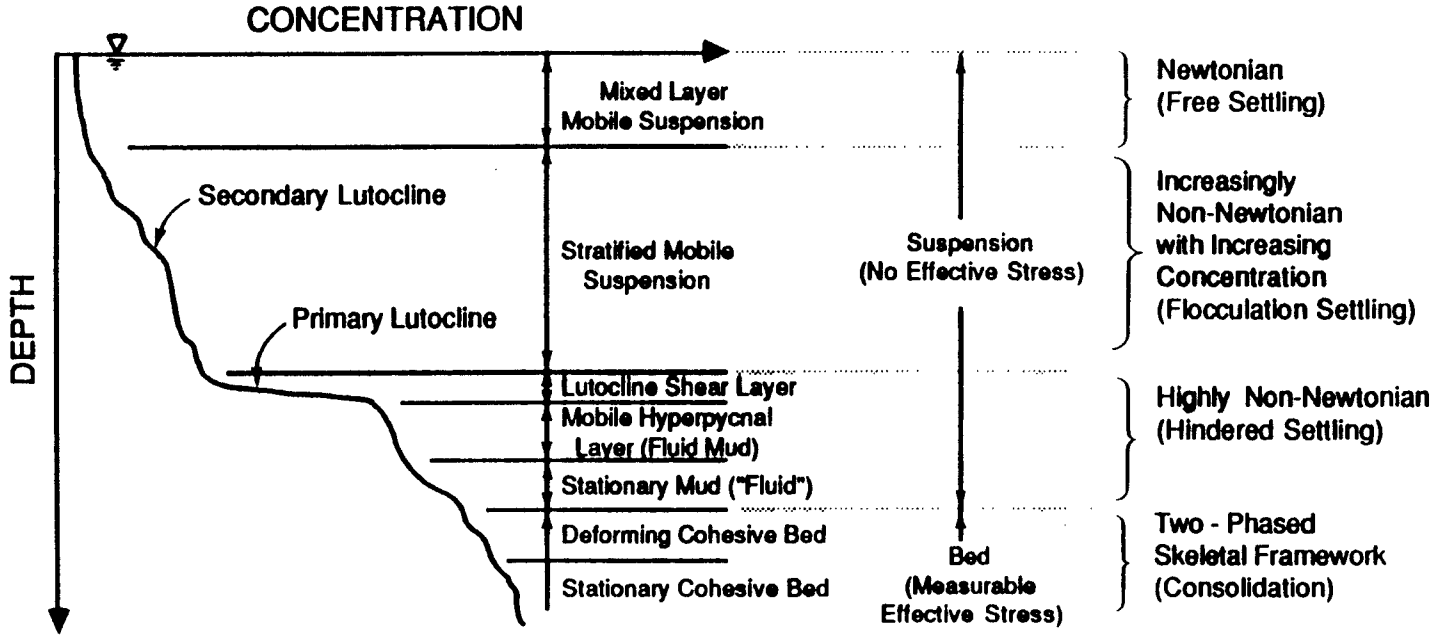

Figure 3.3: Concentration profile definitions.

correspond to the settling ranges described in section 3.2 and the bed layers (with concentrations of 200 g/l or higher) in which the particle framework supports a measurable effective stress. In particular, the hindered settling layer includes a primary lutocline shear layer, a mobile hyperpycnal layer (with both horizontal and vertical particle movement and low rate of dewatering) and the stationary mud layer in which horizontal particle movement no longer occurs. The two bed layers can be distinguished by their degree of consolidation and deformation: while the deforming cohesive bed is only partially consolidated and deforms visco-elastically under oscillatory forcing by waves, the stationary bed is well consolidated and shows little deformation.

3.4 Fluxes at the Bed

3.4.1 General Aspects

The bed fluxes are the deposition flux, F_p, and the erosion flux, F_e, which satisfy the bed boundary condition. In the case of cohesive sediment, deposition and erosion of sediment at the bed can be treated as non-simultaneous phenomena, occurring over different ranges of bed shear stress values. A short description of the physical phenomena associated with the bed fluxes is given below.

3.4.2 Deposition Flux

The time rate of sediment deposition per unit bed area (or deposition flux, F_p) can be defined as

$$F_p = \frac{dm}{dt} = -pW_sC \tag{3.44}$$

where p is the probability of sediment deposition, W_s the settling velocity and C the near-bed sediment concentration. The probability of deposition, due to Krone,

is defined as

$$p = (1 - \frac{\tau_b}{\tau_{cd}}) \tag{3.45}$$

where τ_b and τ_{cd} are the bottom shear stress and a critical shear stress for deposition, respectively. This concept reflects the fact that the deposition of flocs is controlled by near bed turbulence or, more specifically, by the rate of shearing $\partial u/\partial z$ at $z = z_b$. For a floc to stick to the bed it must be strong enough to withstand the near bed shear stress; weaker flocs are disrupted and resuspended. The deposition process is, then, also an effective sorting mechanism, controlling the size distribution of the suspended flocs.

For non-uniform sediment, experimental data (Mehta and Lott, 1987) show that complete deposition will occur if the bed shear stress, τ_b, drops below a critical value τ_{c1} (see figure 3.4). For increasing bed shear stress a residual concentration C_f (less than the initial concentration C_0) will remain, as long as τ_b is less than another critical value τ_{cM} (for $\tau_{c1} < \tau_b < \tau_{cM}$ the ratio C_f/C_0 is a function of τ_b only and increases with it). For shear stresses higher than τ_{cM} no deposition takes place and the initial concentration remains; τ_{cM} is, consequently, an upper value of shear stress for deposition. The solution of 3.44 corresponding to the case of non-uniform sediment is then (Mehta and Lott, 1987)

$$\frac{C}{C_0} = \sum_{i=1}^{n} \Phi(W_s^i) \exp\{-[1 - \frac{\tau_b}{\tau_{c1}}(\frac{W_s^{min}}{W_s^i})^m]\frac{W_s^i}{h}t\} \tag{3.46}$$

where

$$m = \frac{\ln(\frac{\tau_{cM}}{\tau_{c1}})}{\ln(\frac{W_s^{max}}{W_s^{min}})} \tag{3.47}$$

and h is the flow depth, $\Phi(W_s^i)$ is the frequency distribution of W_s^i (settling velocity class), W_s^{min} and W_s^{max} being the extreme values that define the range of the settling velocities; in the case of uniform sediment, for which $\tau_{c1} = \tau_{cM} = \tau_{cd}$

$$\frac{C}{C_0} = \exp[-(1 - \frac{\tau_b}{\tau_{cd}})\frac{W_s}{h}t] \tag{3.48}$$

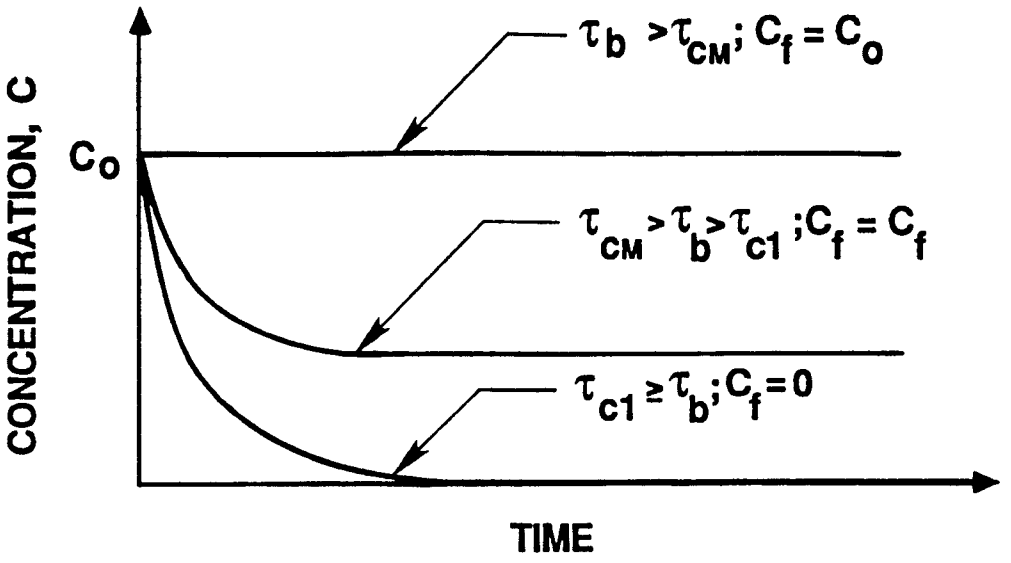

Figure 3.4: Typical time concentration relationship during deposition. From Mehta and Lott, 1987.

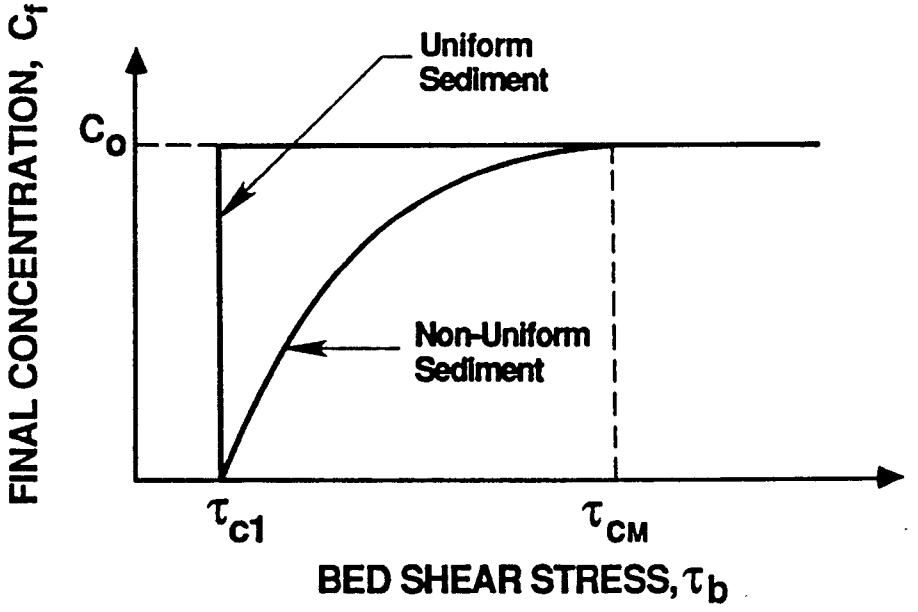

Figure 3.5: Dependence of C_f on τ_b for uniform and non uniform sediments. From Mehta and Lott, 1987.

Furthermore the probability of deposition will, for the case of non-uniform sediment, be expressed as

$$p_i = 1 - \frac{\tau_b}{\tau_{ci}} \tag{3.49}$$

which corresponds to a "settling by class" concept: for a given fraction i of the suspended sediment, if τ_b is greater than τ_{ci} (but less than τ_{cM}) no sediment will deposit while, eventually, another class, j, of coarser sediment may have $\tau_{cj} >> \tau_b$ and virtually no sediment will remain in suspension. The size distribution of the suspended sediment is, consequently, not only a function of the bottom shear stress but also of the initial size distribution and settling properties of each sediment class.

3.4.3 Erosion Flux

Erosion of cohesive sediment has generally been observed to occur in one of two modes: particle by particle and mass erosion. The former mode corresponds to the case in which particles separate from the bed in an individual basis, as a result of hydrodynamic erosional forces exceeding cohesive bonding, frictional and gravitational forces; in the latter case portions of the bed become unstable and large masses of sediment are resuspended, bed failure occurring below the surface. Particle by particle erosion is, however, the most common erosional mechanism in estuaries; under the action of bottom shear stresses higher than the bed shear strength, removal of particles and decrease in bed elevation (scour) will proceed until a bed layer of higher strength, equal to the applied stress, is found. This increase in bed shear strength with depth is due to changes in the floc structure after deposition, during consolidation and gelling. In general and for uniform sediment, the bed shear stresses which are necessary to keep sediment in suspension are much lower than those necessary to erode it; consequently the critical shear stress for erosion is higher than the previously defined τ_{cd}.

The time rate of increase of suspended sediment mass per unit area of the bed

(rate of erosion) can be described as

$$F_e = \frac{dm}{dt} = f(\tau_b, \tau_s, \alpha_1, \alpha_2 \ldots \alpha_n) \tag{3.50}$$

where τ_b is the time mean bottom shear stress, τ_s the bed shear strength and the α_i are other erosion resistance defining parameters. The difference $\tau_b - \tau_s$, the excess shear stress, is one of the common features of some of the existing formulas for the erosion flux, such as the proposed by Kandiah (1974) for uniform beds

$$F_e = \alpha_1 (\frac{\tau_b - \tau_s}{\tau_s}) \tag{3.51}$$

where α_1 is an empirical erosion parameter defined as

$$\alpha_1 = F_e|_{\tau_b = 2\tau_s} \tag{3.52}$$

For non-uniform beds, Parchure and Mehta (1985) proposed

$$F_e = \alpha_2 \exp\{\alpha_3 [\tau_b - \tau_s(z)]^{\frac{1}{2}}\} \tag{3.53}$$

where α_2 is known as the floc erosion rate

$$\alpha_2 = F_e|_{\tau_b = \tau_s} \tag{3.54}$$

and α_3 is a factor which is inversely proportional to the absolute temperature. It should be noted that τ_b is defined as a mean value and, consequently, some sediment particles will still be eroded when it equals the bed shear strength. This is taken into account by equation 3.53 but not by equation 3.51.

3.5 The Numerical Model

3.5.1 General Aspects

The vertical transport model developed by Ross (Ross, 1988) solves equation 3.13 through a finite difference scheme, using boundary conditions 3.14 and 3.15. If applied to the simulation of estuarine tidal conditions the following data are required:

1. Tidal hydrodynamics data:

   Tidal period, tidally averaged values of both the surface elevation and the depth averaged flow velocity, tidal amplitudes and time lags (relative to the time origin of computation) of both variables.

2. Sediment parameters:

   These include the concentrations defining the limits of the free settling range, parameters k_1 and n_1 in equation 3.18 and, for each sediment fraction, parameters W_{s0}, k_2 and n_2 (from equation 3.19), concentration C_0 defining the lower limit of the hindered settling range and the percentage by weight of the sediment fraction in the total sample.

3. Stabilized diffusion parameters:

   Empirical parameters α and β (equation 3.43).

4. Bed characteristics:

   These include the upper limit of the bed shear stress range for deposition $\tau_{cM} = \tau_{cd}$ (see equations 3.44, 3.45 and 3.48), the critical shear stress for erosion τ_s and the erosion empirical constant a (see equation 3.66).

5. Initial concentration profile:

   The values of sediment concentration at each grid point are required.

3.5.2 Numerical Procedure

For each time step a hydrodynamics routine computes the surface elevation H and the depth averaged velocity $\overline{u}$ using the input tidal data; the bed average shear stress τ_b is computed using the relation

$$\tau_b = \rho g R S \tag{3.55}$$

where S is the water surface slope, and Manning's formula

$$\overline{u} = \frac{1}{n} R^{\frac{2}{3}} S^{\frac{1}{2}} \tag{3.56}$$

which, considering $R \simeq H$ leads to

$$\tau_b = \rho g \frac{n^2}{H^{\frac{1}{3}}} \overline{u}^2 \tag{3.57}$$

The main limitations of this approach are related to the fact that Manning's formula was originally obtained from open-channel, hard bed, non-stratified flow data. It should be noticed that the Darcy-Weisbach friction factor (which can be related to Manning's n) changes with concentration and that the shear stress increases in the case of flows with suspended sediment (Ippen, 1971).

Within the water column, at the elevations corresponding to grid points, i, below the water surface, the neutral mass diffusivities are calculated through equation 3.33. Mass diffusivities corresponding to a stratified case are then obtained through equation 3.43. The diffusion fluxes are computed for each sediment class j through a forward difference scheme (i increasing downwards)

$$f_d(i,j) \simeq K(i) \frac{C(i+1,j) - C(i,j)}{\Delta z} \tag{3.58}$$

and the diffusion flux gradient is computed through backward differencing

$$\frac{df_d(i,j)}{dz} \simeq \frac{f_d(i,j) - f_d(i-1,j)}{\Delta z} \tag{3.59}$$

The settling fluxes are computed at each grid point, i, by

$$f_s(i,j) = W_s(i,j) C(i,j) \tag{3.60}$$

after $W_s(i,j) = W_s(i,j)(C(i,j))$ is computed, using formulas 3.18 and 3.19 for flocculation and hindered settling, respectively, or a constant value, if the concentration falls within the free settling range. The settling flux gradient, in the range

of concentration for which the settling flux grows with C is, again, computed using backward differences

$$\frac{df_s(i,j)}{dz} \simeq \frac{f_s(i,j) - f_s(i-1,j)}{\Delta z} \tag{3.61}$$

but a forward difference scheme is used in the hindered flux range

$$\frac{df_s(i,j)}{dz} \simeq \frac{f_s(i+1,j) - f_s(i,j)}{\Delta z} \tag{3.62}$$

The concentration at every grid point within the water column is, then, computed as

$$C^{t+\Delta t}(i,j) = C^t(i,j) - \Delta t\left(\frac{df_s(i,j)}{dz} + \frac{df_d(i,j)}{dz}\right) \tag{3.63}$$

(where the negative sign is required for consistency with equation 3.13) and the accumulated concentration as

$$C^{t+\Delta t}(i,0) = \sum_j C^{t+\Delta t}(i,j) \tag{3.64}$$

At the bed a flux is computed, corresponding to one of three cases as defined by the value of the bed shear stress τ_b:

1. For $\tau_b < \tau_{cd}$ a depositional flux is defined for each class of sediment as

$$F_b(j) = F_p(j) = W_s(j)C(j)\left(1 - \frac{\tau_b}{\tau_{cd}}\right) \tag{3.65}$$

   In this case, although different sediment fractions are considered for the settling velocities and concentrations a single value for τ_{cd} is used. The sediment deposited during each calculation step of a depositional period is accumulated into a variable D_b which corresponds to the mass of sediment accumulated at the bottom per unit area.

2. For $\tau_{cd} < \tau_b < \tau_e$ an entrainment flux is defined, allowing the freshly deposited sediment (during the period in which $\tau_b < \tau_{cd}$) to be resuspended at a constant rate during a given time T (specified from field data interpretation). If when

$\tau_b = \tau_s$ some of the previously suspended sediment still remains at the bed, an entrainment flux corresponding to the resuspension of that sediment quantity is specified, consequently allowing mass conservation in the water column.

3. For $\tau_b > \tau_s$ an erosional flux is defined as

$$F_b(j) = F_e(j) = -\alpha_1(\frac{\tau_b}{\tau_s} - 1) \tag{3.66}$$

which corresponds to a normalized excess shear stress concept. In this case $\alpha_1 = a\exp(-2.33\tau_s)$ as determined by Villaret and Paulic (1986).

The mass of sediment eroded per unit bed area is accumulated into a variable E_b, allowing τ_s to be recalculated at each time step, in the form

$$\tau_s^{t+\Delta t} = \tau_s^t + kE_b \tag{3.67}$$

This increase in the bed shear strength reflects increasing bed resistance to erosion with depth, due to consolidation and gelling. The new value of the concentration at the bed, for each sediment fraction, is computed as

$$C^{t+\Delta t}(b,j) = C^t(b,j) - \Delta t(\frac{F_b(j)}{\Delta z} + \frac{df_s(b,j)}{\Delta z} + \frac{df_d(b,j)}{\Delta z}) \tag{3.68}$$

and the accumulated concentration as

$$C^{t+\Delta t}(b,0) = \sum_j C^{t+\Delta t}(b,j) \tag{3.69}$$

3.5.3 Discussion

The description of the physical phenomena included in the model in the form presented in the previous sections shows some limitations. These are essentially related to the description of conditions close to the bed and to the effects of sediment stratification on the flow.

The first aspect is related to the bed boundary condition. Bed definition has been associated with the development of effective shear stress due to particle interaction leading to the formation of a structure. Above the structured bed two layers, the stationary fluid mud and the mobile fluid mud, exist (see figure 3.3). The near bed phenomena include bed fluidization and fluid mud entrainment into the mobile suspension layers and settling and bed formation as the opposite phenomena, together with consolidation and gelling of the structured bed. These complex features are, obviously, not completely described by a simple erosion-deposition model. In particular, fluidized mud has no shear strength but wave generation and breaking, under shear flow, at the fluid mud-mobile suspension interface, easily cause fluid mud entrainment; the rate of erosion expression, defined as a function of the excess shear stress, although generally applicable to moderate concentration environments, consequently gives a poor description of the behavior of high concentration fluid muds.

The effects of sediment stratification on the flow have been discussed by several authors. Although the Von Karman constant has been reported to decrease with C (Vanoni, 1975, Ippen, 1971) this fact has recently been contested (Coleman, 1981). Changes in the velocity profile and, specifically, in $d\overline{u}/dz$ are, however, commonly accepted, as shown in equation 3.35 by Φ. This function has classically been expressed in the form of equation 3.39, following Munk and Anderson (1948), in which the coefficients α' and β' reflect globally, the effect of stratification. A more detailed analysis was presented by Mc Cutcheon (1981) leading to a velocity profile that includes the effect of the density gradient; other corrected forms of the logarithmic profile for the case of flows with suspended sediment can be found in Ippen (1971) and Coleman (1981). These analyses could allow the direct computation of E_s and, through the Schmidt number of K_s.

CHAPTER 4
FIELD AND LABORATORY EXPERIMENTS

4.1 General Aspects

As described in Chapter 3, modeling of the processes involved in the simulation of the vertical concentration profile requires the collection of data defining both suspended sediment and bed properties. These data are essentially related to the suspended sediment settling velocities and to the bed erosion parameters and can be obtained through laboratory tests. Additionally, the definition of the flow's stabilized diffusion parameters can be obtained through adequately designed field experiments, enabling the computation of turbulent mass diffusion coefficients and mass fluxes. Field data are also necessary to evaluate the overall accuracy of a model's predictions.

The laboratory and field experiments carried out within the scope of the present study are described in this chapter. The laboratory tests were done at the Hohai University, Nanjing (People's Republic of China) using sediment collected at the field measurement site located in Hangzhou Bay. A description of the laboratory procedures and obtained results is presented in the section 4.2. The field environment, the experiment's methodology and the field data pre-processing methods are included in section 4.3.

4.2 Laboratory Tests

4.2.1 Grain Size Test

The grain size test was done according to standard hydrometer test procedures (ASTM, 1988) with slight modifications. These modifications are related to the sample preparation, which generally followed Standard Practice ASTM D2217 (procedure B, applicable to samples at moisture content equal or higher than the natural moisture content). The steps followed in the sample preparation were:

1. Collection of a moist sample containing at least 65 g of particles passing the 2.0 mm sieve.

2. Wet sieving of the sample through a 0.1 mm sieve which confirmed that the sample only contained finer particles.

3. Removal of salt from the sample. For this purpose distilled water was added and the suspension shaken, before being allowed to decant for 24 hours. After this period the excess water was carefully removed. This step was repeated once.

Hydrometer test procedures generally followed Standard Practice ASTM D422 with the exception of sediment sample dispersion which was not done. The grain size distribution is presented in figure 4.1 and shows the floc distribution existing in the natural environment. Although the clay fraction cannot be determined it is assumed to be small (Su et al., 1984). The median floc diameter is 23 μm, slightly higher than the range of median diameters indicated by Su at al. (1984) for Hangzhou Bay (10 to 13 μm for the suspended load and 16 μm for the bed material); this might be a result of the non-deflocculation of the sample.

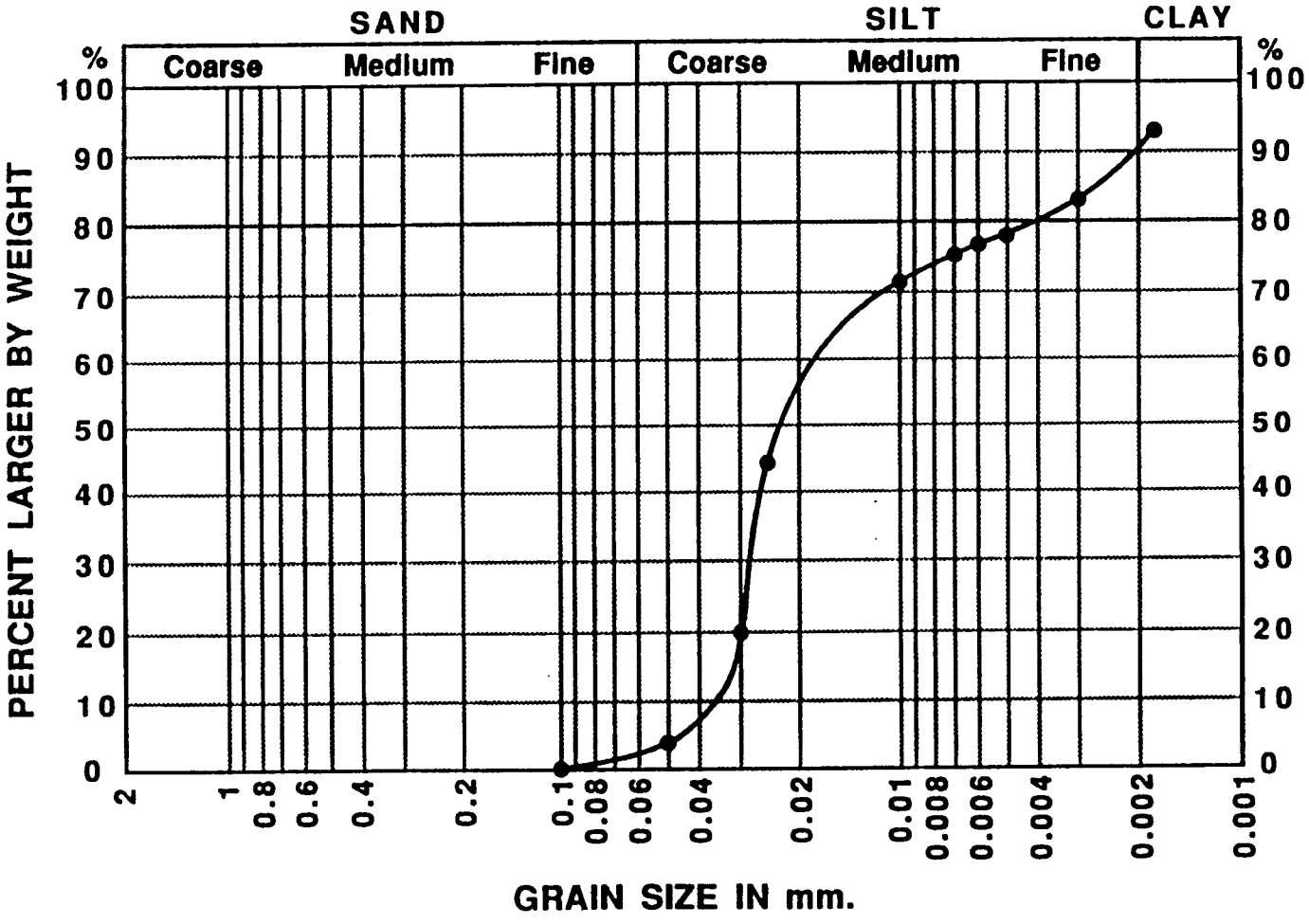

Figure 4.1: Grain size distribution.

4.2.2 Settling Velocity Tests

A settling column is needed for this test. The column used at Hohai University consisted of a 18.7 *cm* diameter tube, 1 *m* long, fitted with 5 *mm* inner diameter taps at six elevations. Tap hoses were 5 *cm* long and were fitted with clamps. The elevations of the taps from the bottom were (in *cm*): 15, 30, 45, 60, 75 and 90.

The experimental procedure used for the test was as follows:

1. High concentration sediment slurry was diluted with salt water to desired initial concentration and required volume (27.45 liters to fill the settling column). The suspension was thoroughly premixed in a large container.

2. After preparation the suspension was poured into the settling column and completely mixed for at least 2 minutes. This was achieved through mechanical mixing.

3. Immediately after removal of mixing device the first set of samples ($\simeq 100\,ml$ per sample) was taken. Samples were collected in glass bottles which were tightly capped, labeled and stored. Sampling was repeated at fixed times (5, 15, 30, 45, 60, 90, 120 and 180 minutes, for example) after the beginning of the test. Water depths and temperatures were recorded at each sampling time. The sampling hoses were always flushed (to remove the suspension left in the previous sampling) before each withdrawal.

4. Gravimetric analysis was used to determine the concentration of each sample. This was done by weighing a known volume of well mixed suspension ($100\,ml$) in a laboratory beaker of known weight. The sediment concentration in the volume was then obtained through the use of the equation

$$C = k(M_T - M_W) \tag{4.1}$$

where k is the inverse of the volume of suspension in the beaker and M_T, M_W are the masses of the suspension and of the same volume of salt water.

The test was carried out fourteen times, using several combinations of initial concentrations 2.0, 10.0, 20.0 and 30.0 g/l and salinities of 2.0, 10.0 and 30.0 ppt.

From the test results, values of the settling velocity, W_s, corresponding to a given concentration, C, can be determined (Vanoni, 1975, Ross, 1988) by considering that, in a settling column ($z = 0$ at the surface, increasing downwards):

$$\frac{\partial C}{\partial t} + \frac{\partial W_s C}{\partial z} = 0 \tag{4.2}$$

which is a continuity equation for sediment settling under quiescent conditions. Integration of equation 4.2 with respect to z gives

$$(W_s C)|_{z=D} = -\frac{\partial}{\partial t}\int_0^D C\, dz = -\frac{\partial}{\partial t}\overline{C}_D \tag{4.3}$$

At $t = 0$ the concentration is uniform throughout the settling column; for $t > 0$, integration of the concentration profile between the free surface and the D levels produces $\overline{C}_D$ values. The slope of a plot of $\overline{C}_D$ versus t at each depth will produce the right-hand side of equation 4.2 and, since the C values are known, W_s can be computed. A plot of W_s versus C values obtained in the settling tests done with Hangzhou Bay sediment is presented in figure 4.2; also shown in the figure are the curves of equations 3.18 and 3.19. Such curves were obtained by least-squares fitting, considering $\overline{W}_{s0} = 1.094\, mm/sec$ and $C_0 = 4.0\, g/l$.

4.2.3 Erosion Tests

An annular flume was used for the erosion test. The flume that was used for this test is similar to the one at the University of Florida, with a channel width of 20 cm, depth of 46 cm and a mean radius of 76 cm. A plexiglass annular ring of width slightly less than the channel width of 20 cm is suspended inside the channel in such

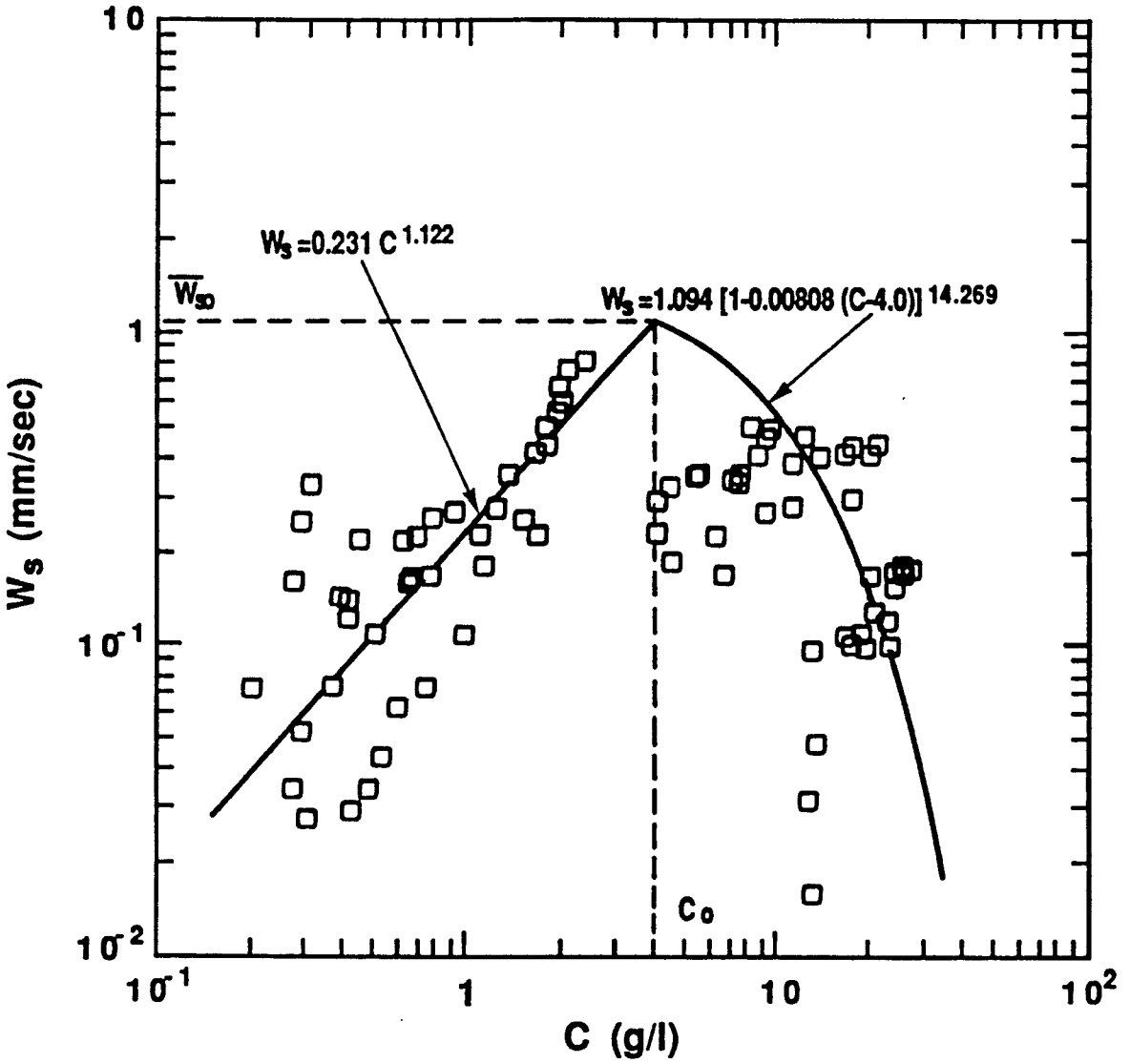

Figure 4.2: Settling velocity as a function of concentration for Hangzhou Bay sediment.

a way that it is in complete contact with the water column. During operation the ring and channel are rotated in opposite directions to minimize secondary currents. Taps are located on the outside wall of the channel, allowing sampling from the water column. The concentrations of the samples are determined by gravimetric analysis, similar to that used in the settling column tests.

The steps followed in the erosion tests were:

1. A placed bed was is used to obtain a relationship between the bed shear strength and the uniform density of the bed. A thick slurry (with selected approximate density) of local bed sediment (sieved to remove shell and plants) was mixed for one hour and placed into the annular flume to uniform depth. Salt water was carefully added to the flume, until adequate depth was reached. A similar slurry was placed in a bucket to allow bed density determination.

2. Four different shear stresses, τ_b, were selected and applied in a stepwise manner during 90 min each. The first was 0.1 N/m^2 and the remaining were obtained by increments of 0.2 N/m^2. A suspension sample was taken at the beginning of the test. Suspension samples ($\simeq$ 100 ml) were also taken at times 2, 5, 10, 15, 20, 25, 30, 40, 50, 60, 75 and 90 min after the beginning of each period of constant applied stress. Samples were taken, in each case, from taps at the top and at the bottom of the water column and an average suspension concentration was calculated and assumed representative of the entire water column. Salt water was periodically added to maintain the initial water depth.

Each test was carried out four times for the first three values of τ_b, with bed bulk densities of 1.2, 1.3, 1.4 and 1.7 g/cm^3 and once for $\tau_b = 0.7\ N/m^2$ with a bed bulk density of 1.7 g/cm^3. Plotting the rate of erosion (suspended sediment mass eroded per unit bed surface area per unit time) versus the applied shear stress (fig. 4.3) a critical shear strength value ($\tau_s = 0.05\ N/m^2$) is obtained. From this

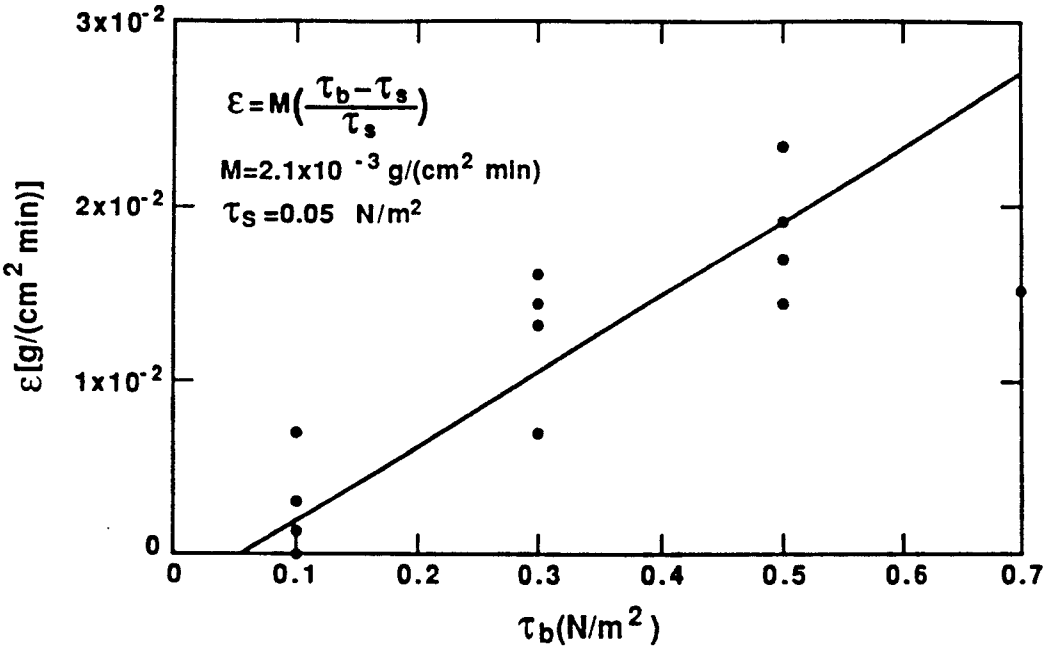

Figure 4.3: Erosion rate versus applied bottom shear stress for Hangzhou Bay sediment

value, and the pairs ϵ_i, τ_{bi} (erosion rate, applied bottom shear stress), a value for $M = 2.1 \times 10^{-3}\, g/(cm^2\, min)$ in the erosion rate expression, $\epsilon = M[(\tau_b - \tau_s)/\tau_s]$ is obtained.

4.3 The Field Experiment

4.3.1 The Measurement Site

The selected field experiment was close to the south shoreline of Hangzhou Bay, a high sediment concentration, meso-tidal environment, located in the East China Sea (figure 4.4). A summary of its most important oceanographic features is presented by Su et al. (1988) in their study of a plume front in the bay and by Su and Xu (1984) who modeled the bay's depositional patterns. A description of Hangzhou Bay's environment based on information provided by these authors is presented in the following paragraphs.

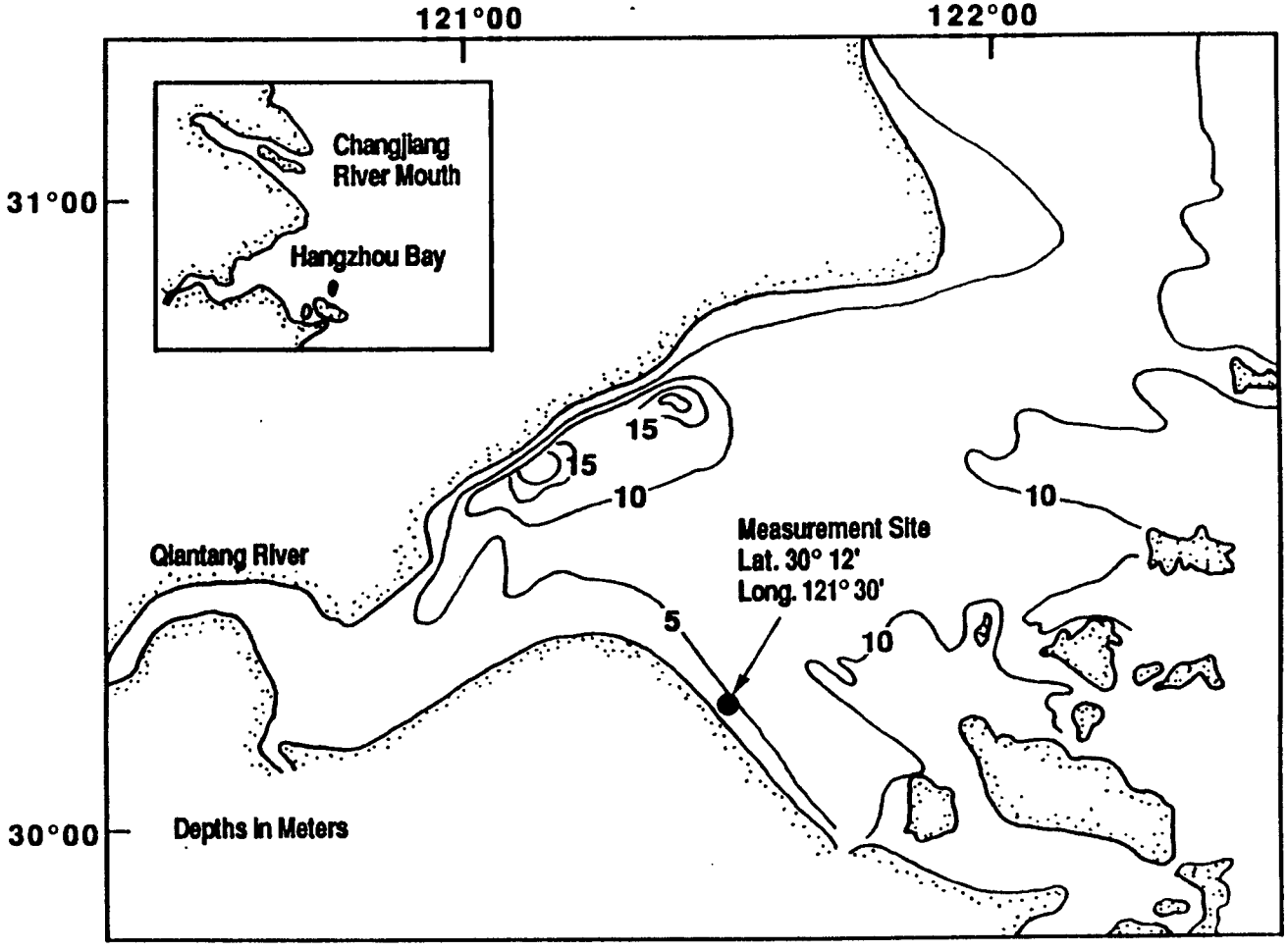

Figure 4.4: Location of the measurement site in Hangzhou Bay.

Hangzhou Bay is the outer region of the Qiantang estuary. It is approximately 100 Km long and its width decreases from 90 Km at the mouth to 20 Km at its western end. Due to this sharp reduction in width the tidal range (about 3 m at the mouth) increases rapidly and a tidal bore develops about 10 Km further upstream of the bay. This bore traps all but the finest sediment of fluvial origin; the retained part accumulates in a sandbar located under the bore. Sediment in the bay is predominantly fine and medium silt: the median size of the suspended load ranges from 10 to 13 μm while that of the bed material is 16 μm.

The rivers upstream from Hangzhou Bay discharge an average water flow of 42 Km^3 per year and an average suspended sediment load of $7.9 \times 10^9 Kg$ per year. Due to the different characteristics of the incoming water relative to the coastal waters a plume is formed. The high fresh water flow causes salinity to be usually less than 30 *ppt* at the mouth; the inner part of the bay is considered to be well-mixed.

Hangzhou Bay itself is a shallow and relatively flat water body, with a 10 m average depth. The bathimetry of the east part of the bay has remained generally stable in the last decades but a 40 Km stretch of the south shoreline, close to the measurement site, has accreted steadily at a rate of 20 m per year for the last six centuries. The accreted material, silt and fine sand, is believed to have offshore origin (Su et al., 1988).

North of Hangzhou Bay lies the mouth of the Chiangjiang River which has an average annual water flow of 925 Km^3 and an annual sediment discharge of 486×10^9 Kg. This river is believed to be an important sediment source for Hangzhou Bay, since mineral composition of both sediments is similar. At the mouth of the Chiangjiang River two plumes are formed (a main plume and a secondary plume), due to the different salinities of the river and coastal waters.

The main Chiangjiang plume is directed southward by the winds during winter, its front being located 50 Km away from the bay's mouth. During the summer

months the water and sediment discharges of the Chiangjiang increase and the main plume front moves to an area located 100 Km seaward of the bay; however, the action of the northbound Taiwan Warm Current and of southerly winds turn the plume to the northeast, where sediment is deposited. This sediment can be resuspended during winter storms, added to the river's winter sediment load and directed southward, entering Hangzhou Bay through its mouth.

The secondary Chiangjiang plume is permanently directed towards the bay, entering it through a localized area at the northern end of its mouth. This plume front aligns itself with the Qiantang river plume front (except in neap tides during low runoff seasons) forming a single NE/SW oriented front. A good correlation is found between high near bottom sediment concentrations and the position of this salinity front. Sediment carried by the secondary Chiangjiang plume and by the Qiantang plume all year round causes high near bottom sediment concentrations at the low density (landward) side of the front; sediment initially carried by the main Chiangjiang plume also accumulates at the high density (seaward) of the front during winter. Tidal resuspension of sediment along the front, although inhibited by stratification, combined with strong cyclonic along- front surface currents then cause southwestward transport of sediment and accretion of the south bank of Hangzhou Bay.

Some of the sediment transport patterns described above are represented in figure 4.5. These features show the complexity of suspended sediment transport patterns in Hangzhou Bay.

4.3.2 Field Experimental Procedures

The field measurement program was carried out from the 14^{th} to the 16^{th} of May, 1988 in the Andong area of the south shore of Hangzhou Bay. The measurements

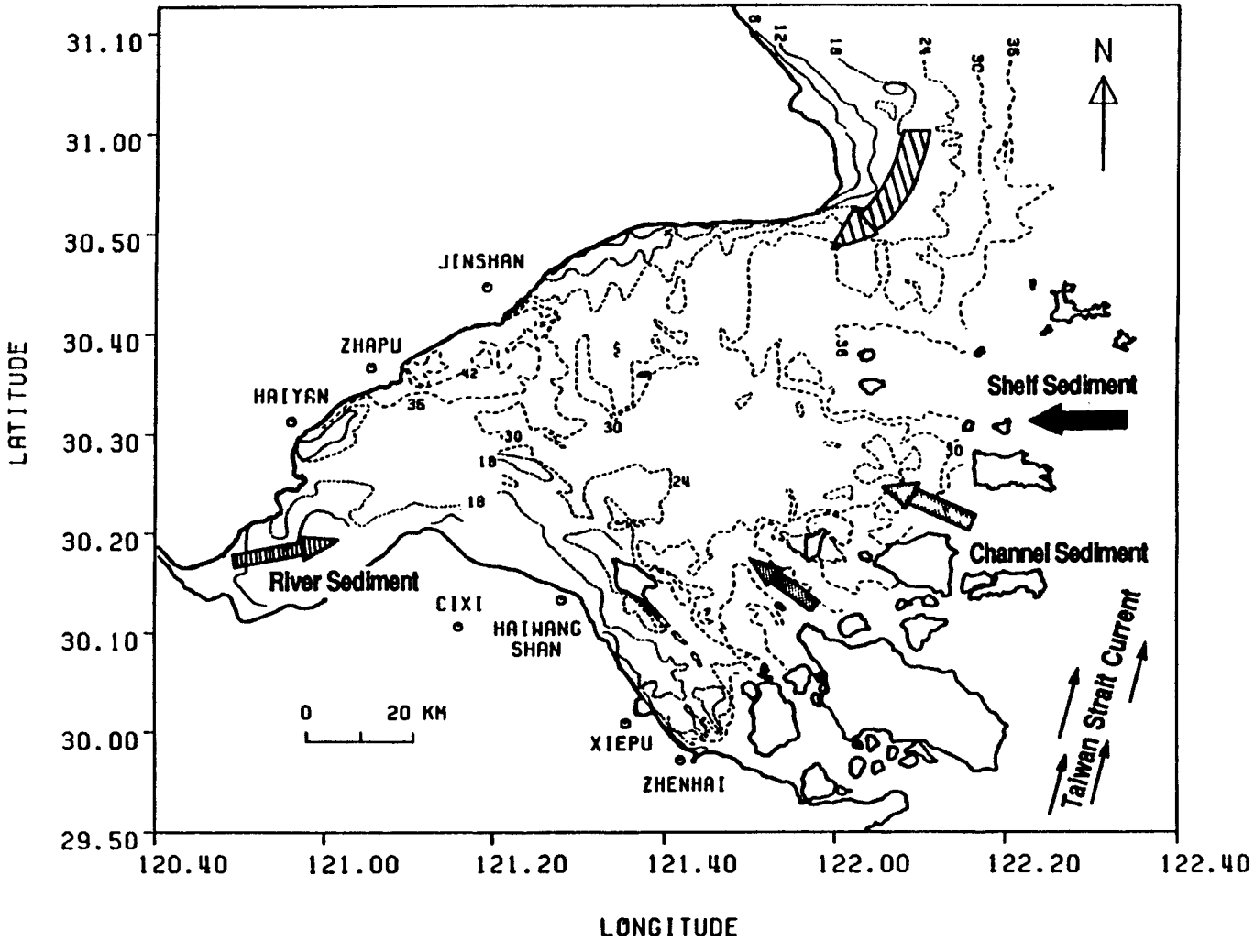

Figure 4.5: Sediment transport patterns in Hangzhou Bay. Courtesy of Dr. Hsiang Hwang.

were made by a joint team of the Coastal and Oceanographic Engineering Department of UF and of the Hohai University.

A measurement tower (fig. 4.6) was installed to accommodate a pressure gage, two turbidity meters and two electromagnetic current meters, at two different levels. A turbidity meter (Partech SDM16), an EM current meter (Marsh McBirney, model 512, with a ball diameter of 4 cm) measuring along two horizontal directions (x and y) and the pressure gage were installed at the lower level. A turbidity meter (Partech TT10 self cleaning unit) and a second EM current meter (of the same model) measuring along an horizontal and a vertical direction (x and z) were located at the upper level. The x direction was taken along the dominant direction of the ebb/flood current (at an angle of 140^o to the magnetic N).

The measurement data were sampled at a rate of 4 Hz and recorded with data-loggers. A preliminary measurement took place on May, 13^{th}, with the purpose of testing the equipment (deployment C1). Two experiments were then carried out: in the first, on May, 14^{th}, six sampling periods of 10 minutes each, separated by intervals of 30 minutes, were measured (deployment C2); in the second which begun on May, 15^{th}, fifteen sampling periods of 5 minutes each, separated by 60 minute intervals and encompassing a full tidal cycle, were measured (deployment C3). During the study period wave action was generally weak. The quality of the measured data was considered to be acceptable, except in the case of pressure data which was, in general, poor; transducer malfunction during experiment C3 also caused the loss of the velocity data at the lower measurement level for the last 9 sampling periods and of concentration at both levels during low concentration periods. Due to these facts the affected data blocks were not used in subsequent analyses.

A summary of wave data (significant wave height H_s, modal period T_m and bandwidth parameter of the spectrum ϵ), corresponding to the data blocks of de-

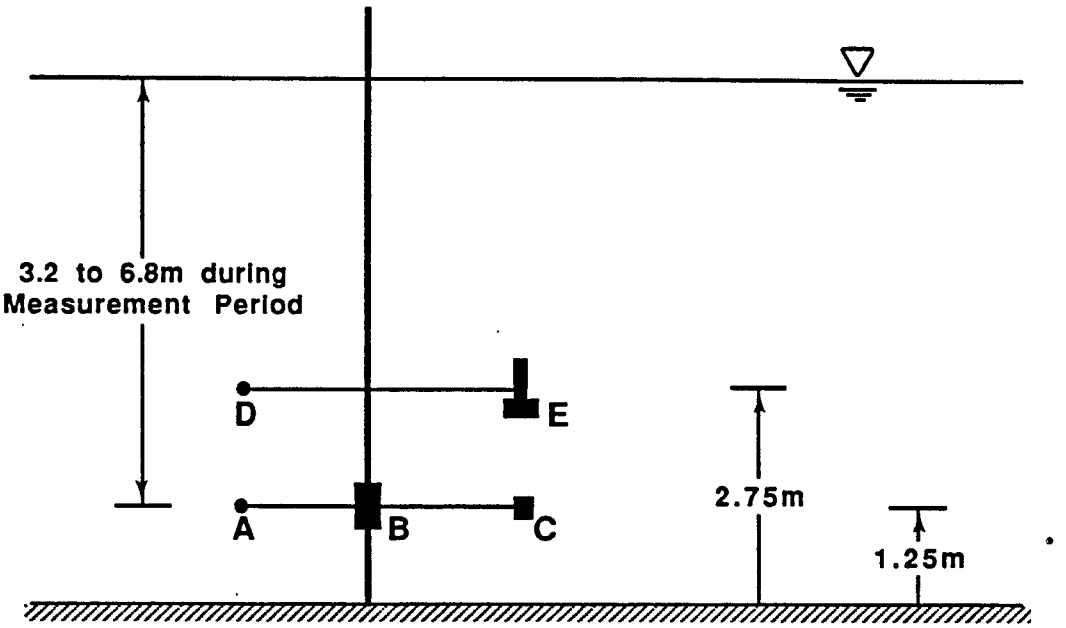

A - EM Meter, Channels 4 (u_1), 5 (v_1)

B - Pressure Gage, Channel 1

C - Turbidity Meter, Channel 3

D - EM Meter, Channels 6 (w_2), 7(u_2)

E - Turbidity Meter, Channel 2

Figure 4.6: Measurement tower and positions of the equipment used in Hangzhou Bay.

Table 4.1: Summary of wave data during the measurement period

Data Block	$H_s\,(cm)$	$T_m\,(sec)$	ϵ
CH24	12	2.98	0.327
CH25	22	2.67	0.199
CH26	33	2.41	0.206
CH36	117	2.03	0.271
CH37	96	2.67	0.226
CH38	122	2.15	0.117
CH315	31	2.98	0.375

ployments C2 and C3 of acceptable quality, is presented in table 4.1 . The values of the significant wave height generally confirm that the wave action was weak during the measurement period; it should be noted that the highest values of H_s correspond, approximately, to LW slack in deployment C3.

4.3.3 Data Pre-processing

After decodification the data records measured in Hangzhou Bay were pre-processed in order to separate the different physical processes involved. In general terms, a measured variable e can be represented as

$$e = \overline{e} + e_t + \tilde{e} + e' \tag{4.4}$$

where $\overline{e}$ is the time-average part, e_t the tidally induced part (tidal trend), $\tilde{e}$ the wave induced part and e' the turbulent part.

For the analysis of the random variations involved both $\overline{e}$ and e_t must be eliminated from the records. In general e_t can be assumed to have a linear variation with time during short measurement periods as was the case; however, due to the importance of plume effects in the local sediment dynamics, trends (tidal or others) were removed through subtraction from the original records of cubic spline curves representing such trends. These curves were defined for each record by a set of points $\overline{e}_n$ which were the average values of groups of n points of the original records; in

the present case a value of $n = 60$ (15 *sec* averaging) was used. The spline curves defined in such a way showed quasi-linear trends in the case of pressure and velocity records and more complex features in the case of sediment concentration data (probably due to plume effects), as expected. Examples of trend removal from the measured records are presented in figure 4.7.

Once the time average part and the trend are removed from each record, a new variable e_1 can be defined, including both the wave induced and turbulent effects:

$$e_1 = \tilde{e} + e' \tag{4.5}$$

The separation of these effects from velocity and concentration records can be done through the use of the wave coherent part of the pressure record, in the following way. Considering that the remaining part of the pressure record is

$$p_1 = \tilde{p} + p' \tag{4.6}$$

and since only the wave induced pressure fluctuations are of interest, the highest detectable wave frequency at the pressure gage level will separate the high frequency (turbulence induced) pressure fluctuations p' from the $\tilde{p}$ component which is assumed to result from waves only. The highest detectable wave frequency can be obtained through linear wave theory, assuming that, for the measured depths and the short period waves observed during the experiment, deep water conditions exist. Under these assumptions and for an average distance d from the pressure gage to the water surface (during the measurement period), the shortest wavelength detected by the gage during the measurement period will be

$$L_0 = 2d \tag{4.7}$$

and the corresponding frequency

$$\overline{f} = \frac{1}{T} = \sqrt{\frac{g}{2\pi L_0}} = \sqrt{\frac{g}{4\pi d}} \tag{4.8}$$

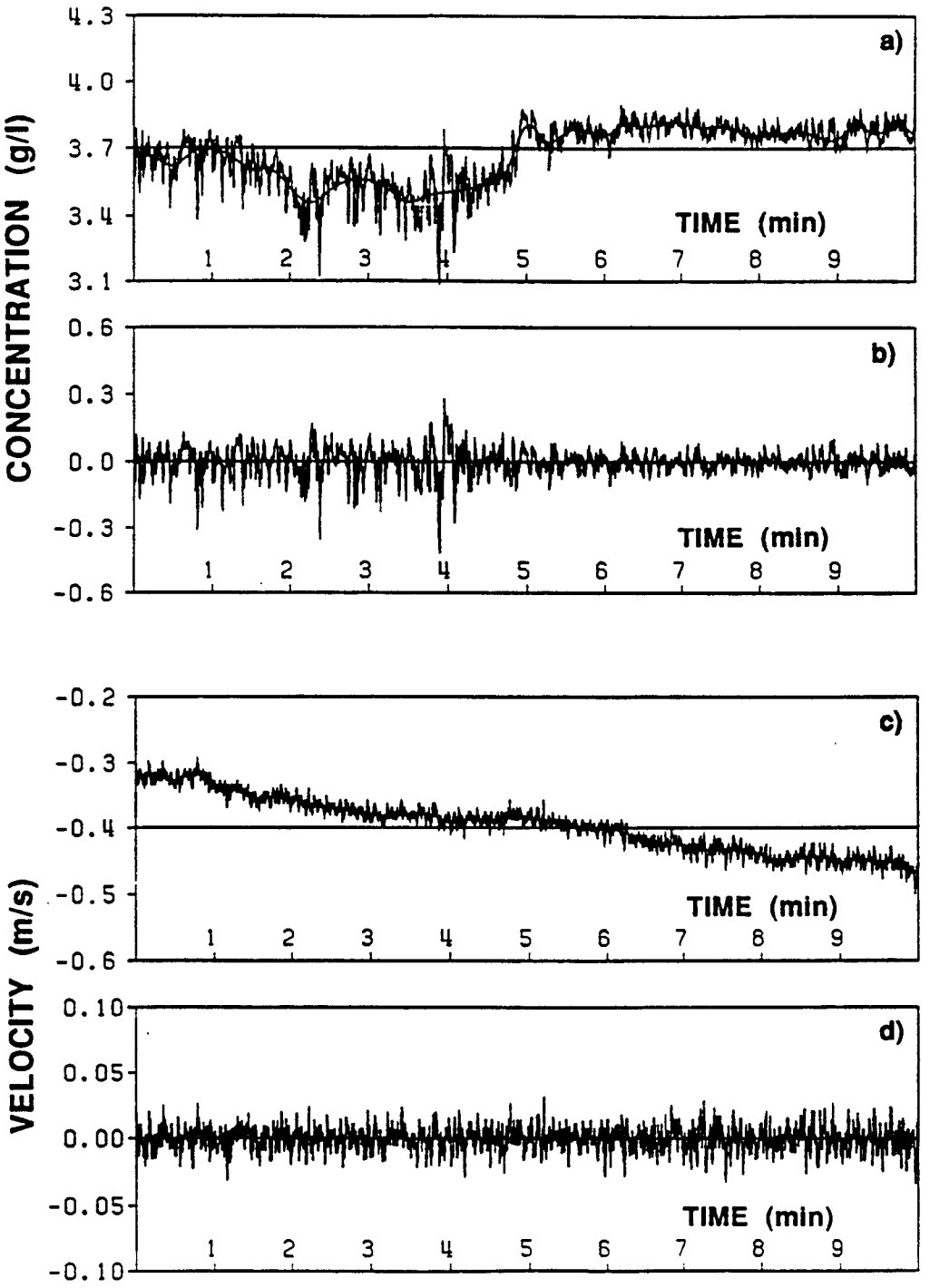

Figure 4.7: Trend removal from the measured records (deployment C2, data block 2). a) Measured c_2 (upper level); b) c_2 after trend removal; c) measured u_2 (upper level); c) u_2 after trend removal.

The values of $\overline{f}$ which were computed using this method ranged from 0.34 to 0.50 sec^{-1}. Higher frequencies, resulting from turbulent effects will, consequently, have to be filtered out (lowpass filtering). Defining a finite Fourier transform pair as

$$X(f,T) = \int_0^T x(t)e^{-2\pi ift}\,dt \tag{4.9}$$

$$x(t) = \int_0^T X(f,T)e^{2\pi ift}\,df \tag{4.10}$$

where $x(t)$ is a generic random process and $X(f,T)$ its finite transform, and a frequency response function $H_F(f)$ of the filter as

$$H_F(f) = \begin{cases} 1 & f \leq \overline{f} \\ 0 & f > \overline{f} \end{cases}$$

the filtered time series $\overline{x}(t)$ will be given by

$$\overline{x}(t) = \int_0^T X(f,T)H(f)e^{2\pi ift}\,df \tag{4.11}$$

This procedure can be applied to the pressure data by considering $x \equiv p_1$ and, consequently, $\overline{x} \equiv \tilde{p}$.

Once $\tilde{p}$ is obtained, the wave induced parts of the velocity ($\tilde{u}$, $\tilde{v}$, $\tilde{w}$) and concentration ($\tilde{C}$) records can be filtered out. Considering again a generic variable e_1, a complex transfer function of $\tilde{p}$ to $\tilde{e}$ is defined as

$$L_{\tilde{e}}(f,T) = \frac{C_{\tilde{p}e_1}(f,T)}{S_{\tilde{p}}(f,T)} \tag{4.12}$$

where $C_{\tilde{p}e_1}$ and $S_{\tilde{p}}(f,T)$ are the complex cross spectrum of $\tilde{p}$ and e_1 and the power spectrum of $\tilde{p}$, respectively. These are defined, for the finite interval T as

$$C_{\tilde{p}e_1}(f,T) = \frac{1}{T}\tilde{P}^*(f,T)E_1(f,T) \tag{4.13}$$

$$S_{\tilde{p}}(f,T) = \frac{1}{T}\tilde{P}^*(f,T)\tilde{P}(f,T) \tag{4.14}$$

where $\tilde{P}$ and E_1 denote the finite Fourier transforms of $\tilde{p}$ and e_1, respectively, and $\tilde{P}^*$ is the complex conjugate of $\tilde{P}$. Equation 4.12 is valid assuming that e' and $\tilde{p}$ are completely uncorrelated and, consequently:

$$\frac{C_{\tilde{p}\tilde{e}}(f,T) + C_{\tilde{p}e'}(f,T)}{S_{\tilde{p}}(f,T)} \simeq \frac{C_{\tilde{p}\tilde{e}}(f,T)}{S_{\tilde{p}}(f,T)} = L_{\tilde{e}}(f,T) \tag{4.15}$$

The complex finite spectrum of $\tilde{e}$ can, then, be computed as

$$\tilde{E}(f,T) = L_{\tilde{e}}(f,T)\tilde{P}(f,T) \tag{4.16}$$

and the wave coherent time series

$$\tilde{e} = \int_0^T \tilde{E}(f,T)e^{2\pi i f t}\, df \tag{4.17}$$

The turbulent part of the record can, finally, be obtained as

$$e' = e_1 - \tilde{e} \tag{4.18}$$

Examples of this filtering procedure are presented in figure 4.8.

It should be noted that the previous method relies on two basic assumptions:

1. $\tilde{p}$ and p' can be completely separated through lowpass filtering and there are no turbulent contributions at frequencies lower than $\overline{f}$.

2. $\tilde{p}$ and e' are completely uncorrelated and, consequently $C_{\tilde{p}e'} = 0$.

An evaluation of the validity of these assumptions can be made by computing the correlation coefficients between the time series of $\tilde{p}$ and $\tilde{e}$ or e'. Such coefficients showed, generally, values of 0.7 or higher for the $\tilde{p}$ and $\tilde{e}$ time series and of 0.3 or lower for the $\tilde{p}$ and e' series; these values could be a result of the poor quality of the pressure data. As a general rule a better correlation was found between $\tilde{p}$ and $\tilde{u}$, $\tilde{v}$, $\tilde{w}$ than between $\tilde{p}$ and $\tilde{c}$; u', v', w' also showed worse correlation with $\tilde{p}$ than c' with $\tilde{p}$.

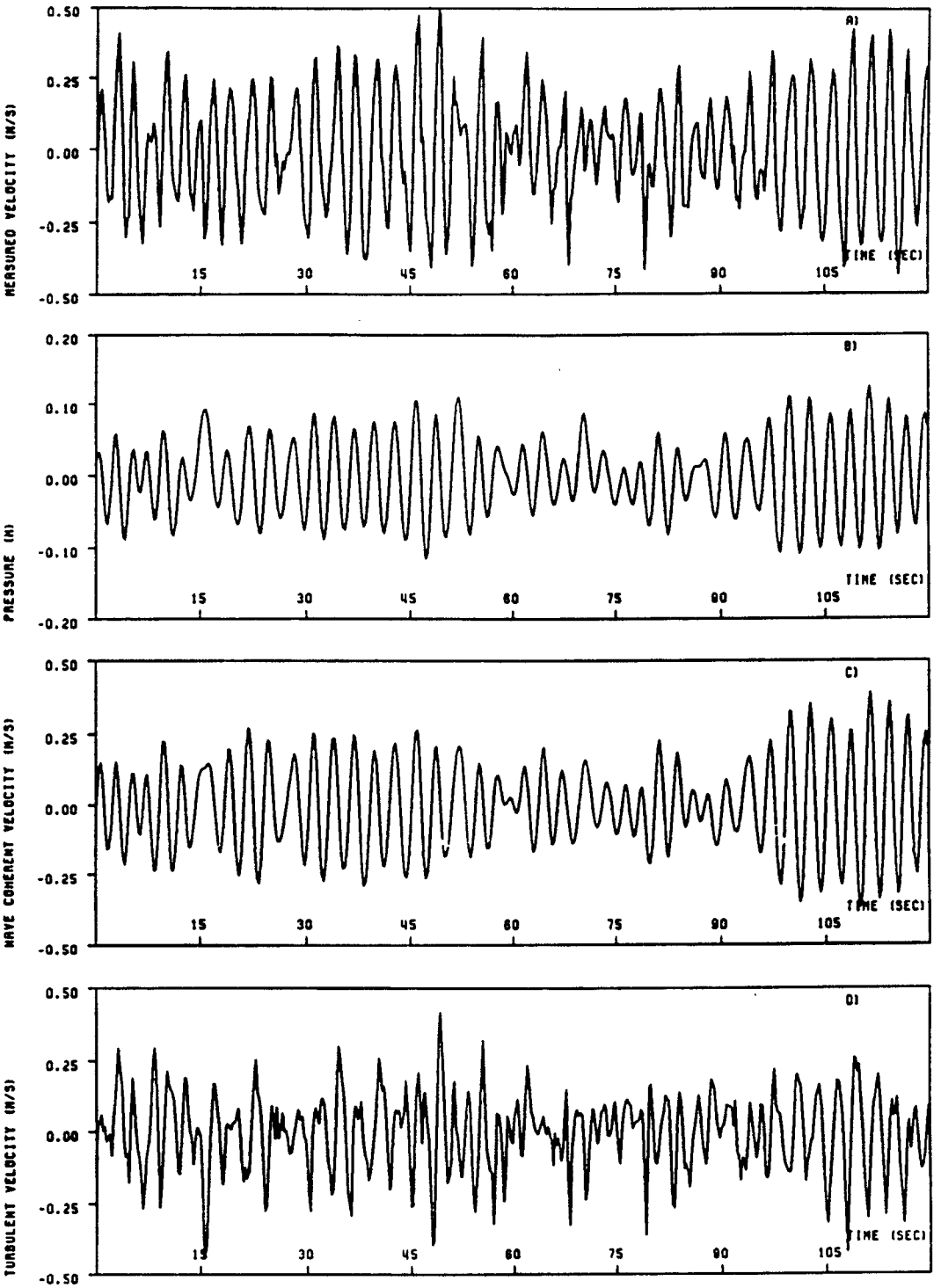

Figure 4.8: Examples of the filtering procedure applied to the measured u_2, velocity data at the upper level (Deployment C3, block 7). a) measured u_2; b) pressure record; c) $\tilde{u}_2$; d) u_2'.

CHAPTER 5
RESULTS AND DISCUSSION

5.1 General Aspects

The numerical model described in Chapter 3, the field data measured in Hangzhou Bay and the laboratory parameters describing the local fine sediment properties and processes were used to investigate the influence of fine-sediment properties, bed parameters and stabilized-diffusion characteristics in the vertical concentration profile of a high concentration environment. In particular, the effects of sediment time-lagged response to flow variations, expressed by the characteristic hysteresis loop, in a sediment-stratified environment, were investigated. The results of a sensitivity analysis of the numerical model to variations in the parameters describing key physical processes are presented in section 5.2, while the influence of the same parameters in the lagged response of sediment to flow changes are included in section 5.3. The measured field data and in particular the properties of its random variations are analyzed in section 5.4. Finally an evaluation of the importance of fine sediment-flow hysteresis in transporting sediment in Hangzhou Bay is presented in section 5.5.

5.2 Sensitivity Analysis

5.2.1 General Aspects

In order to investigate the sensitivity of the model to the variation of some of the key parameters describing the physical processes involved, several applications were made under similar conditions. In each of these applications, however, a significant

parameter was changed, allowing the evaluation of its influence in the computed concentration profiles. For this type of analysis, water depth and depth average velocity data corresponding to deployment C2 were used (measurement period of 2.5 hours; 30 *min* between measurements). Sinusoidal variations of both parameters were assumed. From deployment C3 (which encompassed a full tidal cycle) a tidal period of 13 hours, the mean water depth and mean depth average velocity were obtained; these values were used to determine the tidal amplitudes and time lags of both parameters for deployment C2, through least-squares fitting.

The resulting expressions were:

$$H = 6.404 + 1.153 \cos(27.565\,t - 322.855)$$

$$\overline{u} = -0.144 + 1.352 \cos(27.563\,t - 265.592)$$

in which H and $\overline{u}$ are the water depth and depth average velocity in m and m/sec, respectively, and t the time, in hours, elapsed since the beginning of deployment C2.

Typical sediment reference parameters for settling, relevant to high concentration environments, were used in the simulation. Equations 3.18 and 3.19 with $C_0 = 13.3\,g/l$ and $\overline{W}_{s0} = 0.297\,mm/sec$ were used with the following parameters: $k_1 = 0.018$, $n_1 = 1.082$, $k_2 = 0.00468$ and $n_2 = 12.1067$ (Hayter et al., 1982). The reference bed erosion and deposition parameters used in the simulation were $a = 0.2 \times 10^{-3}\,Kg/(m^2 sec)$, $\tau_s = 0.2\,N/m^2$ and $\tau_{cM} = \tau_{c1} = \tau_{cd} = 0.1\,N/m^2$ (Ross, 1988).

The initial concentration profile used in the simulations is presented in figure 5.1. The lower portion of the profile was defined based on the concentrations measured during deployment C3 in a tidal situation similar to that found at the beginning of deployment C2 (ebb tide, accelerating velocities). The steep slope of the profile in this zone results from the small differences in between the concentrations at the measurement elevations during the field experiment. Two lutocline layers, a main

(lower) lutocline and a secondary (upper) one, were also included with the purpose of investigating their evolution under conditions corresponding to the several values of the parameters; such features are typical of high sediment concentration environments (Kirby, 1986). A mixed layer, usually found in the upper layers of the water column (Ross, 1988), completed the profile. The measured concentrations, obtained during deployment C2 at elevations $z = 1.25\,m$ and $z = 2.75\,m$ were used in the simulated profiles as reference values.

The parameters whose influence was investigated were those related to diffusion under stratified conditions, settling velocity and bed erosion, since the hydrodynamic conditions during deployment C2 did not correspond to those of a depositional period. The results obtained in this type of analysis are presented in figures 5.2 to 5.6.

5.2.2 Settling Velocity

The influence of the settling velocity in the concentration profile is documented in figure 5.2 . A reference peak settling velocity of $\overline{W}_{s0} = 0.297\,mm/sec$ was chosen and profiles were generated for that value as well as for peak settling velocities $\overline{W}^a_{s0} = 5\,\overline{W}_{s0}$ and $\overline{W}^b_{s0} = 10\,\overline{W}_{s0}$. In all the plots the same value of the stability parameters $\beta = 20.0$ and $\alpha = 2.0$, erosion parameter $a = 0.2 \times 10^{-3}$ and critical shear stress for erosion $\tau_s = 0.2\,N/m^2$ were maintained. The above diffusion parameter values correspond to a highly stabilized water column (diffusion is strongly inhibited) while the erosion parameters lead to a moderate erosion flux. From figure 5.2 it can be seen that the initial concentration profile strongly influences the profiles obtained with the reference $\overline{W}_{s0}$ in which both lutoclines' positions are virtually constant during the calculation period. The combination of strongly inhibited diffusion with low settling velocities consequently produces balanced fluxes and a concentration profile which is virtually steady in time.

An increase in the settling velocities, however, produces increased settling fluxes which will prevail over the diffusive fluxes. It can be seen that for $\overline{W}_{s0}^{a}$ and $\overline{W}_{s0}^{b}$ the upper lutocline has virtually disappeared at $t_0 + 60\ min$ while the lower lutocline steadily drops in the water column, the faster evolution corresponding to the higher settling velocities (the same situation seems to occur close to the surface where a new secondary lutocline develops). The evolution for the concentration profile for $\overline{W}_{s0}^{b}$ is, furthermore, characterized by the appearance of a new secondary lutocline layer for $t_0 + 90\ min$ and $t_0 + 120\ min$, independent of the original profile; this secondary lutocline slightly drops in the water column, merging with the rising main lutocline into a single feature for $t_0 + 150\ min$, a phenomenon that has been clearly observed in settling column tests. This single lutocline obtained with $\overline{W}_{s0}^{b}$ occupies a similar final position as that obtained with $\overline{W}_{s0}^{a}$ which seems to indicate an 'equilibrium' lutocline position under the diffusion and erosion conditions assumed for the calculation. The value of C measured at $z = 2.75\,m$, however, shows a much higher value than those generated by the model using the $\overline{W}_{s0}^{a}$ and $\overline{W}_{s0}^{b}$ values.

5.2.3 Erosion Flux

In order to investigate the influence of the erosional characteristics at the bed on the concentration profile, the vertical model was used with values of the erosion constant a of $a_r = 0.2 \times 10^{-3}$ (reference value), $a_a = 10\,a = 0.2 \times 10^{-2}$ and $a_b = 100\,a = 0.2 \times 10^{-1}$, corresponding respectively to moderate, high and very high erosion fluxes (the total amounts of sediment eroded and suspended during the 150 minute computation period were respectively of 8.7 Kg/m^2, 15.8 Kg/m^2 and 22.5 Kg/m^2). Such erosional situations should not be considered, however, as an ubiquitous feature in estuarine environments since a rapidly eroding bed would quickly be scoured to 'equilibrium' levels at which the increasing bottom shear strength would be comparable in magnitude to the applied stresses.

The remaining parameters, kept constant in all three cases were the stability parameters $\beta = 20.0$, $\alpha = 2.0$, the peak settling velocity $\overline{W}_{s0} = 1.485\ mm/sec$ and critical shear stress for erosion $\tau_s = 0.2\ N/m^2$.

The immediate result of the increase in the erosion constant by one and two orders of magnitude is an increase in the amount of sediment added to the water column during the computation by factors of, approximately, two and three. The consequence of such an increase in the amount of suspended sediment can easily be observed in figure 5.3 . In the cases of the profiles corresponding to a_a and a_b, a strong dependence of the computed profiles on the initial conditions is apparent. Moreover, both the upper and the lower lutoclines persist throughout the computation period, showing little variation of their respective positions; both profiles are similar in shape, differing only in their near-bottom concentrations, naturally higher in the case corresponding to a_b in which more sediment is eroded and suspended.

By contrast the profiles corresponding to the reference erosion constant show little dependence on the initial conditions, the upper lutocline quickly disappearing and the lower lutocline lowering its position in the water column as a result of settling dominating over diffusion (it should be noted that the value used for $\overline{W}_{s0}$ in this case corresponds to $\overline{W}^a_{s0}$ in the previous set of calculations, the stabilized diffusion parameters being the same).

The influence of the amounts of suspended sediment is apparent on the evolution of the concentration profiles; by increasing the amount of suspended sediment, buoyancy stabilization is increased and upward diffusion is further decreased. The concentration profiles tend to assume 'stable configurations', with the excess of eroded sediment (i.e. between the cases computed with a_a and a_b) accumulating close to the bed due to greater inhibition to vertical mixing.

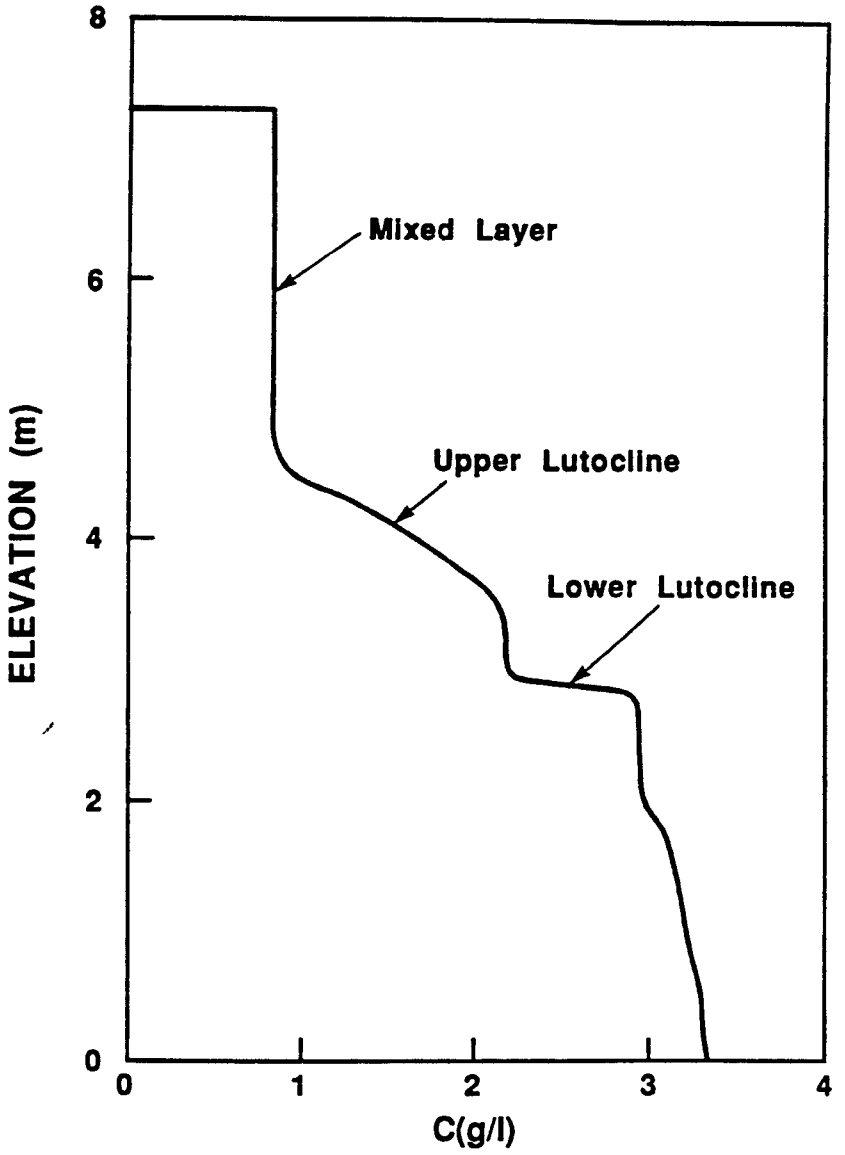

Figure 5.1: Initial concentration profile.

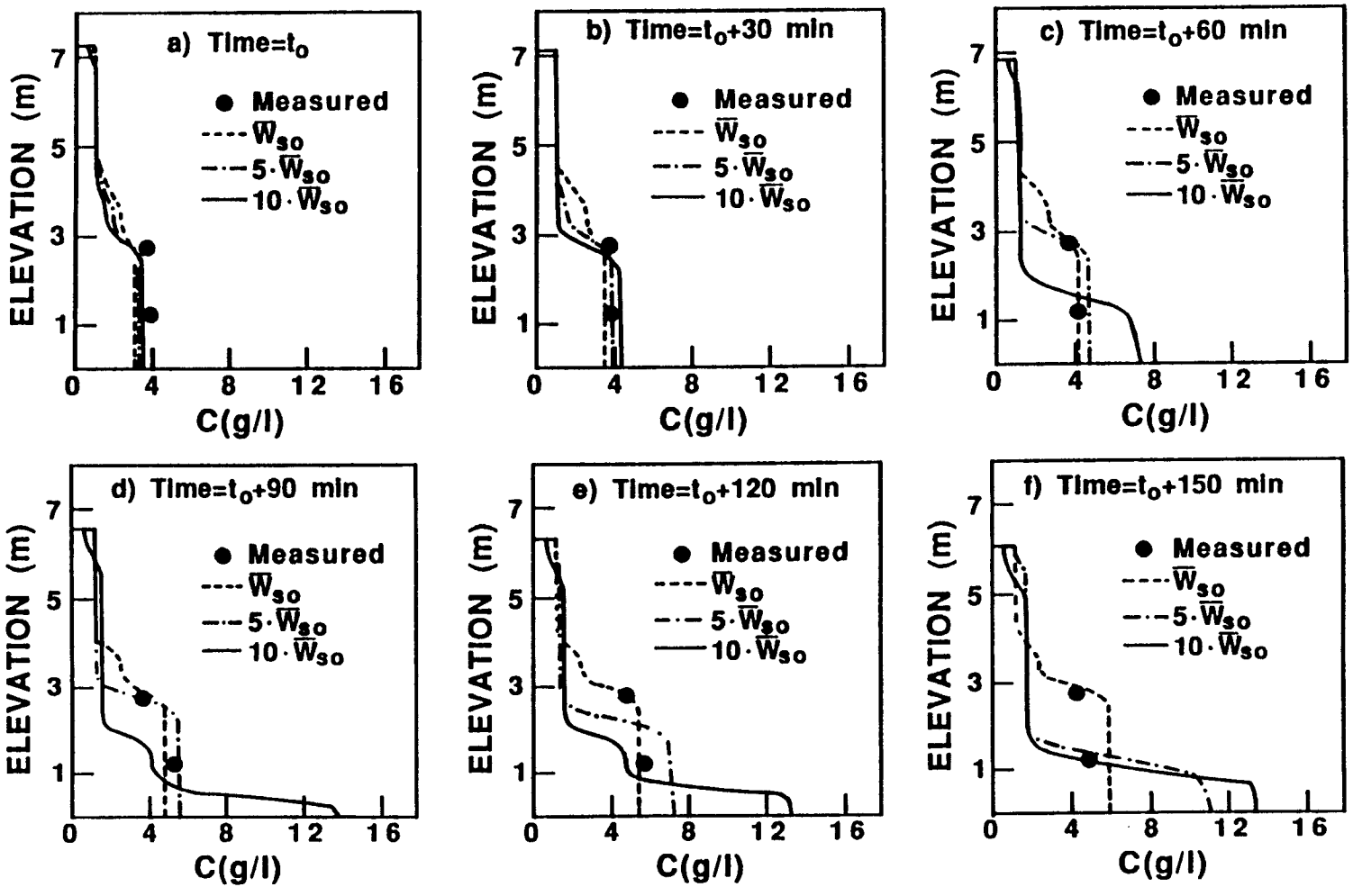

Figure 5.2: Simulated profiles with different settling velocities.

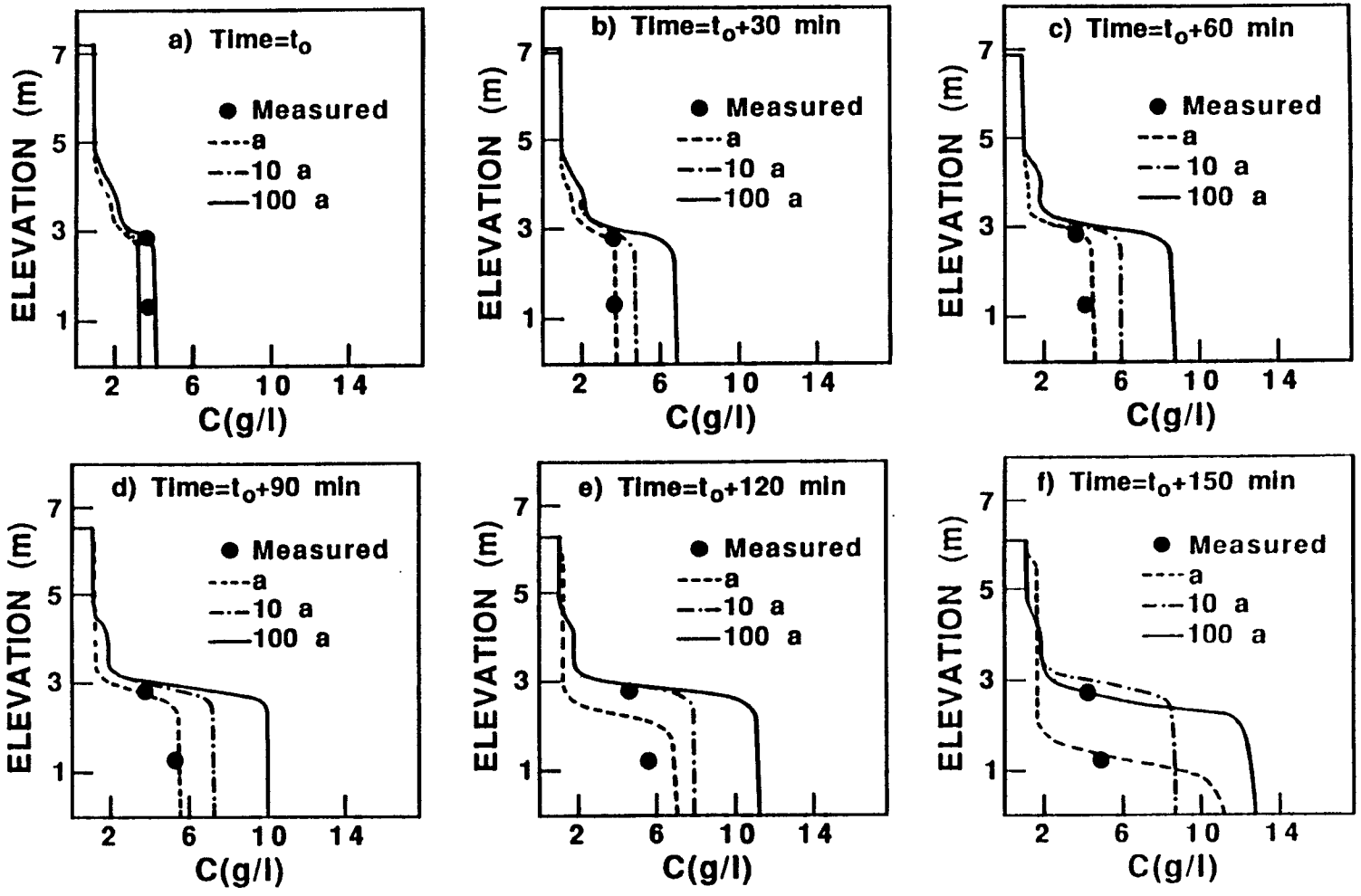

Figure 5.3: Simulated profiles with different erosion conditions.

5.2.4 Diffusion

The influence of both diffusion stabilized parameters was analyzed under conditions of moderate erosion ($a = 0.2 \times 10^{-3}$,$\tau_s = 0.2\ N/m^2$) and moderate peak settling velocity $\overline{W}_{s0} = 1.485\ mm/sec$. First, concentration profiles were computed for a fixed value of $\beta = 12.0$ and values of $\alpha = 1.0$, $\alpha = 2.0$ and $\alpha = 3.0$ (figure 5.4).

It is apparent from the figure that for a situation of low diffusion stabilization ($\alpha = 1.0$), diffusion prevails over settling and the concentration profile becomes virtually uniform, a slight lutocline layer developing only close to the surface.

For $\alpha = 2.0$ the concentration profile becomes increasingly steady, suffering little variation during the computation period, which would indicate equilibrium between the settling and diffusive fluxes. A single lutocline is maintained, approximately halfway through the water column, its position dropping only slightly at $t_0 + 150\ min$.

Increased stabilization, corresponding to $\alpha = 3.0$, shows a stronger dependence on the initial profile, the upper lutocline disappearing slowly with time. The lower lutocline, however, due to the decrease in the diffusive flux, drops in the water column, with another secondary feature being apparent for $t_0 + 150\ min$. In this case the settling flux seems to be more important than the stabilized diffusive flux.

Comparison of the measured values with the computed profiles indicates that $\alpha = 2.0$ should be an adequate value for this parameter. This value was, consequently, adopted together with the previous erosion and settling values for the analysis of the second stability parameter β (figure 5.5).

Once again, from the profiles corresponding to more stabilized situations ($\beta = 16.0$ and $\beta = 20.0$) a stronger dependence on the initial profile is observed. In general, the lower lutocline drops in the water column with time for the cases of higher stabilization ($\beta = 16.0$ and $\beta = 20.0$), remains stable for $\beta = 12.0$ or rises slightly for $\beta = 8.0$, corresponding to the different magnitudes of the stabilized

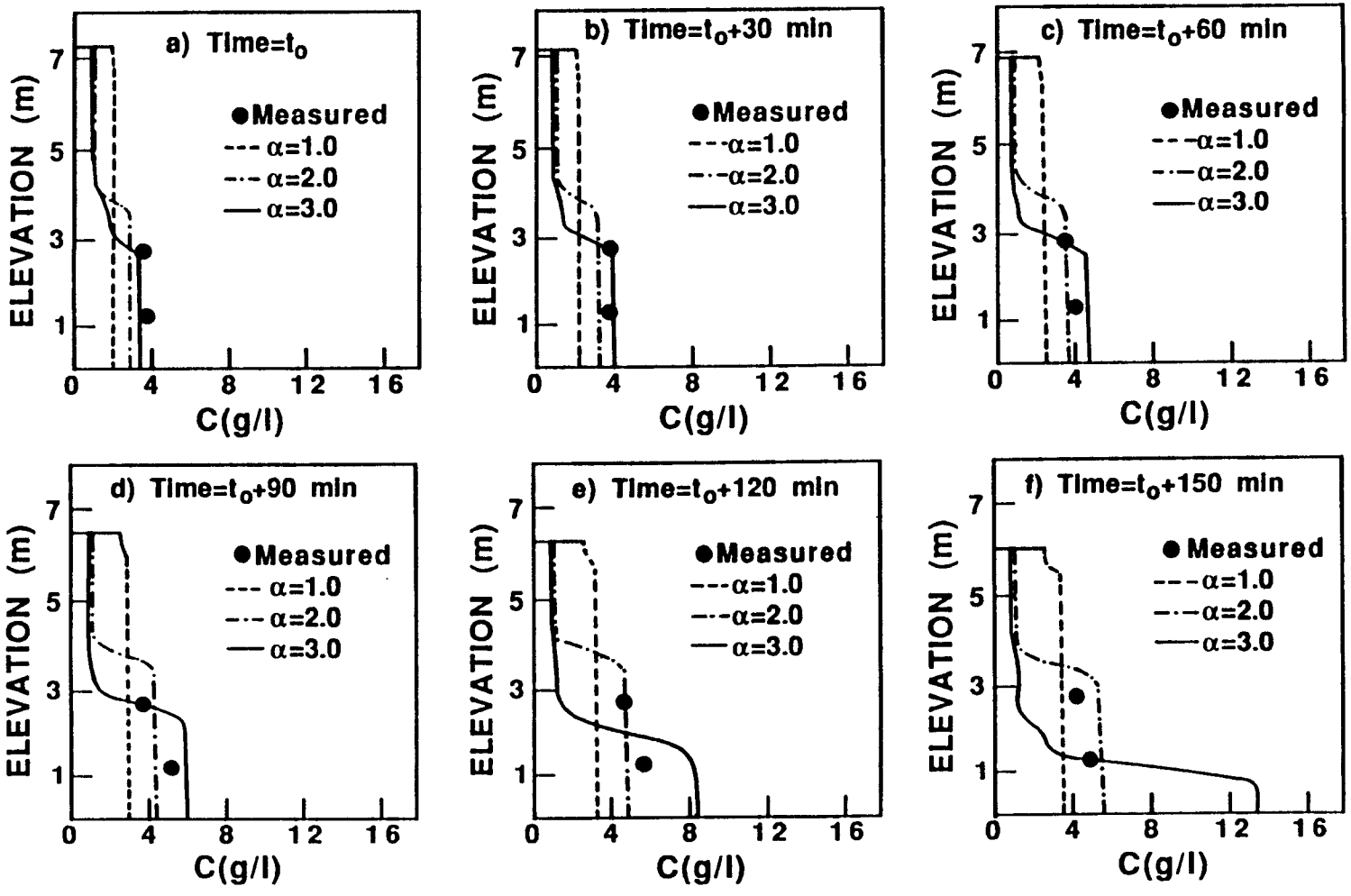

Figure 5.4: Simulated profiles with different values of diffusion parameter α.

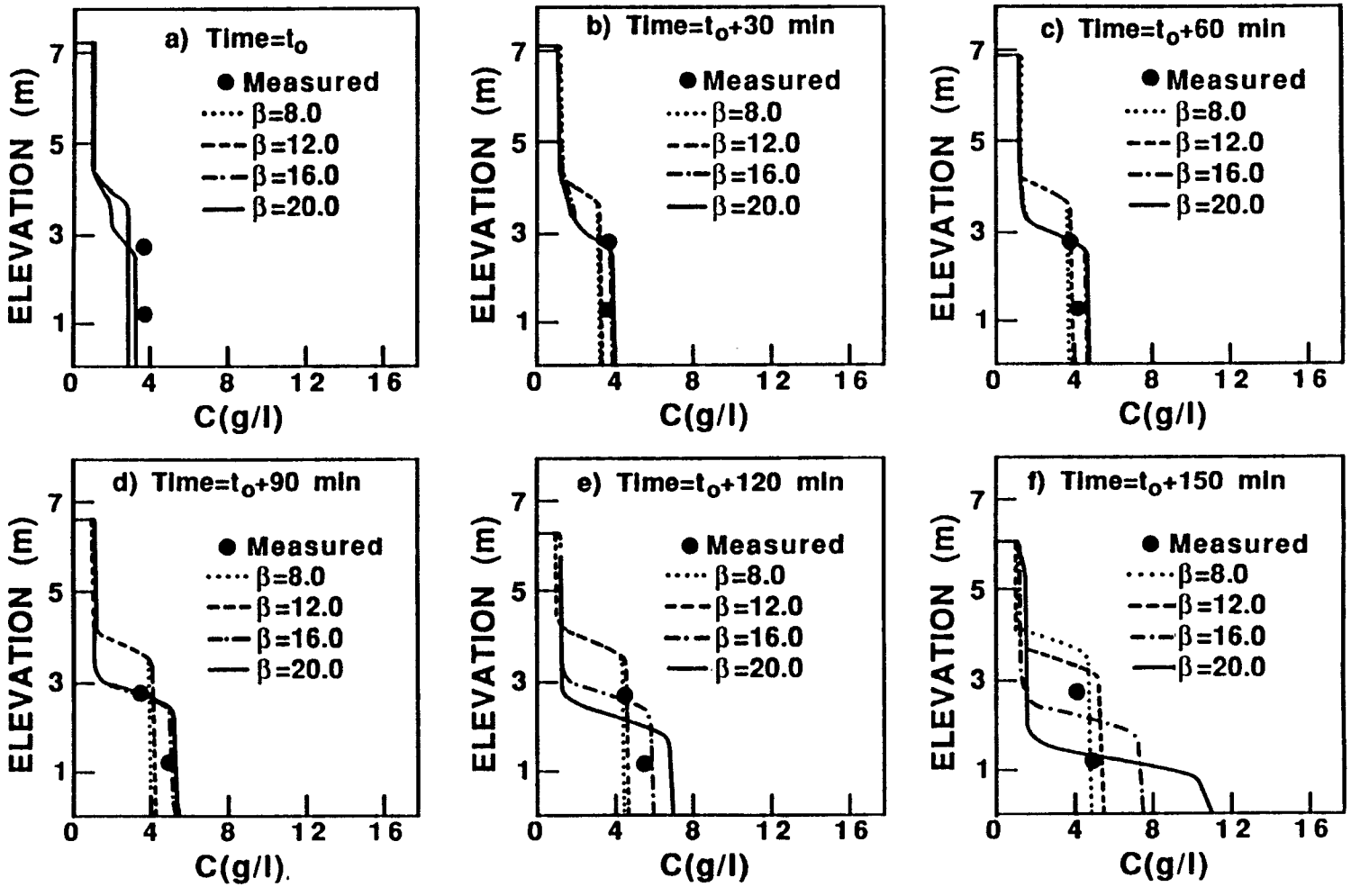

Figure 5.5: Simulated profiles with different values of diffusion parameter β.

diffusive flux relative to the settling flux.

Finally, concentration profiles were computed for different values of β (with $\alpha = 2.0$) by using a low value for the peak settling velocity $\overline{W}_{s0} = 0.297\, mm/sec$ and allowing higher erosional fluxes at the bottom ($a = 0.1 \times 10^{-2}$ and $\tau_s = 0.2\, N/m^2$).

It can be observed from figure 5.6 that for a low value of the stability constant $\beta = 4.0$, the concentration profile quickly becomes uniform, diffusion dominating over settling, while for highly stabilized conditions ($\beta = 20.0$) equilibrium is apparent, producing profiles strongly dependent on the initial conditions. An intermediate value of $\beta = 8.0$ shows a more realistic evolution in accelerating flow conditions; the lower lutocline moves upward in the water column, responding to velocity increase, before reaching an 'equilibrium position'.

5.3 Modeling of Flow-Sediment Hysteresis

5.3.1 General Aspects

The physical mechanisms supporting sediment motion in the water column and those occurring at the bed provide a general description of sediment dynamics in turbulent flows, under the assumptions leading to equation 3.13. Diffusion, settling and deposition parameters and bed properties, such as the depth dependent bed shear strength and the erosion parameters, consequently determine sediment behavior and the nature of its response to variations in hydrodynamic conditions. The importance of this response (especially in time) is further emphasized due to the complexity of tidal flows in natural environments (as happens in estuarine and coastal flows) and has practical engineering consequences.

Several researchers have identified the mechanisms for sediment response in time to changes in flow conditions, expressed by such time-averaged parameters as the bed shear stress). For decreasing estuarine currents, concentrations are usually higher than for increasing currents. The lags associated with this sediment-flow

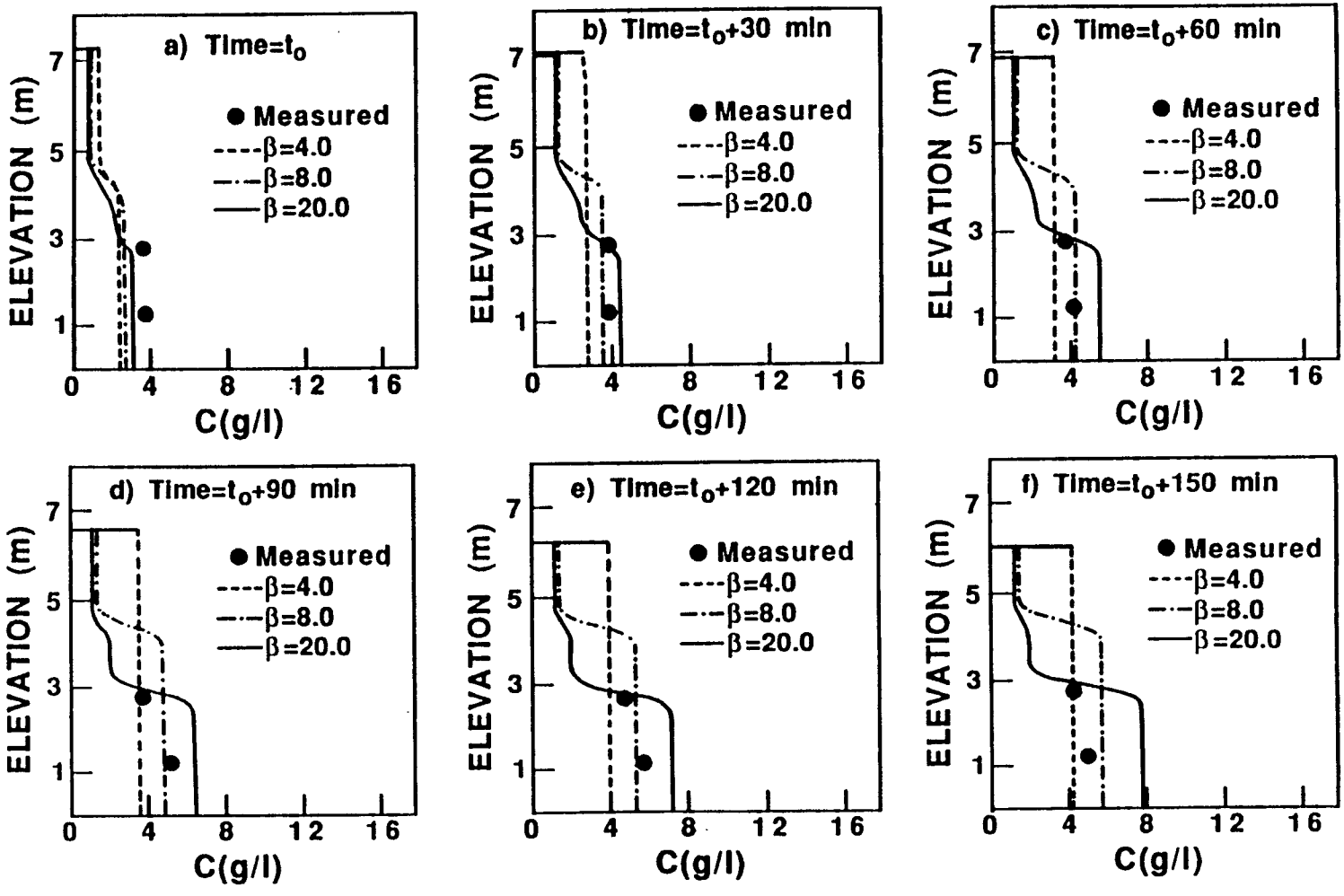

Figure 5.6: Simulated profiles with different values of β with high erosional fluxes at the bottom.

hysteresis can be identified, following Dyer and Evans (1989) and Postma (1967) as

1. A lag associated with settling, corresponding to the time that a sediment particle, in suspension at a certain elevation in the water column, takes to reach the bed once the transport velocity (or $\overline{u}|\overline{u}|$) has decreased below a minimum value. This settling lag is associated with the settling velocities of the sediment particles and will, consequently, be dependent on the aggregation conditions and on the concentration dependent settling velocity range.

2. A lag associated with the diffusion process, corresponding to the time taken by a sediment particle once entrained from the bed to be diffused to upper layers in the water column. This diffusion lag is associated with the stabilization characteristics in the water column and will depend on the amount of sediment available for resuspension as well as on the vertical concentration gradients.

3. A lag associated with the time difference between the occurrence of a transport velocity or $\overline{u}|\overline{u}|$ in the water column and the occurrence of higher values of the same parameters causing bed erosion. This scour lag is associated with the resistance of the top bed layer to erosion and, particularly, to the critical shear stress for erosion.

4. A lag associated with bed consolidation, corresponding to the fact that in cohesive consolidated beds, the bed shear strength increases with bed consolidation time. This effect is called erosion lag.

These lag mechanisms can, then, be 'superimposed' to explain the fact that sediment concentrations usually lag hydrodynamic forcing. If a tidal flow is considered, and beginning at low water slack, a scour time lag occurs before sediment resuspension in the accelerating flow begins, to which a diffusion lag associated with particle diffusion to upper layers should be added; furthermore, once the flow begins to

decelerate a certain time is needed for the sediment to settle and a settling lag should be added.

During slack water a residual sediment concentration will remain in the water column, corresponding to the finer fractions of the sediment under the effect of residual turbulence.

A rough comparison between the magnitudes of the settling lag and of the diffusion lag can be made by considering the concept of a time dependent mean height of suspension $\overline{z}$ introduced by Monin and Yaglom (1971), cited by Dyer (1986)

$$\overline{z} = 0.77\,\kappa u_* t \tag{5.1}$$

Considering $\kappa = 0.4$ and u_* having a magnitude in the order of $1\ cm/sec$ a vertical distance Δz of $1m$ would correspond to a diffusion time lag of about $5min$. The same vertical distance Δz for a settling velocity of the order of magnitude of $1\ mm/sec$ would produce a settling lag of about $16\ min$ or, roughly, three times the diffusion lag.

Besides the lags associated with sediment and bed properties, other flow characteristics contribute to flow-sediment hysteresis. Direct measurements (at an elevation of about $2\,m$ from the bed) of the turbulent Reynolds stresses and turbulent kinetic energy, plotted versus current velocity also showed an hysteresis effect; in both cases lower values occur in the period of accelerating current than in the decelerating part of the tidal flow (Gordon (1975), McLean (1983) cited by Dyer (1986)). Since the sediment concentrations in the water column are related bed shear stress (through bottom erosion/deposition characteristics), of which the Reynolds stresses are an indicator, and mass diffusivity is related to turbulence intensity, these results should also contribute to flow-sediment hysteresis, even if different hysteresis patterns may occur at different levels and, particularly, at the bed (Lavelle and Mofjeld (1983)).

Flow-sediment hysteresis plots are usually presented in the form of average concentration versus a flow parameter which can be either the velocity $\overline{u}$ (averaged to eliminate turbulent fluctuations) or the quantity $\overline{u}|\overline{u}|$ which is proportional to the bed shear stress. Two such plots are presented in figures 5.7 and 5.8 corresponding respectively to measurements in the Rappahannock Estuary (Nichols (1986)) and in the Humber River estuary (Dyer, personal communication). As a general feature concentrations are observed to lag the flow parameter although more complicated patterns also occur. In particular, in figure 5.8 at the $0.5\,m$ elevation the maximum shear stress lags the maximum concentration for both flood and ebb situations; this might be caused by lutocline formation below the measurement level and, later, by its rise to upper layers, the concentration maximum at the $0.5\,m$ elevation corresponding to the presence of the lutocline at that level. A possible interpretation of this type of feature is qualitatively sketched in figure 5.9 which would indicate the possibility of two types of hysteresis loops (one for lower and the second for upper layers in the water column) in case lutoclines develop in the concentration profile.

5.3.2 Modeling Results

The vertical transport model developed by Ross (Ross, 1988) was used to generate plots of the average concentration C versus $\overline{u}|\overline{u}|$ and to investigate the physical mechanisms explaining the hysteresis phenomenon. The hydrodynamics parameters used in the simulation were, again, those corresponding to deployment C2 in Hangzhou Bay, time t_0 corresponding to peak flood current and a uniform concentration profile (with $C = 4.25\,g/l$) being adopted to start the calculation at time $t_0 - 60\,min.$

A reference (case A) simulation is shown in figures 5.10 to 5.12; for this case stabilized diffusion parameters $\alpha = 2.0$ and $\beta = 1.0$ were used as well as $W_{s0} = 4.77\,mm/sec$ ($C_0 = 8.3\,g/l$) and critical shear stresses for deposition and erosion

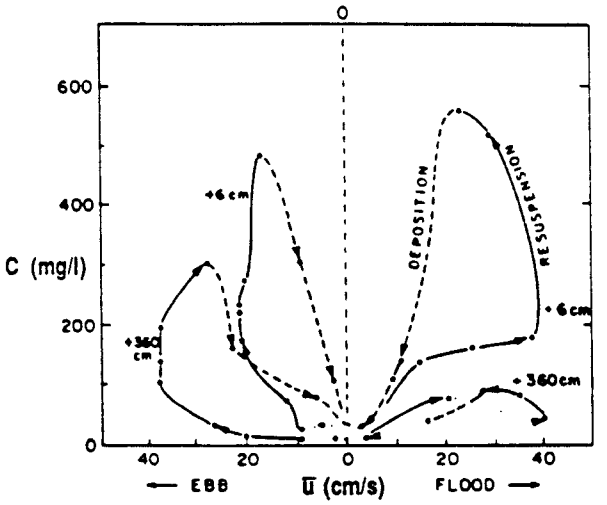

Figure 5.7: Flow-sediment hysteresis. Resuspension, solid lines; deposition/settling, dashed lines;indeterminate, dotted lines. From Nichols (1986).

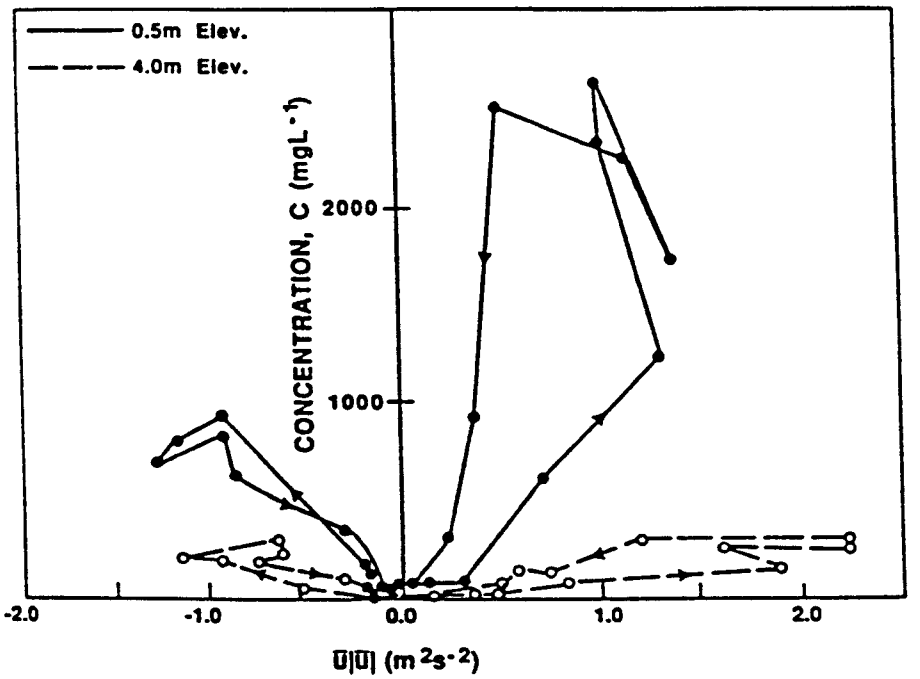

Figure 5.8: Flow-sediment hysteresis measured in the Humber River estuary (courtesy of Prof. Keith Dyer, Plymouth Polythecnic, Plymouth U.K.).

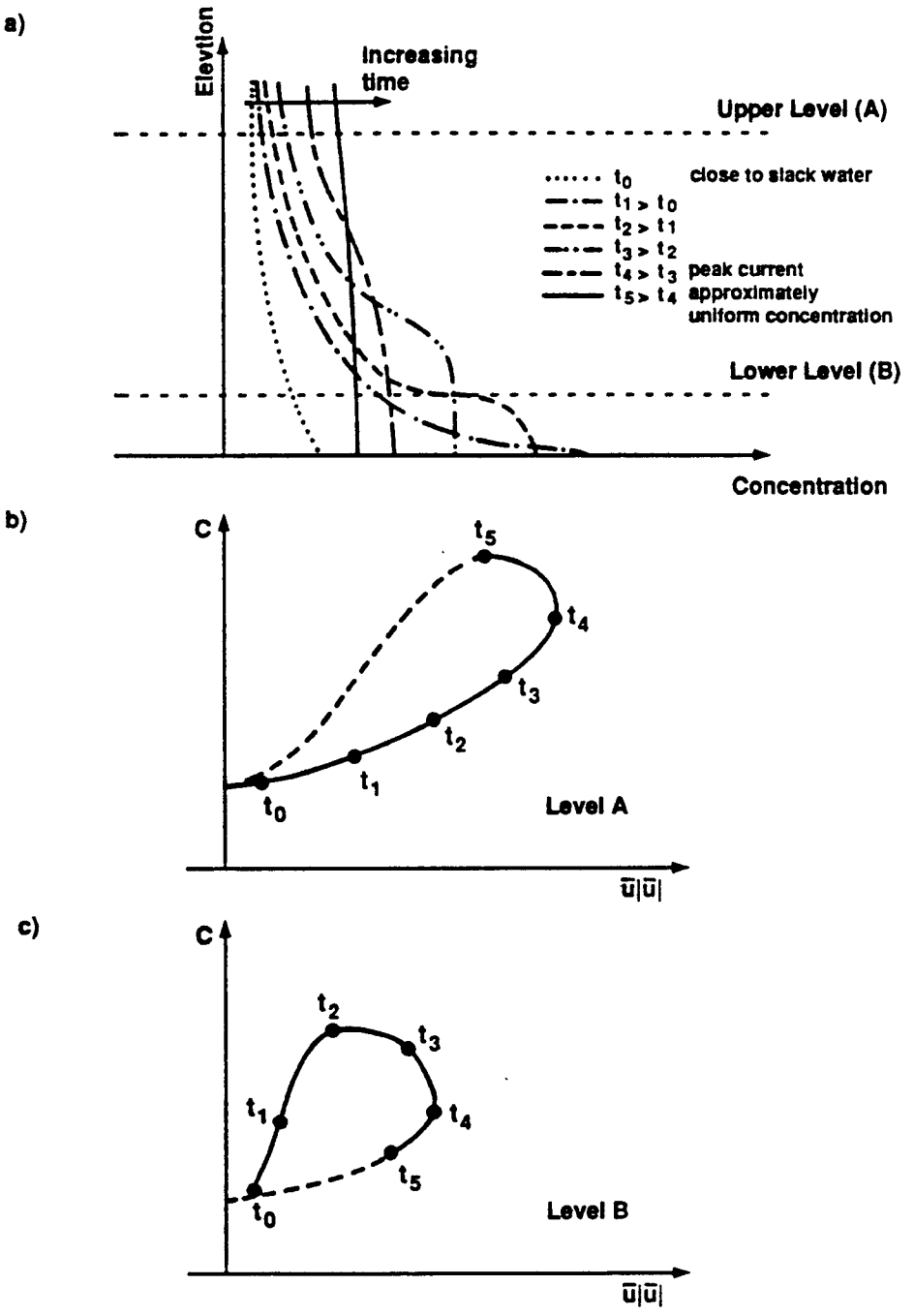

Figure 5.9: Qualitative hysteresis loops at different elevations in cases of lutocline formation.

$\tau_d = 5.0\ N/m^2$ and $\tau_s = 15.0\ N/m^2$. Plots of C vs. $\overline{u}|\overline{u}|$ were obtained for elevations 1.25 and 2.75 m above the bed (figure 5.10). In this figure and in figures 5.13, 5.14 and 5.15 the elapsed times, in minutes, are indicated close to the computed points. For the previous elevations and for an elevation of 0.25 m above the bed plots of the concentration C versus time and of the vertical gradient of the net flux (right-hand side of equation 3.13) versus time are presented in figures 5.11 and 5.12; in the last case a positive value corresponds to a resuspension/diffusion dominated situation while deposition/settling is indicated by a negative net flux gradient.

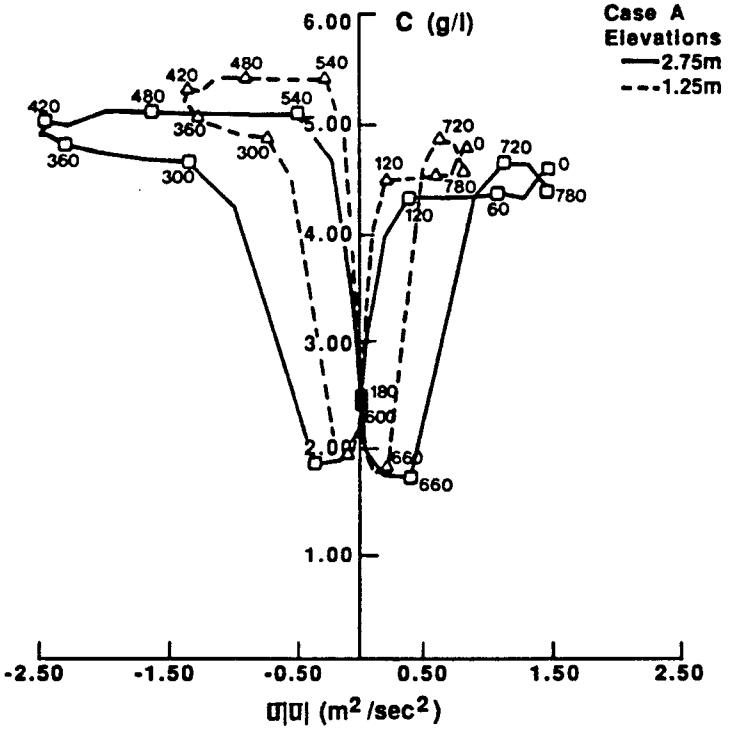

Figure 5.10: C vs. $\overline{u}|\overline{u}|$ for case A.

It can be seen that for both elevations (figure 5.10) the concentration lags the shear stress in the ebb flow while the opposite happens during flood; the time lag between maximum values of both variables is of 60 min in the first case and 40 min in the second (a Δt of 20 min between calculations was used). The computed slack water residual concentrations were slightly higher after the ebb than after the flood, although residual concentrations showed little variation between HW and LW

slacks or, even, between the two elevations, indicating almost uniform concentration profiles. Figure 5.11 shows the evolution of the concentration with time for the three elevations, higher values naturally being obtained near the bottom. Comparison between this figure and figure 5.12 which shows the corresponding average net flux gradients between calculation times allows the definition of the main periods during which settling and deposition or resuspension and diffusion took place.

Deposition settling/phenomena are clearly dominant around slack water (120 to 220 and 520 to 620 *min*, HW and LW slacks occurring at 180 and 600 *min*, respectively) while resuspension/diffusion dominate the re-entrainment periods that follow (up to 300 and 720 *min*, respectively). The magnitude of these fluxes, if compared with those occurring the remaining of the computation period emphasizes the importance of bed conditions in the evolution of the concentration profile since, clearly, the much higher values of the net flux gradients during deposition and re-entrainment periods are due to these phenomena.

A variation in the diffusion parameters allows the evaluation of the dispersion lag effects in the hysteresis mechanism (case B). Figure 5.13 was obtained with the same settling and bed parameters as in case A, with β taking a value of 2.0 and $\alpha = 2.0$; this corresponds to increased stabilization in the water column, upward mixing of sediment being further inhibited. This situation is confirmed by comparison between figures 5.10 and 5.13: higher values of the peak concentrations are found in case B than in case A, the differences in concentration between the two cases increasing with the proximity to the bed. The residual slack water values are similar in both cases. Although the general shape of the curves in figures 5.10 and 5.13 is the same, the ebb maximum concentrations are observed to lag the shear stress by an additional 20 *min* relative to case A; this reflects an increase in the dispersion lag due to higher diffusion stabilization. The flood lag remains unchanged relative to case A. The net flux gradients corresponding to case B showed general agreement

with those found in case A; the peak values were, however, higher in case B.

In order to evaluate the settling lag effects (case C) the peak settling velocity was decreased ($W_{s0} = 1.19\, mm/sec$), all the remaining parameters in case A being the same. From figure 5.14 it can be seen that the shear stress lags the concentration in the ebb by 140 *min* while in the flood C lags the shear stress by 60 *min* (both values are higher than those found in case A). The decrease in the settling velocities also causes a decrease in the peak concentrations but, more significantly, a sharp increase in the residual concentrations around slack water. The net flux gradients corresponding to case C were found to be smaller than those corresponding to case A, particularly during deposition and resuspension dominated periods, the importance of bed phenomena to the concentration profile being once again apparent.

Finally, the influence of bed conditions was investigated (case D) by making $\tau_d = 1.0\, N/m^2$ and $\tau_s = 11.0\, N/m^2$ ($\Delta\tau = \tau_s - \tau_d$ is constant relative to case A), all the other parameters in case A remaining constant.

The results are presented in figure 5.15 and show that in the ebb C lags the shear stress by 60 min, while in the flood the shear stress lags C by 100 min (an additional 60 min relative to case A). The decrease in the critical shear stress for deposition decreases the deposition period around slack water and, consequently, causes higher values of the residual concentration relative to the reference case, while the peak concentrations have similar values during the ebb and slightly higher values during the flood. Comparison of the flux gradients showed that the peak diffusive fluxes are lower and the peak settling fluxes higher in case D relative to case A.

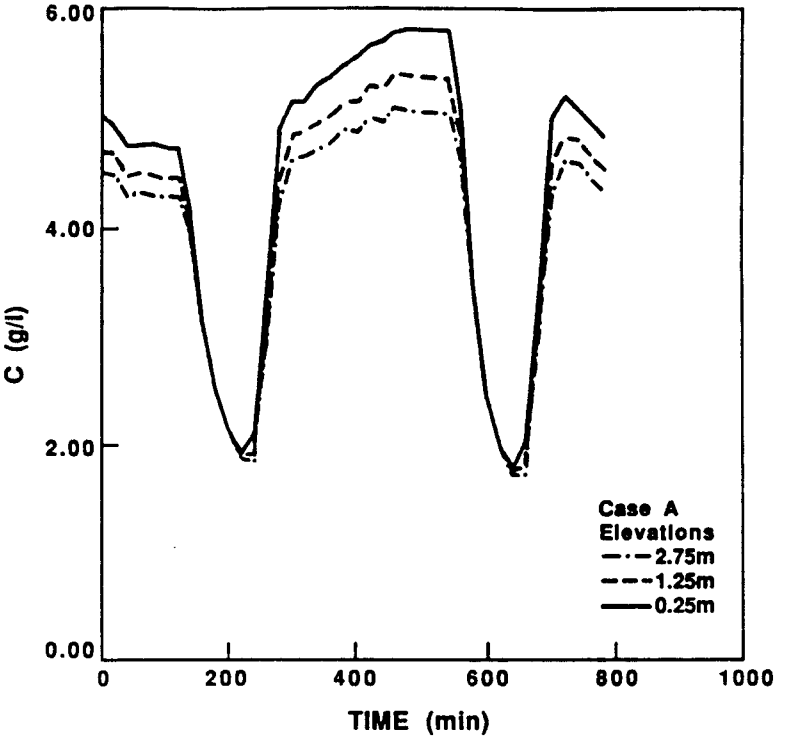

Figure 5.11: C vs. time for case A.

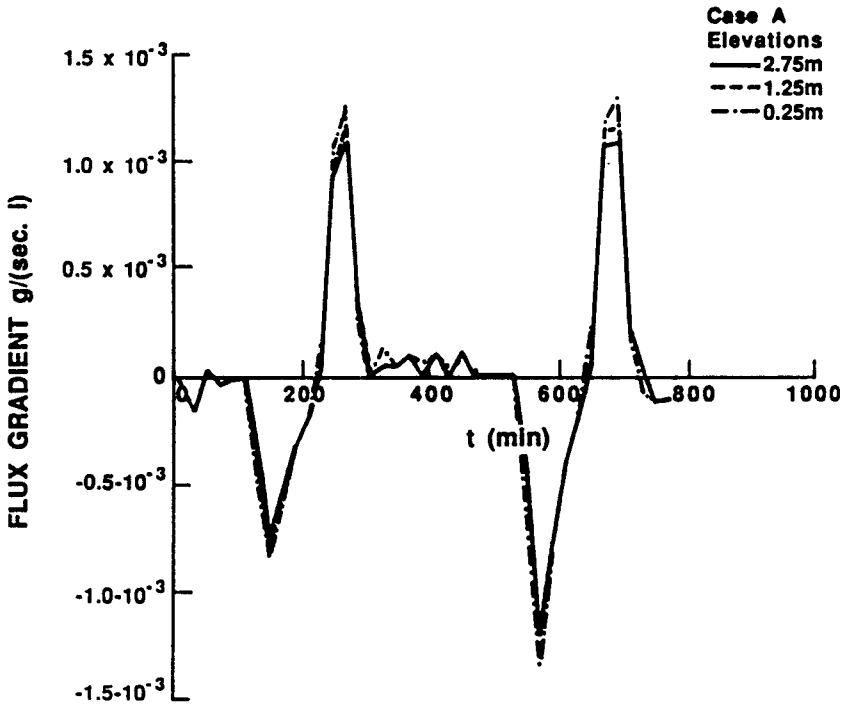

Figure 5.12: Vertical gradient of the net flux vs. time for case A.

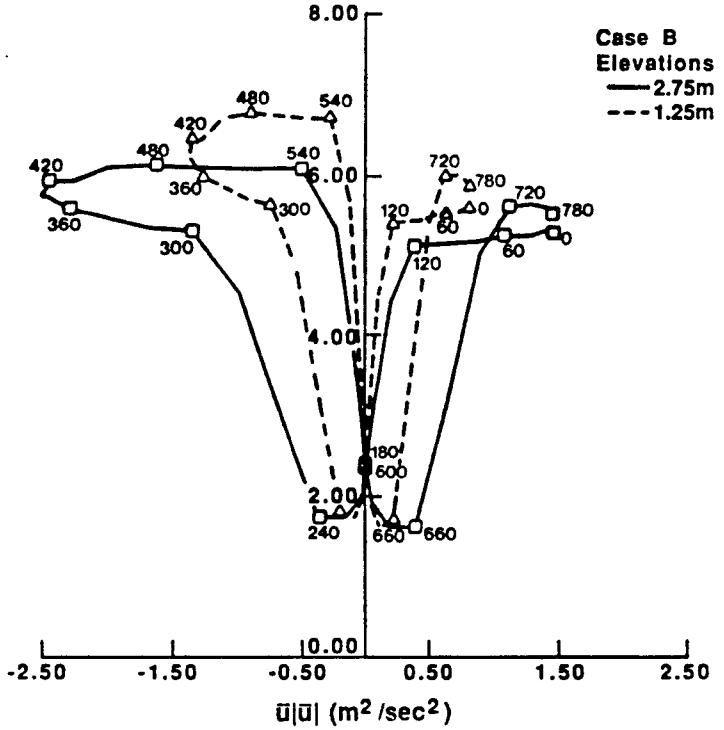

Figure 5.13: C vs. $\overline{u}|\overline{u}|$ for case B.

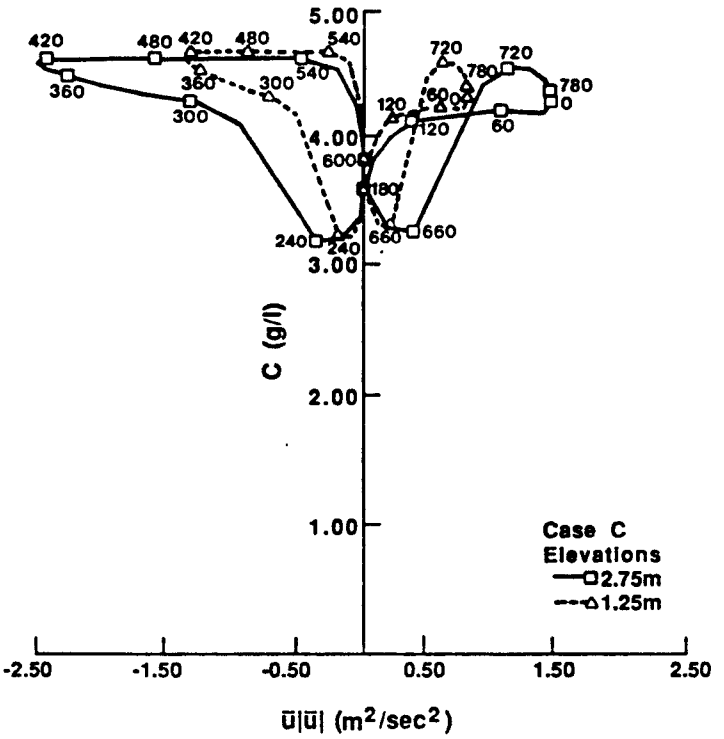

Figure 5.14: C vs. $\overline{u}|\overline{u}|$ for case C.

5.4 Field Data Analysis

5.4.1 General Aspects

The data measured in Hangzhou Bay during the field experiment produced 6 data blocks of 10 minutes each in the case of deployment C2 and 15 blocks of 5 minutes each in the case of deployment C3 (some of the records in C3 blocks could not be used due to transducer malfunction, as mentioned in Chapter 4). Each data block consisted of pressure data at the lower level, concentration and velocity data along two axis at two levels, as described in Chapter 4. Deployment C2 corresponded to an ebb flow period, while deployment C3, which began during an ebb flow situation included the following LW and HW and the beginning of the following ebb, including, consequently, a full tidal cycle.

The mean values of the measured concentrations in the data blocks ranged from 3.7 to 4.7 g/l and from 3.8 to 5.7 g/l at the upper and lower levels, respectively, during deployment C2; during deployment C3 average concentrations attained upper values of 4.8 and 5.0 g/l at the upper and lower levels, respectively, but dropped below 1 g/l during LW slack, a short period for which no measurements were available. These values clearly show the high concentration nature of the Hangzhou Bay environment.

The measured mean value of the longitudinal velocity $\overline{u}$ (i. e. in the direction of the dominant ebb/flood currents) at the upper level during deployment C3 (the only complete set of measurements for a tidal cycle) showed maximum velocities of 1.3 and 1.6 m/sec for ebb and flood flows, respectively. The value of the mean velocity in the y direction, $\overline{v}$, at the lower level consistently showed values one to two orders of magnitude lower than the corresponding $\overline{u}$ value at the same level, confirming that the alignment of the x axis of measurement was along the predominant direction of the flow. At the upper level $\overline{w}$ also showed values that were lower than the corresponding $\overline{u}$ by one to two orders of magnitude.

All the records for which no instrument malfunction had occurred were pre-processed according to the methods described in Chapter 4 to eliminate the time-average part and the trend. These resulted in records of e_1 type variables (concentration or velocity) in which turbulent and wave induced effects are superimposed. These records correspond to the conditions actually existing in the field, i.e. to the velocity fluctuations acting upon the sediment particles and to the measured resulting concentration variations. The poor quality of the pressure data prevented the filtering of the wave-coherent parts from most of the records and the procedure described in Chapter 4 was only applied to three complete data blocks of deployment C2 and to four data blocks of deployment C3 in which some of the records could not be used due to transducer malfunction. This procedure produced records of turbulent variables of the e' type.

5.4.2 Stationarity Analysis

The time varying nature of tidal flows prevents long term stationarity of turbulence, although semi-stationarity can occur for short records. The same situation exists in the case of variables of the e_1 type resulting from superposition of a turbulent component and a wave-coherent component. The stationarity hypothesis has, consequently, to be tested for each record in order to allow the use of the statistical parameters of the random variations. For this purpose a test for stationarity given by Bendat and Piersol (1971) was applied to all records of the types e_1 and e'.

The test assumes that any given record will be long enough to reflect the non-stationarity of the data (if that is the case) and to allow the non-stationary trends to be differentiated from the random fluctuations of the data; this is considered to occur in the case of the Hangzhou Bay data records which have durations of several minutes. In order to apply the test the random variations were assumed to be completely described by their mean values and variances.

The sample records were divided into N equal time intervals ($N = 20$ and $N = 10$ for 10 minute and 5 minute records, respectively, for uniformity) and the mean value and variance of each interval were calculated. The sequences of mean values and variances

$$\overline{x}_1, \overline{x}_2, \ldots, \overline{x}_N$$

$$\overline{s}_1, \overline{s}_2, \ldots, \overline{s}_N$$

were then tested for the presence of underlying trends using the non-parametric test described by Bendat and Piersol (1971), page 122. Median values were calculated and the number of runs, n, (sequences of values higher or lower than the median) determined for each of the sequences. The hypothesis of stationarity can be accepted at the $\alpha = 0.05$ level of significance if

$$6 < n \leq 15 \quad (N = 20)$$

$$2 < n \leq 9 \quad (N = 10)$$

Results of the test applied to records of the generic type e_1 (for concentrations and velocities) showed stationarity for the mean values in 95% of the cases and for the variance in 92% of the cases. From these values, deployment C3 (shorter records) showed stationarity of the mean values in 97% of the cases and of the variance in all the cases. For records of the generic type e' stationarity was found for the mean value in 94% of the cases and for the variance in 97% of the cases. Again deployment C3 showed stationarity of both the mean value and the variance in all the cases. None of the records of both types showed simultaneous non-stationarity of both the mean value and the variance.

5.4.3 Spectral Analysis

Suspended sediment transport by turbulent flows is a complex phenomenon strongly dependent upon the turbulent properties of the two phase water/sediment

system. The quantity of suspended material, for instance, should influence the turbulent properties of the flow, sediment suspension causing damping of turbulence intensity (Soulsby et al., 1984); the superposition of wave action upon a turbulent tidal flow is, furthermore, an additional source of complexity. In order to determine some turbulence characteristics, spectral analysis was performed on the available records of both the e_1 and e' types.

A theoretical derivation (Tennekes and Lumley, 1972) indicates that for high Reynolds numbers the Eulerian time spectra of u, v, w should show an inertial advective subrange proportional to a $-\frac{5}{3}$ power of the frequency. The power spectrum of a given variable as a function of the frequency f, $S(f)$, (equation 4.14) can be converted to a function of the wavenumber k, $E(k)$, through Taylor's hypothesis, by making

$$\begin{aligned} k &= \frac{2\pi f}{\overline{u}} \\ E(k) &= \frac{\overline{u}}{2\pi} S(f) \end{aligned}$$

where $\overline{u}$ is the mean advective velocity and, consequently, $E(k)$ should be proportional to $k^{-\frac{5}{3}}$. In the case of settling particles and despite the fact that no theoretical derivation of a spectrum appears to be available (Bedford at al., 1989) the tacit assumption that sediment behaves as a turbulent scalar analogous to temperature has been commonly accepted (Soulsby et al., 1984). In the case of temperature, at Reynolds numbers large enough to produce an inertial subrange in the energy spectrum and when the heat conductivity is small, an inertial convective subrange exists in which the spectrum of temperature variance, $E_\theta(k)$ is, again, proportional to $k^{-\frac{5}{3}}$ (Tennekes and Lumley, 1972).

Spectra of variables C_1 and C_2 (concentrations at the upper and lower levels, respectively), u_1 and v_1 (horizontal velocity components at the lower level), u_2 and w_2 (longitudinal and vertical velocity components at the upper level) and of the additional variables $r = c_2 w_2$, $q = u_2 w_2$, were obtained. A Fast Fourier Transform

routine was used to compute the spectra as a function of frequency, the spectra being smoothed by averaging of the estimates in blocks of 20 points. The spectra were then converted to $E(k)$ through the use of Taylor's hypothesis. Examples of the computed spectra corresponding to block 4 of deployment C2 are presented in figures 5.16 and 5.17, for variables of the type e_1 and e', respectively. In the case of records of the e_1 type (wave coherent and turbulent parts) the dependence which was apparent (from the median value of the slope) for high values of k was of $k^{-\frac{7}{3}}$ for the concentration at both levels, $k^{-\frac{8}{3}}$ for the v and w components of the velocity and $k^{-\frac{5}{3}}$ for u at both levels. The slope of $-\frac{3}{3}$ obtained for the u_2 spectrum in figure 5.16 is, in this respect, non-representative of the general observed trend. The spectra of variables r and q for records of the e_1 type showed a $k^{-\frac{3}{3}}$ and $k^{-\frac{2}{3}}$ dependence, respectively.

In the case of records of the e' type (turbulent part only) the observed slopes showed similar values relative to the corresponding e_1 spectra (fig. 5.17).

The small number of data records of the second type makes comparison of both sets of results difficult; however, some general aspects seem apparent:

1. In the cases of variables v and w in which the normalized turbulent intensities

$$\frac{\sqrt{\overline{(v_1')^2}}}{\overline{v}} \tag{5.2}$$

$$\frac{\sqrt{\overline{(w_2')^2}}}{\overline{w}} \tag{5.3}$$

were, at least, one order of magnitude higher than the corresponding values in the x direction (due to the low values of $\overline{v}_1$ and $\overline{w}_2$), the slopes of the spectra did not agree with the theoretically derived values.

2. The slopes of the concentration spectra were steeper than those theoretically derived for temperature and generally assumed as valid for sediment particles.

The normalized turbulent intensities for all the measured velocity components of the e_1 type in deployment C3 showed their highest values during the period of

lowest sediment concentration, close to LW slack; this result seems to support the hypothesis of turbulent intensity damping by suspended sediment (Soulsby et al., 1984). The wavelength corresponding to the peak of the concentration spectra ($\lambda = 2\pi/k$), representing the dominant clouds, had average values of about 4 m.

5.5 Flow-Sediment Hysteresis in Hangzhou Bay

The time lags in sediment response to flow changes described in section 5.3 are the basic mechanisms contributing to flow-sediment hysteresis in estuaries and coastal bays. Measured flow-sediment hysteresis, is consequently a fundamental indication of the role of time lagged sediment response or, equivalently, of the importance of vertical mass transport in the suspended sediment regime of a water body. This is a direct consequence of the net effect of such lags which, as shown in fig. 2.1 is reflected in the landward transport of sediment.

The role of vertical mass transport in the general transport patterns in Hangzhou Bay could be hypothesized through an analysis of fig. 4.5 which clearly shows landward transport of sediment into the bay. This hypothesis was examined through numerical simulations and the use of field data, as described in the following paragraphs.

The one dimensional numerical model was used to generate a plot of C vs. $\overline{u}|\overline{u}|$ (figure 5.18) corresponding to the settling properties of Hangzhou Bay sediment, shown in Chapter 4. The remaining simulation parameters were those used in case A of section 5.3, which used the hydrodynamics parameters of deployment C2, except the initial concentration for which a value of 3.25 g/l, uniform in the water column, was taken. Flow-sediment hysteresis is apparent from the figure. The dependence of the same variables measured during deployments C2 and C3 is presented in figure 5.19 and, despite the lack of data corresponding to a full tidal cycle, the hysteresis

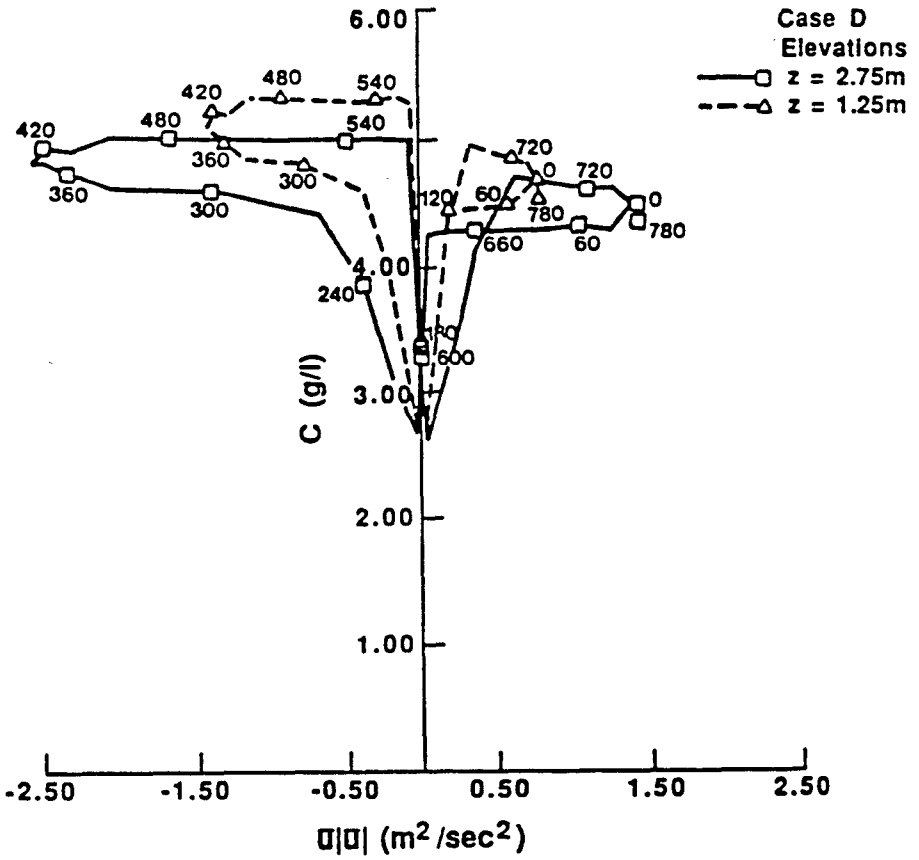

Figure 5.15: C vs. $\overline{u}|\overline{u}|$ for case D.

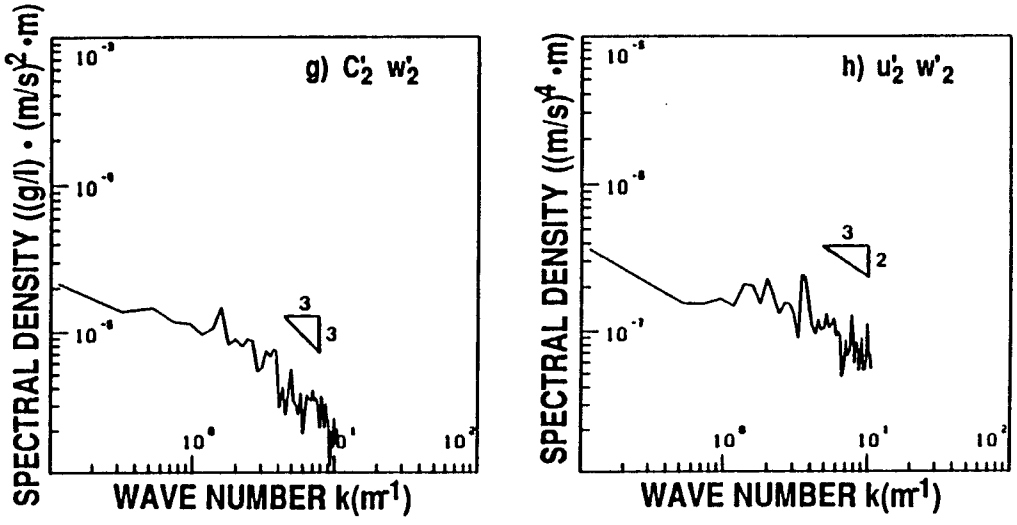

Figure 5.16 (cont.): g) $C_2'w_2'$ h) $u_2'w_2'$.

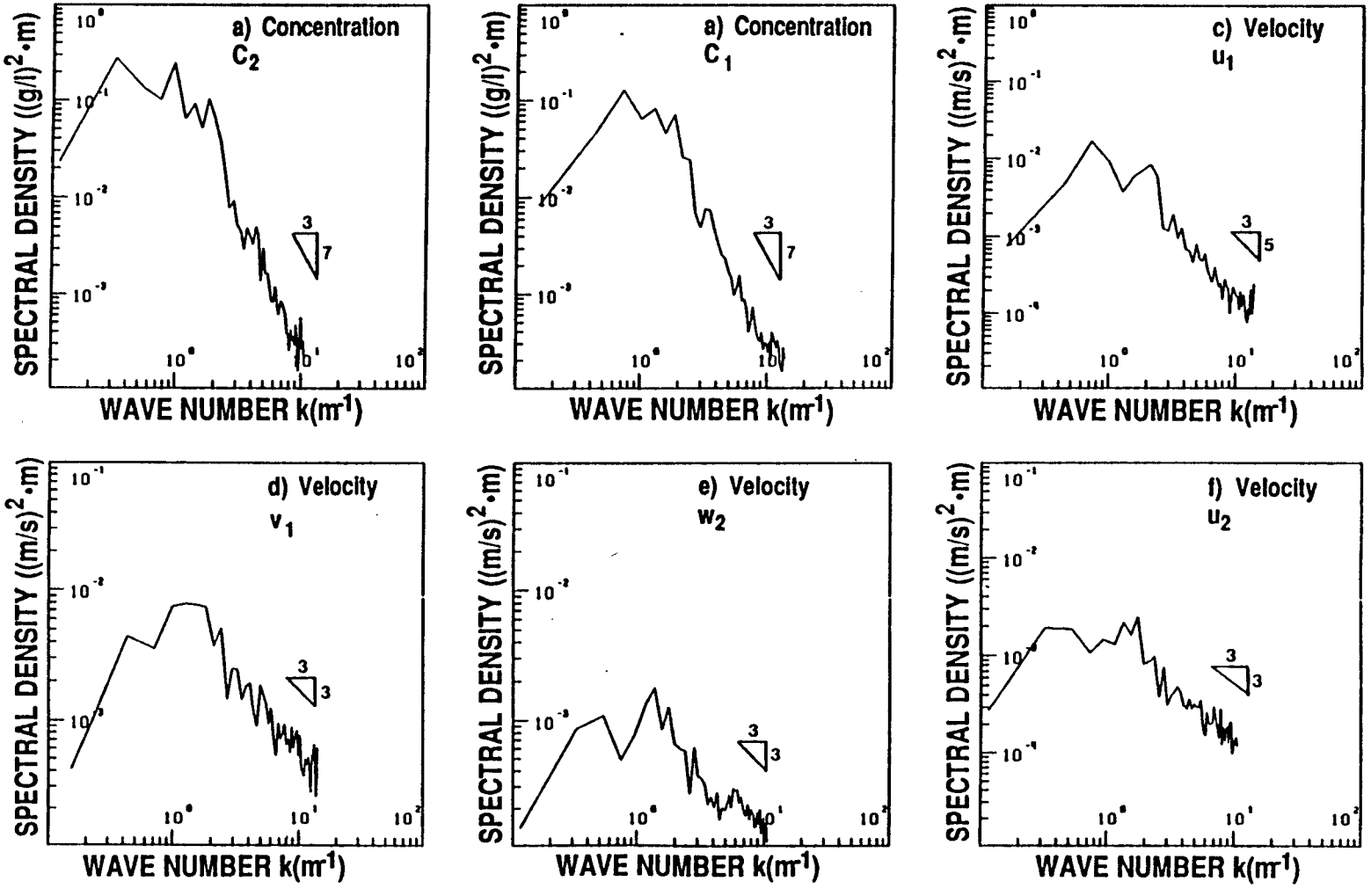

Figure 5.16: Examples of computed spectra for variables of the e_1 type. a) C_2; b) C_1; c) u_1; d) v_1; e) w_2; f) u_2

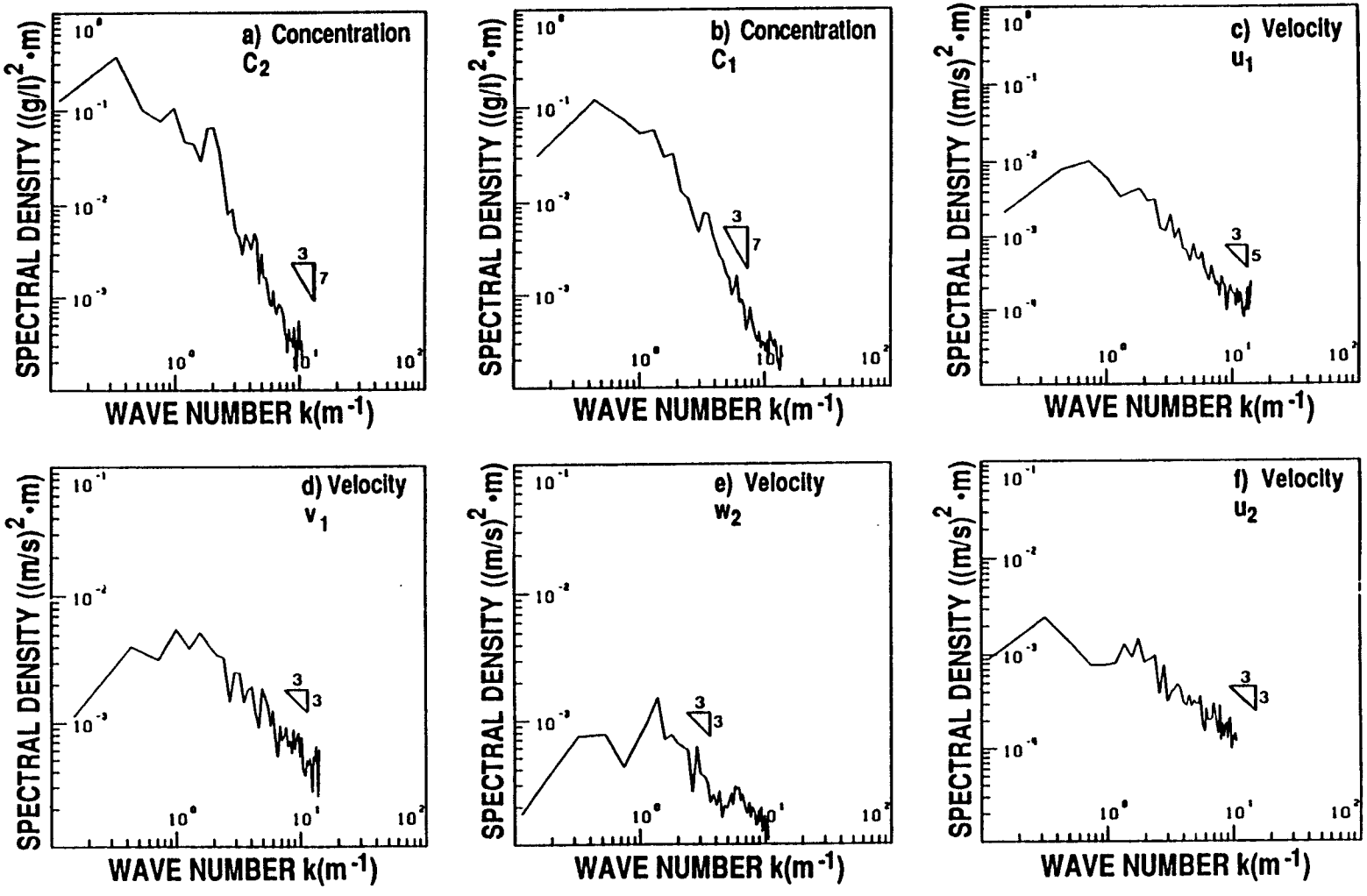

Figure 5.17: Examples of computed spectra for variables of the e' type. a) C_2; b) C_1; c) u_1; d) v_1; e) w_2; f) u_2

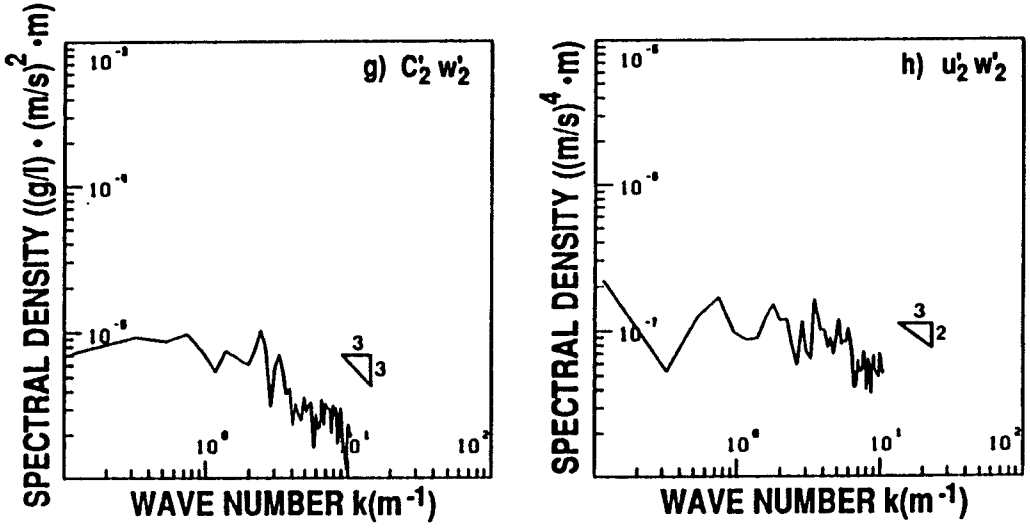

Figure 5.17 (cont.): g) $C_2'w_2'$ h) $u_2'w_2'$.

phenomenon is globally confirmed. Qualitative agreement is observed between the model's results and those measured in the field experiment during deployment C2.

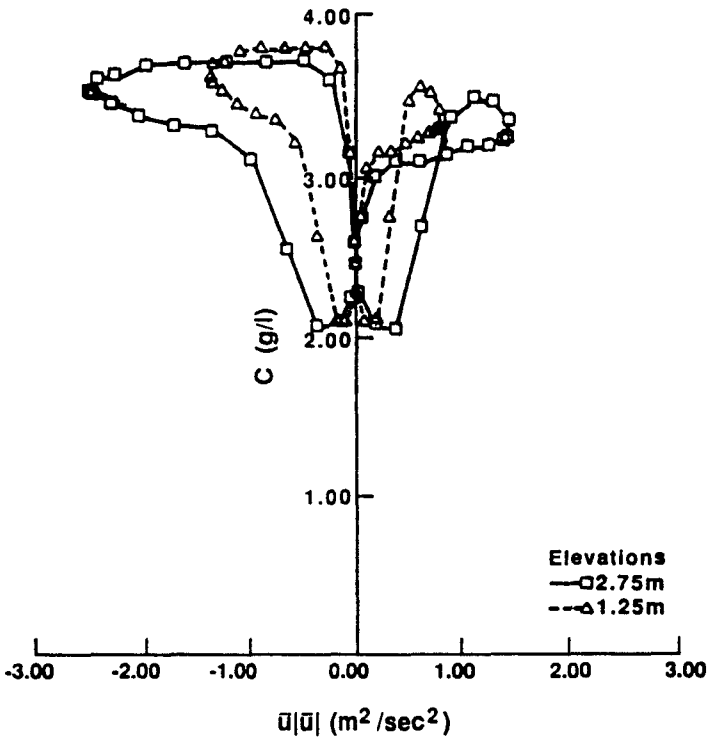

Figure 5.18: Hysteresis loops simulated using Hangzhou Bay sediment settling properties.

In order to verify the hysteresis phenomenon detected in terms of mean sediment concentrations and flow parameters the measured 'turbulent' properties (wave effects and turbulence, e_1) of the flow were investigated. Figure 5.20 shows a plot of the Reynolds stresses at the upper measurement level vs. the mean horizontal velocity, while figures 5.21 to 5.23 show the turbulent variances (which contribute to the 'turbulent' kinetic energy) of u (at both levels), v (at $z = 1.25\,m$) and w (at $z = 2.75\,m$) vs. $\overline{u}$. Despite the small number of data points qualitative hysteresis loops could be drawn, showing higher values of the variables during decelerating flow periods. Since the Reynolds stresses at a given elevation are an indicator of the bed shear stress and consequently related to sediment concentration through erosion/deposition conditions at the bottom, figure 5.20 is consistent with

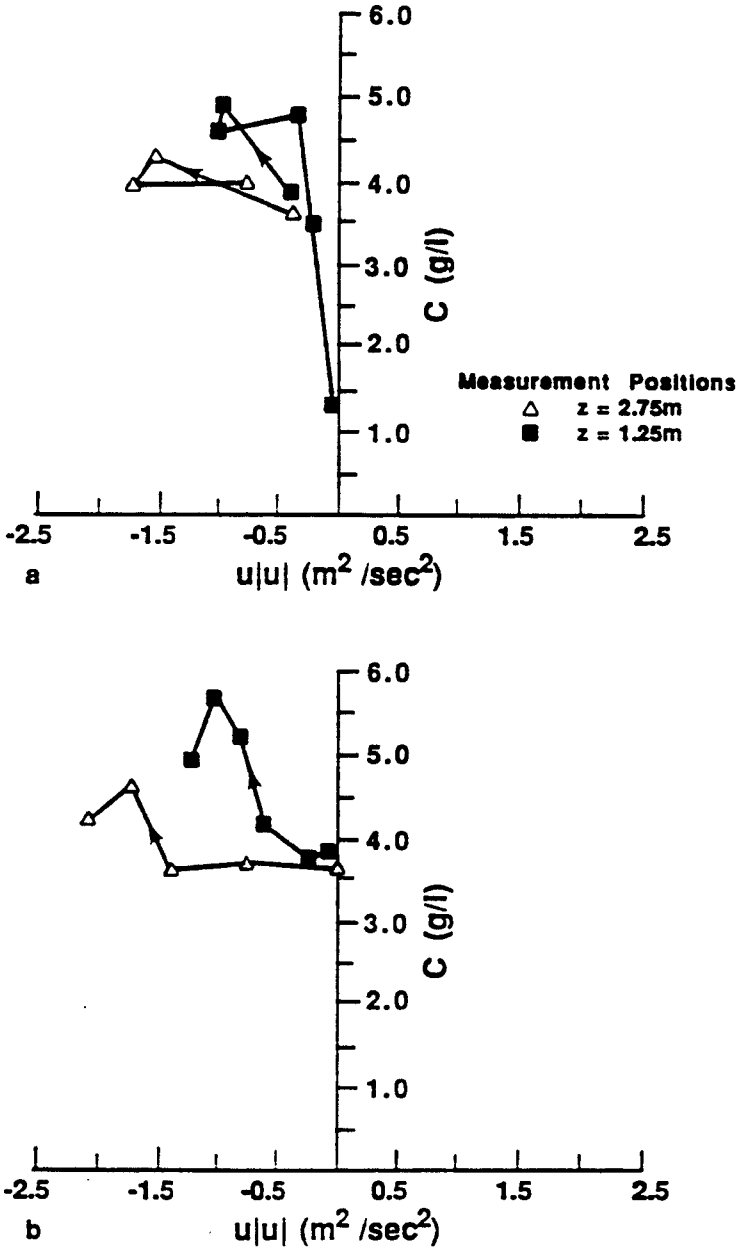

Figure 5.19: Measured hysteresis loops: a) Deployment C3; b) Deployment C2.

the previously assumed hypothesis. Figures 5.21 to 5.23 provide additional support to the hypothesis, since higher 'turbulent' kinetic energy will cause, through increased upward diffusion, higher sediment concentrations during the decelerating periods in the upper layers of the flow.

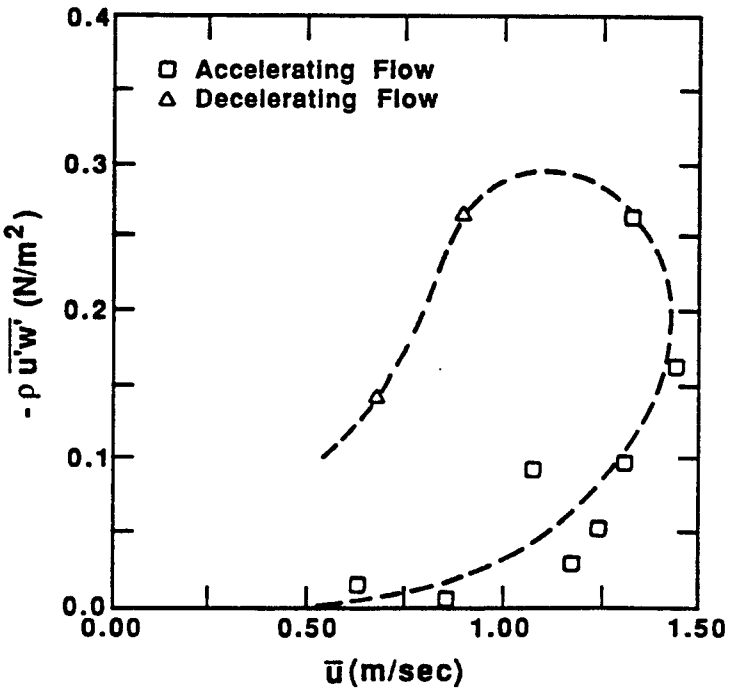

Figure 5.20: Hysteresis in Reynolds stresses.

The importance of vertical mass transport in the suspended sediment regime in Hangzhou Bay seems, consequently, to be confirmed not only through the behavior of the mean parameters (mean concentration-flow hysteresis) but also of the 'turbulent' variables related to erosion/deposition and mass diffusion.

The qualitative nature of the results of the model simulation was evaluated in the light of some of the parameters measured in the field or resulting from laboratory tests. The mass and momentum diffusivities resulting from records of the e_1 type (corresponding to the actual field conditions) were calculated through the use of

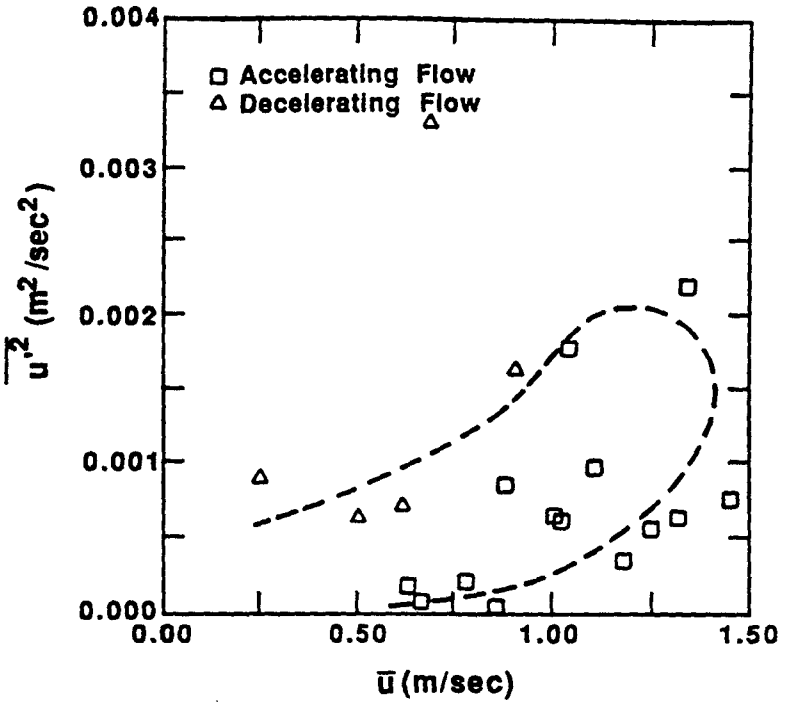

Figure 5.21: Hysteresis in u variance.

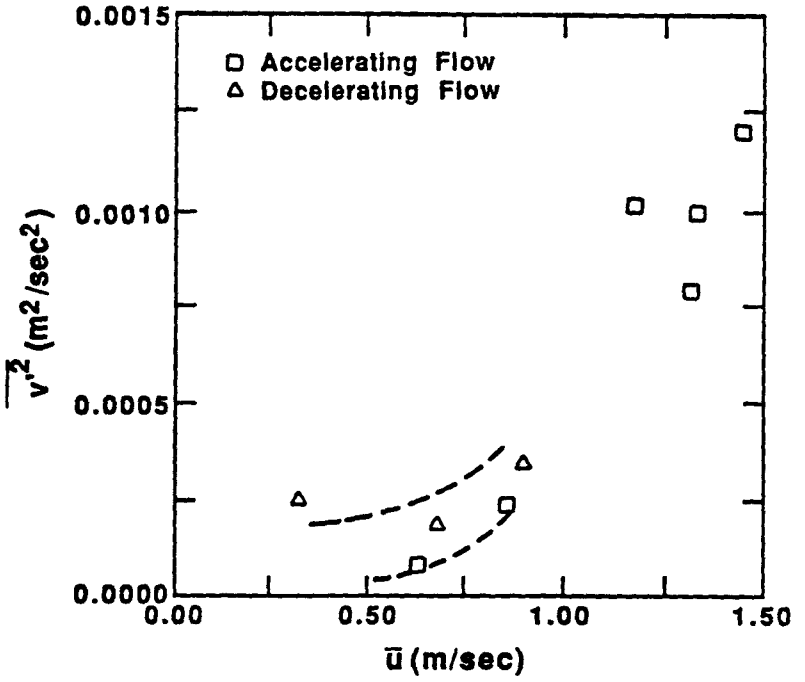

Figure 5.22: Hysteresis in v variance.

the difference formulas

$$K_s = -\frac{\overline{w'c'}}{\Delta C/\Delta z} \tag{5.4}$$

$$E_s = -\frac{\overline{w'u'}}{\Delta \overline{u}/\Delta z} \tag{5.5}$$

which give only rough approximations to the value of the diffusivities since $\Delta z = 1.5\ m$ is a rather large value. The mass and momentum diffusivities and the Schmidt numbers computed using this approach are shown in tables 5.1 and 5.2 together with the depth averaged longitudinal velocities (negative values denoting ebb velocities). For turbulence under conditions of local equilibrium a flux Richardson number defined as

$$Ri_f = \frac{g\overline{\rho' w'}}{\overline{\rho} \overline{u'w'}(\partial \overline{u}/\partial z)} = \frac{Ri}{S_t} \tag{5.6}$$

represents the efficiency of conversion from turbulent kinetic energy to potential energy (Abraham, 1989); Ri_f also reflects, relative to the gradient Richardson number, the difference between mass and momentum diffusivities under stratified conditions. The computed values of the flux Richardson number are presented in table 5.2. The mass diffusivities calculated by the model (using Hangzhou Bay sediment settling parameters) for values of $\overline{u}_D$ similar to those of table 5.1 are presented for comparison in table 5.3 . The values of K_s which were obtained from the field data were of orders of magnitude of $10^{-3}\ m^2/s$ or lower while the mass diffusivities computed by the model showed, for comparable values of the depth averaged velocities, values of the order of magnitude of 10^{-2}, much higher than the former. This fact confirms the need for a more accurate description of turbulent diffusion when modeling sediment-stratified flows. The measured values of K_s compare favorably with those used by van Leussen and Winterwerp (1988) (4×10^{-3} and $4 \times 10^{-4}\ m^2/sec$ for estuaries showing slight and strong stratification conditions, respectively). If time scales for vertical mixing and settling are defined as $T_d = H^2/K_s$ and $T_s = H/W_s$ respectively, their ratio T_s/T_d is the Peclet number for the suspension (Teeter, 1986) and reflects

Table 5.1: Measured mass diffusivities.

$\overline{u}_D$ (m/sec)	K_s (m^2/sec)
-1.221	3.29×10^{-4}
-1.163	5.60×10^{-5}
-0.861	3.21×10^{-5}
0.416	1.24×10^{-4}
0.762	2.53×10^{-3}
1.137	3.45×10^{-4}
1.336	8.12×10^{-4}
1.454	1.91×10^{-4}

Table 5.2: Measured momentum diffusivities, Schmidt and flux Richardson numbers.

$\overline{u}_D$ (m/sec)	E_s (m^2/sec)	S_t	Ri_f
-1.418	6.81×10^{-4}		
-1.276	4.92×10^{-4}		
-1.260	1.30×10^{-3}		
-1.221	3.08×10^{-4}	0.94	0.090
-1.163	1.37×10^{-4}	2.45	0.042
-0.861	7.71×10^{-5}	2.40	0.277
-0.827	1.36×10^{-3}		
-0.624	7.18×10^{-5}		
-0.603	1.12×10^{-3}		
-0.272	1.53×10^{-2}		
-0.180	2.18×10^{-3}		

the ratio between the settling lag and the diffusion lag. For typical values of the parameters measured in Hangzhou Bay this ratio is, approximately, equal to seven.

The difference between the values of τ_s used in the simulation and that determined for the local sediment (5.0 and 0.05 N/m^2, respectively) also confirms the need to improve the algorithms currently employed to describe the fluxes at the bed. It is obvious that a simplified erosion/deposition description of the bed phenomena is insufficient to simulate the complex manner in which bottom fine sediment is fluidized and entrained.

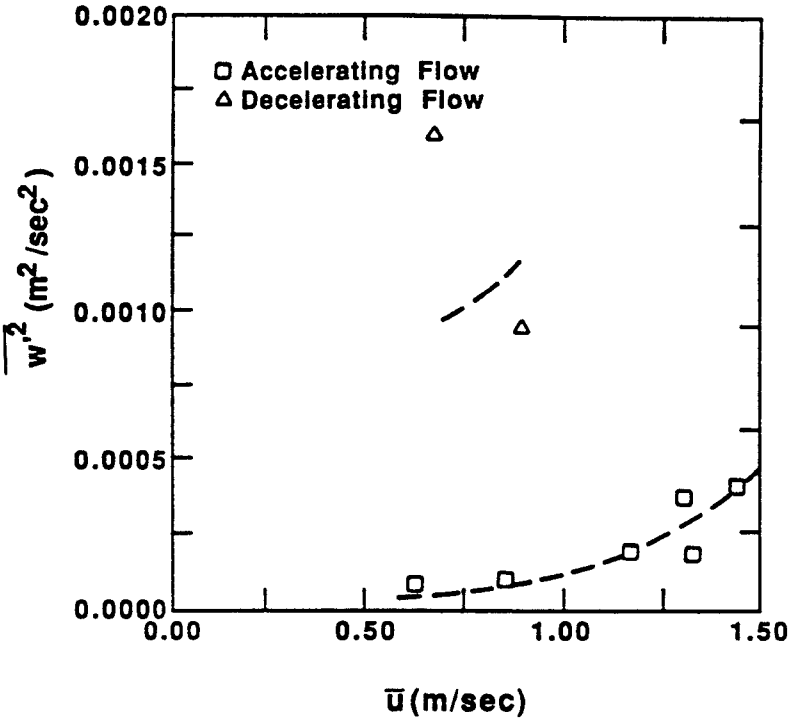

Figure 5.23: Hysteresis in w variance.

Table 5.3: Mass diffusivities computed by the model.

$\overline{u}_D$ (m/sec)	K_s (m^2/sec)
-1.278	8.33×10^{-2}
-1.145	8.49×10^{-2}
-0.809	8.62×10^{-2}
0.441	9.33×10^{-2}
0.796	9.20×10^{-2}
1.139	9.06×10^{-2}
1.208	8.79×10^{-2}

CHAPTER 6
SUMMARY AND CONCLUSIONS

The intensive use of estuarine and coastal waters has led to an increased number of engineering problems involving sediment dynamics and, in particular, of fine sediment fractions. The knowledge of sediment circulation patterns and of the factors affecting the development and location of zones of high turbidity has, consequently, become critical.

Several researchers have attempted to determine the relative importance of the physical processes producing landward transport of sediment in estuaries and causing zones of turbidity maxima to form; such zones contain a high percentage of the available mobile sediment and persist despite the opposing effects of seaward transport by the mean flow and of dilution. The basic tool used to investigate the relative importance of tidally averaged longitudinal mass transport is the decomposition of the relevant variables (velocity, salt or suspended sediment concentration, cross-sectional area) into average components and deviations related to time and spatial variations. Through expansion of the several mass transport terms, followed by tidal-cycle and cross-sectional averaging procedures and elimination of uncorrelated terms, the pertinent physical processes can be identified and their magnitudes evaluated through use of field data. Despite uncertainty factors which make comparison of different methods difficult, some significant results were obtained from such studies:

1. The main transport processes acting to transport salt and sediment landward are related to the tidal pumping phenomenon and to the effect of the vertical gravitational circulation. Tidal pumping results from phase differences

between cross-sectional area and average cross-sectional velocities and concentrations of salt or sediment; the vertical gravitational circulation is the net estuarine type of circulation due to salt water penetration. Both transport processes depend on the vertical concentration profile and, consequently, on the vertical mass transport fluxes.

2. The relative importance of the physical processes transporting salt and sediment landward is different: while tidal pumping seems to be the dominant process transporting sediment, the vertical gravitational circulation dominates the landward transport of salt. This difference can be largely explained by the time lags associated with sediment settling and erosion/deposition which should be added to the diffusion lag which affects both salt and sediment. A rough comparison of the lags associated with settling and diffusion for the case of sediment shows the settling lag to be approximately three times larger than the diffusion lag. A further argument supporting the importance of sediment erosion/deposition lags is related to the fact that tidal pumping of sediment was found to be related to the availability of sediment and to bed erodability.

In order to investigate the influence of the several parameters contributing to sediment lagged response to flow variations a vertical one-dimensional transport model was used together with field data obtained in a high concentration environment (Hangzhou Bay, People's Republic of China).

The numerical model developed by Ross (Ross, 88) solves the vertical sediment transport equation by considering the settling and diffusive fluxes in the water column and simplified erosion/deposition conditions at the bottom. The mass settling accounts for free settling, flocculation settling and hindered settling while the diffusive flux includes a Munk-Anderson type 'correction' to the neutral diffusivity conditions. At the bottom a flux is defined, depending on the mean bed shear stress, reflecting erosion, deposition or re-entrainment of recently deposited sediment. The

sensitivity of the model to several key parameters describing settling, stabilized diffusion and erosion was investigated using hydrodynamic data from Hangzhou Bay. The model was able to reproduce lutocline evolution typical of high concentration environments. The computed profiles essentially reflected lutocline evolution as function of the relation between settling fluxes and stabilized diffusion fluxes, stability conditions changing with different values of the Munk-Anderson coefficients and with the amount of sediment in suspension.

The numerical model was also used to simulate the characteristic fine sediment-flow hysteresis loops (C vs. $\overline{u}|\overline{u}|$) which reflect the lagged response of sediment to changes in flow conditions. Qualitative agreement was obtained between the model's results and hysteresis loops measured by Nichols (1986) and Dyer (personal communication). The effects of variations in the diffusion parameters and in the settling velocity (corresponding, respectively, to diffusion and settling lag effects) and bed conditions were determined; such effects are essentially related to time differences between the peak concentration and the peak shear stress and to the value of the residual concentration around slack water and affect the magnitude of the tidal pumping terms contributing to the longitudinal transport. Computed net vertical flux gradients showed higher values (both upward and downward) close to slack water periods than during the remaining of the tidal period; this fact confirms one of the limitations of the numerical model since, obviously, its schematic erosion/deposition description cannot represent adequately the complex near bed phenomena which include fluidization, entrainment, settling, bed formation, consolidation and gelling. A second limitation of the numerical model is related to modeling of the effects of sediment stratification on the flow and on its diffusion characteristics, which the Munk and Anderson approach globally describes using parameters α and β. Comparison between the mass diffusivities computed by the model and those obtained from field data from Hangzhou Bay showed that, for

comparable depth averaged horizontal velocities, the former were higher by, at least, one order of magnitude. Improvement of turbulence modeling in sediment-stratified environments and of the algorithms describing bed fluxes seem, consequently, to be critical steps in order to achieve better numerical modeling results.

The field data obtained in Hangzhou Bay were used to investigate the significance of lags in sediment response to flow changes in contributing to the transport patterns in the bay. The numerical model was used to generate sediment-flow hysteresis loops using the settling parameters determined through laboratory tests of the bay's sediment. The simulated loops showed qualitative agreement with the measured data corresponding to similar hydrodynamic conditions. The field data, despite limitations resulting from the small number of available data points, showed hysteresis features, a typical indication of the importance of time lagged sediment response or, equivalently, of vertical mass transport. Hysteresis was also detected in terms of microscale parameters resulting from random variations in the velocity (corresponding to superposition of turbulence and wave action). Such parameters, related to the shear stress and to the turbulent energy showed higher values during periods of decelerating flow than during periods of accelerating flow.

The properties of the random variations resulting from the measured field data were investigated through spectral analysis. Two types of data records were analyzed corresponding, respectively, to the superimposed effects of wave and turbulence, e_1 records, and to turbulent effects, e' records (once the wave coherent part of the records was removed); it should be noted that the filtering procedure seems to have produced better results when applied to velocity records than when applied to concentration records. The spectra of the e_1 type of records in the inertial subrange deviated from the theoretically predicted slopes in the cases of the v and w velocity components which showed a -1 dependence of the wavenumber; the slope of the u velocity component spectra showed a $-5/3$ value in the inertial subrange,

in agreement with the theoretical prediction. For the concentration spectra a $-7/3$ dependence on the wavenumber was found, different from the slope theoretically derived for temperature and generally accepted for the case of suspended sediment. Records of the e' type showed spectra with similar slopes in the inertial subrange.

The normalized turbulent intensities for all the measured velocity components of the e_1 type showed their highest values during the period of lowest suspended sediment concentration, a result which seems to support the hypothesis of turbulent intensity damping by suspended sediment.

APPENDIX
CALIBRATION OF THE ELECTRO-OPTICAL TURBIDITY METERS

A.1 General Aspects

The concentration measurements that took place in Hangzhou Bay (People's Republic of China) were made using two of a group of three electro-optical turbidity sensors operating with two Partech consoles currently available at the Coastal and Oceanographic Engineering Laboratory of the University of Florida. Two sensors of the same group were also used with the same Partech consoles in preliminary field experiments in a low concentration environment in the Intracoastal Waterway (Florida) previously to the experiment in Hangzhou bay. The sensors, whose normal ranges of operation are different, are:

1. Partech S1000, dual path transducer, with a normal range of 0 to 200 mg/l;
2. Partech SDM16 transducer, with a normal range of 100 to 50,000 mg/l;
3. Partech TT10, self-cleaning transducer, with a normal range of 100 to 50,000 mg/l.

The Partech type 7000-3RP measuring consoles used with the transducers have the references 19264 and 19265 and have, each, three output channels referenced as FSD1, FSD2 and FSD3. Previously to the field experiments in the Intracoastal Waterway two of the transducers were calibrated in the Coastal and Oceanographic Engineering Laboratory. The linear calibration curves obtained in this experiment for the concentration ranges of interest allowed the use of linear calibration curves in the Hangzhou Bay field experiment. The calibration curves, obtained in the field,

were, for transducer SDM16 with console 19265 and transducer TT10 with console 19264, both operating in channel FSD3, respectively:

$$C = 1.285 \times V + 0.648 \tag{A.1}$$

$$C = 1.549 \times V - 0.130 \tag{A.2}$$

where C is the concentration in g/l and V the instrument's output in volts. The concentration data points used for the field calibration resulted from gravimetric analysis of suspensions collected locally and are consequently representative of the actual field conditions. The laboratory calibration of the transducers used in Florida is presented in the following sections.

A.2 Calibration Media

For the purposes of the field experiment in the Intracoastal Waterway two transducers were calibrated, the S1000 and the SDM16. The instruments were calibrated using local fine sediment from the chosen site and a combination of fresh and local saline water, also from the experimental site.

The local seawater was filtered using a vacuum pump resulting in 24 liters of water. Approximately 20 liters were consumed during calibrations and the remainder was used for clear water zero set-up every morning and evening whilst the instruments were in use.

The local bed samples were processed to provide calibration material. The process is laborious and involves wet sieving through a 62.5 μm screen (#200 mesh) to separate coarse material, which is discarded. The remaining fine material was then desalinated by frequent washing with fresh water (tap water is adequate and was used for this purpose). Ideally the fines should be washed and settled and then tested for the presence of residual quantities of sea salt by use of silver nitrate, a clear solution. In the presence of NaCl a white precipitate forms. Experience has

shown that three to four washings is sufficient and this test was not pursued. The desanded and desalinated fines were then oven dried at 100 °C to drive off all water. The dried flakes of baked silty clay were allowed to cool to room temperature for a period of about twelve hours. The fines were then ground in a rock crusher and pulveriser to furnish a fine flour-like powder. The powder was sieved through a 37 μm screen (#400 mesh) to eliminate coarse particles. Eventually, in excess of 200 g of such fine powder were produced. 196 g were required for the calibrations and the remainder was been preserved in marked containers should further calibrations be required.

The fine powder samples were weighed out into 53 accurately weighed incremental samples. These ranged from 0.06 to 60.0 g and were placed in cleaned sealable sample pots.

It was decided to calibrate both transducers in the range 0-500 mg/l and the SDM16 transducer in the range 100-20,000 mg/l. The physical size of the head of the S1000 transducer dictated the size of the calibration vessel and thus the volume of suspension necessary to immerse the head completely. This value also dictated the weight of sediment to provide the known concentrations. The sediment samples were weighed to four decimal places.

A.3 Siltmeter Calibration Procedure

The Partech transducers were placed in an opaque vessel with rounded corners. Uniform dispersion of the suspensions was achieved using a combination of magnetic and mechanical stirrers. Daylight was excluded from the vessel by use of an opaque plastic sack. The S1000 transducer was calibrated with its black metal shroud in place. The purpose of this shroud is to eliminate any daylight interference.

The windows of the Partech transducers were carefully cleaned and clean fresh water was placed in the calibration vessel. The water was allowed to come to room

temperature equilibrium. The Partech systems were switched on two hours prior to the set-up of the zero reading and maintained in water. This ensured temperature stability and that the device was fully warmed up (two hours is almost certainly an excessive period). The outputs from the instrument at each point on the calibration were displayed and noted from a digital voltmeter (DVM).

The Partech systems were powered externally with a DC power supply driven off the mains and were switched to "Timer Off-External." The zero potentiometers were then set-up to give a zero scale reading and an analog output of close to zero millivolts (a small positive reading was considered to be a good compromise).

The two instruments operate over different concentration ranges meaning that, effectively, two complete and separate calibrations had to be performed.

A.3.1 S1000 Calibration

The Intracoastal Waterway saline water had a brown color. As a precaution therefore it was decided to calibrate the sensitive S1000 in tap water. In the event, later tests showed the instruments to be insensitive to this discoloration of the water.

Usually the span control is set up to cover the full concentration range to be encountered during the field experiment. In the case of the S1000, three initial suspensions could have been used to set up the span control. For example the FSD1 channel could have been set with, say a 100 mg/l suspension to give the maximum volt output, say 250 mg/l to give the maximum full scale deflection on the FSD2 channel and 500 mg/l to give the full scale deflection on the FSD3 channel. The maximum output was found to be 4.54 volts. In this case, lack of material and time constraints prevented this procedure from being adopted. In the event one channel, FSD3, was set to give a maximum output at 500 mg/l and the two remaining span controls were left at a lower setting.

Note that the zero and span controls are slightly interactive and that having set

up the span control, the zero setting must be rechecked in clean water and adjusted if necessary.

The calibration was then carried out in one continuous operation to prevent, as far as possible, the settling out of any suspended material. The powders were introduced incrementally onto the water surface and readings were taken within a short period ($\approx 1\ min$) when all the material had been taken up in suspension and the DVM reading had stabilized. No more than ten increments were permitted to ensure that cumulative weighing errors were eliminated. Fresh suspensions were used at concentrations 100 and 500 mg/l.

The results of the calibration are plotted out as three curves, 1 to 3, in figure A.1 . From the calibration curves it can be seen that the meter extinguished at 500 mg/l on FSD1 and was reaching saturation on FSD3 (as set). The data for FSD2 suggest the meter could be calibrated above 500 mg/l. Note that the calibration is only valid for the console and transducer combination used.

A.3.2 SDM16 Calibration

This transducer was calibrated using local saline water. Tests in which the zero was set up in fresh and saline (colored) water showed only a marginal effect, which was not considered significant.

It was suspected that the manufacturers claims to be able to calibrate this transducer up to 50,000 mg/l were over-optimistic. For this reason, having set the zero controls on the three ranges, the span controls were set up having extinguished the light source by obscuring the beam. A maximum output of 4.5 volts was achieved. All three channels were calibrated with the span controls adjusted to cover this maximum range, but this can be varied on a future occasion to increase the sensitivity and range of channels FSD1 and FSD2.The calibration was otherwise carried out in exactly the same way as that for the S1000 head. Fresh suspensions were

used at concentrations 2,000 and 10,000 mg/l. The calibration curves are plotted as curves 4, 5 and 6 in fig. A.2 .

The SDM16 transducer was also calibrated in fresh water to 500 mg/l as shown in curves 7, 8 and 9 (figures A.3 and A.4). Fresh suspensions were again used at concentrations 100 and 500 mg/l. It should be noted that the span control on channel FSD1 was changed between the two calibrations. If it is desired to use the SDM16 transducer on the low concentration range only data for FSD2 or FSD3 should be used.

A.4 Quality Control and Assessment

The calibrations which were obtained were considered to be adequate but could be improved with more appropriate instrumentation and control of the method. In particular, the need to obtain field samples of suspended sediment during the field deployments, to be dried and weighed to check against the laboratory calibration is emphasized.

In general the calibrations were found to be linear. In the case of the SDM16 head they were linear up to 10,000 mg/l and usable up to 20,000 mg/l where they were virtually extinguished. This was very much as expected.

One reason for caution in using the calibration data is seen in the dual point sample changeovers (100, 500, 2000, 10,000 mg/l). The points could be expected to lie closer together in a more rigorous calibration. Possible reasons for these differences could be:

1. Calibration vessel not in an ideal shape, permitting some settlement on the base during the calibration;

2. Suspensions not sufficiently finely ground leading to a tendency for particle separation and settlement;

3. Weighing errors in the samples;

4. Inadequacy of the apparatus used to maintain a homogeneous suspension. Trials showed increasing the mixing raised the voltage reading, implying raising more material from the base of the vessel. The stirrer caused a problem in that if the stirring rate was raised too high it led to cavitation, which is undesirable. A more suitable mixer is required.

In respect of operational procedures it is essential to carry out a clear water zero check at the beginning and end of each experiment. This is done in either fresh or local filtered seawater in a container and with the container within an opaque plastic bag to exclude daylight. Altering the output to zero at the start of the experiment does not alter the shape of the calibration curve, but ensures it starts at zero and has no offset. The span controls cannot be altered.

Formazine turbidity standards may be used during the course of an experiment if desired to check on the instrument stability. These bear little resemblance to the suspended solids values.

It was not clear why the maximum output was 4.54 as opposed to 5 volts and therefore whether any instruments could be loading the DVM was checked. There was no evidence of this. Also for the calibrations in figures A.1, A.3 and A.4 the zeros of both instruments had drifted between the start and end of the calibrations. In both cases the zeros on channels FSD2 and FSD3 had drifted more than that on channel FSD1. Any reason why the zeros should shift more on one channel setting than another could not be found. No environment factor such as temperature, lens cleanliness or water cleanliness was found to be involved. Transducer SDM16 was more stable during the calibration in fig. A.2, although this change could not be accounted for.

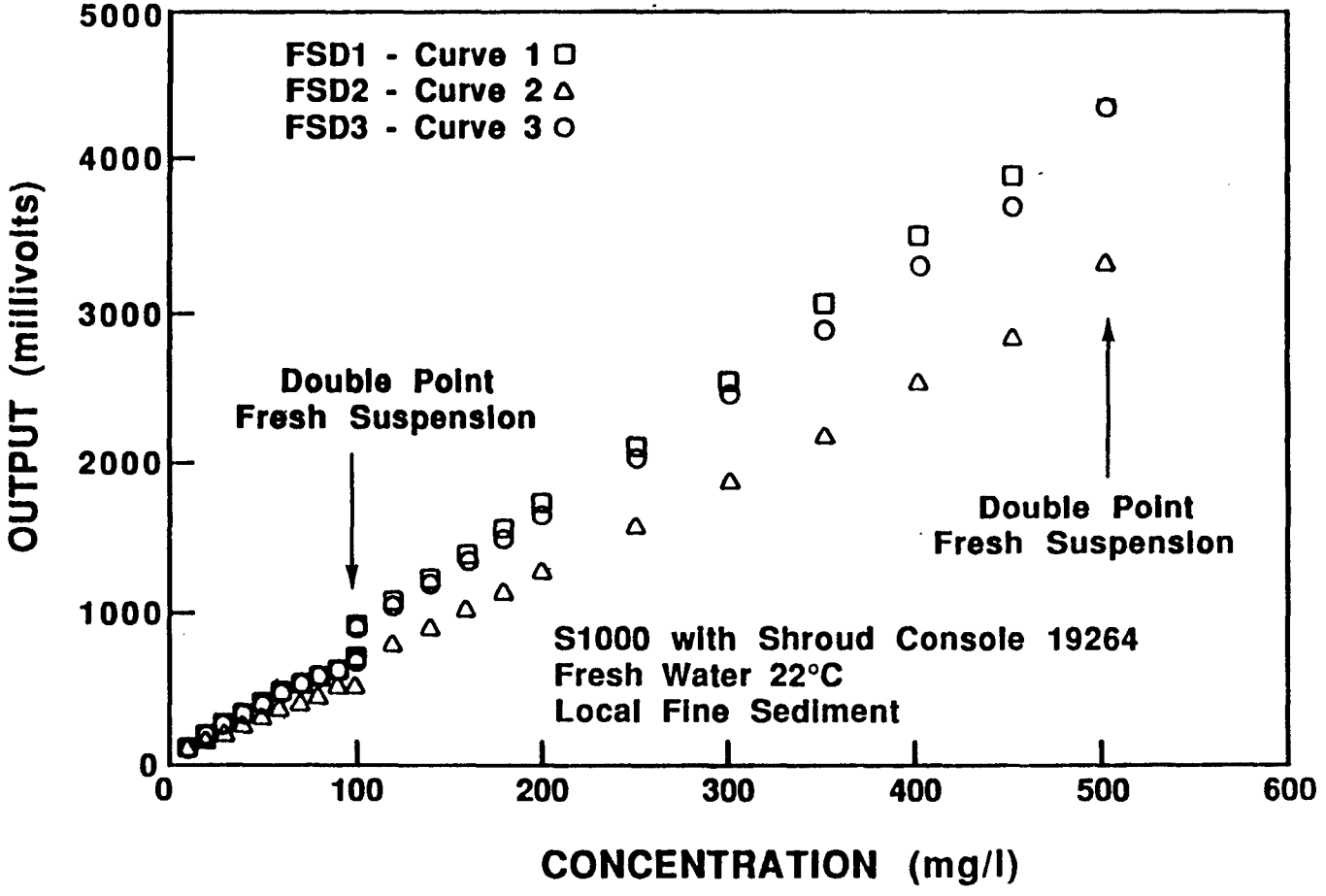

Figure A.1: Calibration curves for the S1000 transducer and console 19264 using fresh water.

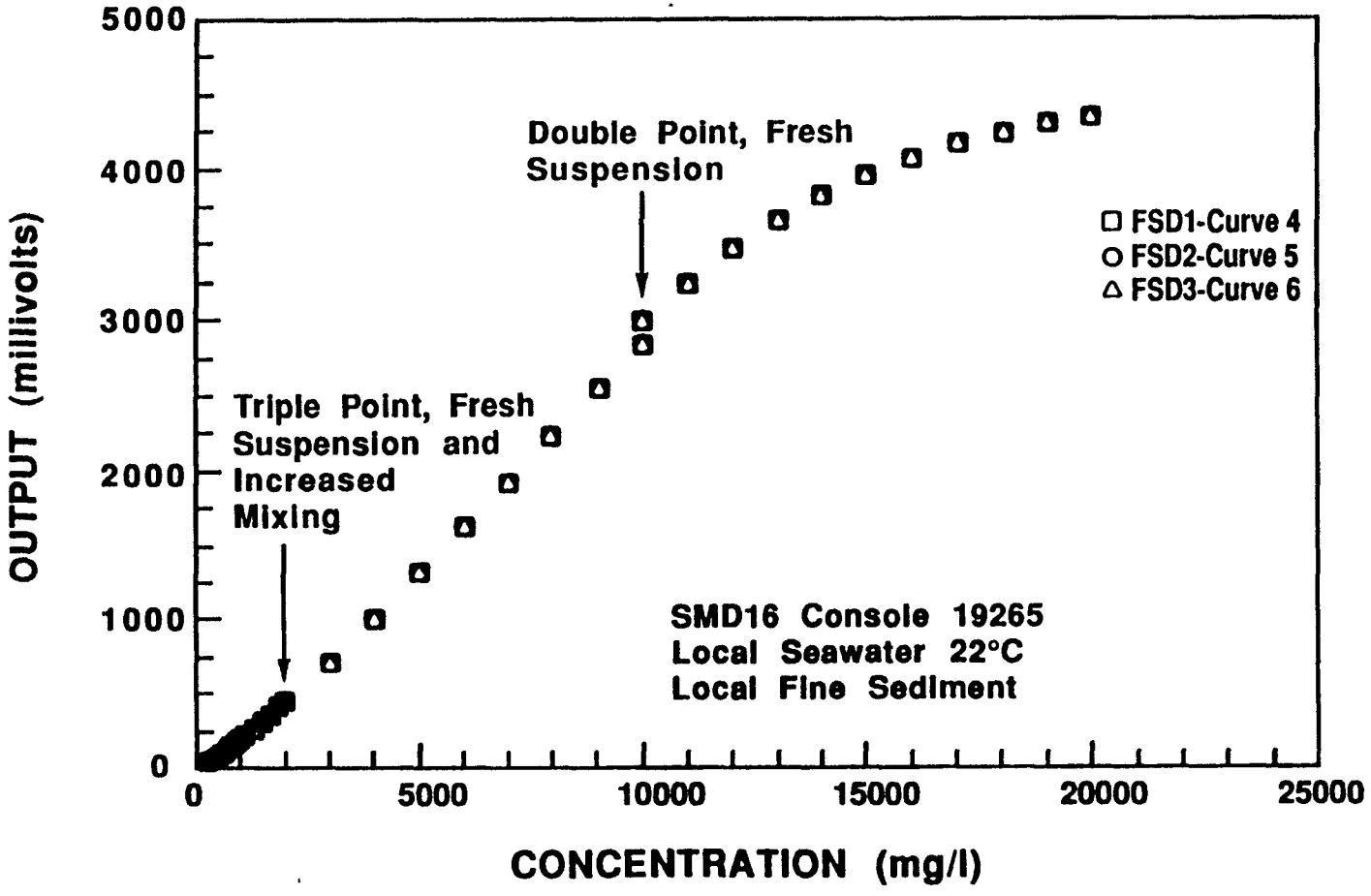

Figure A.2: Calibration curves for the SDM16 transducer and console 19265 using saline water.

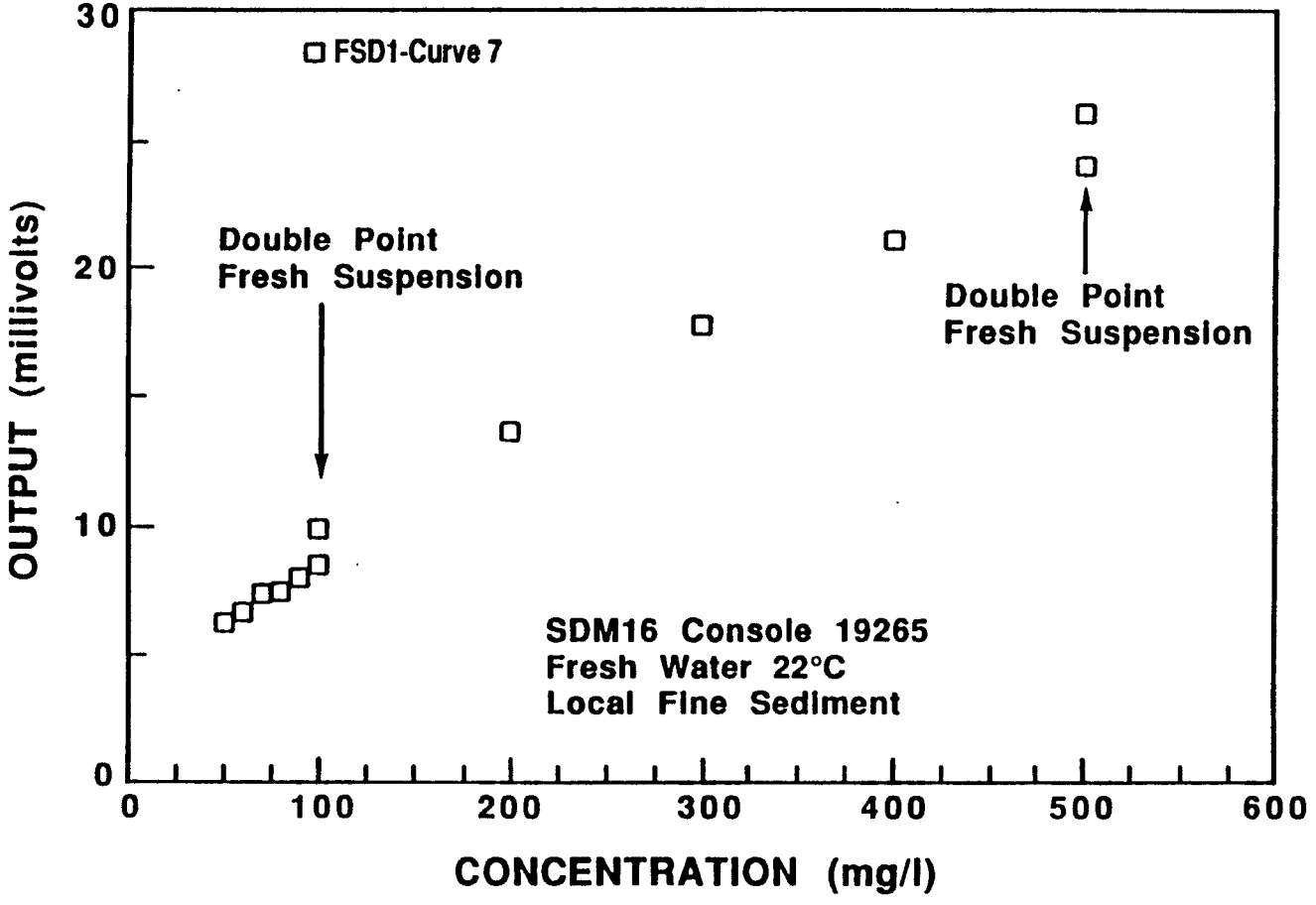

Figure A.3: Calibration curve for the SDM16 transducer and FSD1 channel of console 19265 using fresh water.

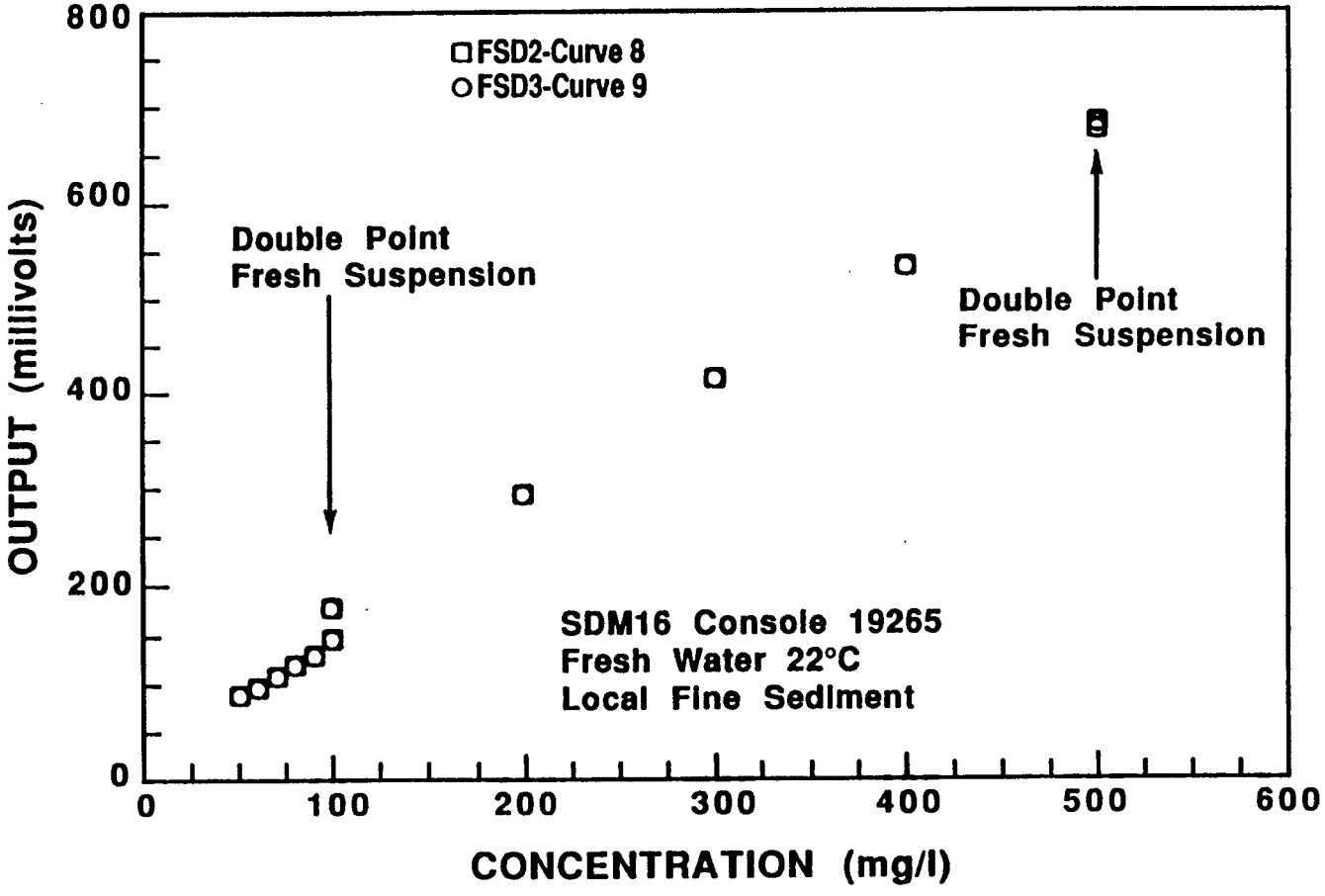

Figure A.4: Calibration curves for the SDM16 transducer and channels FSD2 and FSD3 of console 19265 using fresh water.

BIBLIOGRAPHY

Abraham, G., "Turbulence and Mixing in Stratified Tidal Flows," Physical Processes in Estuaries, W. van Leussen and J. Dronkers, eds., Springer-Verlag, Berlin, 1989.

Allen, G. P., Salomon, J. C., Bassoulet, P., Du Penhoat, Y., and De Grandpre, C., "Effects of Tides on Mixing and Suspended Sediment Transport in Macrotidal Estuaries," Sed. Geol., 26, 1980, pp. 69-90.

Allen, G. P., Sauzay, G., Castaing, P., and Jouanneau, J. M., "Transport and Deposition of Suspended Sediment in the Gironde Estuary, France," Estuarine Processes, Vol II, M. Wiley, ed., Academic Press, New York, 1977.

A. S. T. M., Annual Book of A. S. T. M. Standards, Volume 04.08, American Society for Testing and Materials, Philadelphia, 1988.

Bedford, K. W., Libicki, C., Wai, O., Abdelrhman, M., and van Evra III, R., "The Structure of a Bottom Sediment Boundary Layer in Central Long Island Sound," Physical Processes in Estuaries, W. van Leussen and J. Dronkers, eds., Springer-Verlag, Berlin, 1989.

Bendat J. S., and Piersol A. G., Random Data: Analysis and Measurement Procedures, Wiley-Interscience, New York, 1971.

Bowden, K. F., "The Mixing Processes in a Tidal Estuary," Int. J. Air Wat. Poll., 7, 1963, pp. 343-356.

Bowden, K. F., and Sharaf el Din, S. H., "Circulation, Salinity and River Discharge in the Mersey Estuary," Geophy. J. Roy. Ast. Soc., 10, 1966, pp. 383-400.

Coleman, N. L., "Velocity Profiles with Suspended Sediment," J. Hyd. Res., 19, N° 3, 1981, pp. 211-229.

Dyer, K. R., Estuaries: A Physical Introduction, John Wiley and Sons, London, 1973.

Dyer, K. R., "The Salt Balance in Stratified Estuaries," Estuar. Coastal Mar. Sci., 2, 1974, pp. 273-281

Dyer, K. R., "The Balance of Suspended Sediment in the Gironde and Thames Estuaries," Estuarine Transport Processes, B. J. Kjerfe, ed., Belle W.

Baruch Library in Marine Science N° 7, University of South Carolina Press, Columbia, South Carolina, 1978.

Dyer, K. R., Coastal and Estuarine Sediment Dynamics, John Wiley and Sons, Chichester, U. K., 1986.

Dyer, K. R., "Fine Sediment Particle Transport in Estuaries," Physical Processes in Estuaries, W. van Leussen and J. Dronkers, eds., Springer-Verlag, Berlin, 1989.

Dyer, K. R., and Evans E. M., "A Study of the Dynamics of the Turbidity Maximum," 3rd Workshop on Estuarine Cohesive Sediment Dynamics, Palm Coast, Florida, 1988, in print.

Festa, J. F., Hansen, D. V., "Turbidity Maxima in Partially Mixed Estuaries: A Two-Dimensional Numerical Model," Estuar. Coastal Mar. Sci., 7, 1978, pp. 347-359.

Fischer, H. B., "Mass Transport Mechanisms in Partially Stratified Estuaries," J. Fluid Mech., 53, 1972, pp. 672-687

Fischer, H. B., List, E. J., Koh, R. C. Y., Imberger, J., and Brooks, N. H., Mixing in Inland and Coastal Waters, Academic Press, New York, 1979.

Gordon, C. M., "Sediment Entrainment and Suspension in a Tidal Flow," Marine Geol., 18, 1975, M57-M54.

Hansen, D. V., "Currents and Mixing in The Columbia River Estuary," Ocean Science and Ocean Engineering, Trans. Joint Conf. Exib. Marine Tech. Soc. Am. Soc. Limnology and Oceanography, 1965, pp. 943-955.

Harleman, D. R. F., Transport Processes In Environmental Engineering. A Series of Notes to Accompany Lectures in 1.77 Water Quality Control, Ralph M. Parsons Laboratory, Department of Civil Engineering, M. I. T., Cambridge, Massachusetts, 1988.

Hayter, E. J., and Mehta, A. J., "Modeling of Estuarial Fine Sediment Transport for Tracking Pollutant Movement," UFL/COEL-82/009, Coastal and Oceanographic Engineering Department, University of Florida, Gainesville, Florida, 1982.

Henderson, F. M., Open-Channel Flow, The Macmillan Co., New York, 1966.

Ippen, A. T., "A New Look at Sedimentation in Turbulent Streams," J. Boston Soc. Civ. Eng., 58, N° 3, 1971, pp. 132-161.

Kandiah, A., "Fundamental Aspects of Surface Erosion of Cohesive Soils," Ph. D. Dissertation, University of California, Davis, California, 1974.

Kirby, R., "Suspended Fine Cohesive Sediment in the Severn Estuary and Inner Bristol Channel, U. K.," Report ETSU-STP-4042, Department of Atomic Energy, Harwell, United Kingdom, 1986.

Lavelle, J. W., and Mofjeld, H. O., "Effects of Time-Varying Viscosity on Oscillatory Channel Flow," J. Geophys. Res., 88, N° C12, 1983, pp. 7607-7616.

McCutcheon, S. C., "Vertical Velocity Profiles in Stratified Flows," J. Hyd. Eng., ASCE, 107, N° 8, 1981, pp. 973-988.

McLean, S. R., "Turbulence and Sediment Transport Measurements in a North Sea Tidal Inlet (The Jade)," North Sea Dynamics, J. Sundermann and W. Lenz eds., Springer-Verlag, Berlin, 1983.

Mehta, A. J., "Depositional Behavior of Cohesive Sediments," Ph. D. Dissertation, University of Florida, Gainesville, Florida, 1973.

Mehta, A. J., "Cohesive Sediments in Estuarine Environment," Invited Contribution to AGU Chapman Conference, Bahia Blanca, Argentina, 1988.

Mehta, A. J., and Lott, J. W., "Sorting of Fine Sediment During Deposition," Proc. Coastal Sediments '87, 1, ASCE, New Orleans, Louisiana, 1987, pp. 348-362.

Monin, A. S., and Yaglom, A. M., Statistical Fluid Mechanics: Mechanics of Turbulence, M. I. T. Press, Cambridge, Massachusetts, 1971.

Munk, W. H., and Anderson, E. R., "Notes on a Theory of the Thermocline," J. Mar. Res., 1, 1948, pp. 276-295.

Murray, S. P., and Siripong, A., "Role of Lateral Gradients and Longitudinal Dispersion in the Salt Balance of a Shallow Well Mixed Estuary," Estuarine Transport Processes, B. J. Kjerfe, ed., Belle W. Baruch Library in Marine Science, N° 7, University of South Carolina Press, Columbia, South Carolina, 1978.

Nichols, M. M., "Effects of Fine Sediment Resuspension in Estuaries," Estuarine Cohesive Sediment Dynamics, A. J. Mehta ed., Springer-Verlag, Berlin, 1986.

Nichols, M. M., and Biggs, R. B., "Estuaries," Coastal Sedimentary Environments, R. A. Davis Jr., ed., Springer-Verlag, Berlin, 1985.

Oduyemi, K. O. K., "Turbulent Transport of Sediment in Estuaries," Ph. D. Dissertation, University of Birmingham, Birmingham, U. K., 1986.

Officer, C. B., "Discussion of the Turbidity Maximum in Partially Mixed Estuaries," Est. Coastal Mar. Sc., 10, 1980, pp. 239-246.

Officer, C. B., "Physical Dynamics of Estuarine Suspended Sediments," Marine Geology, 40, 1981, pp. 1-14.

Owen, M. V., "The Effect of Turbulence on the Settling Velocities of Silt Flocs," Proc. XIV Congress, International Association for Hydraulic Research, XIV Congress, Paris, France, 1971, pp. 27-32.

Parchure, T. M., and Mehta, A. J., "Erosion of Soft Cohesive Sediment Deposits," J. Hyd. Eng., ASCE, 111, N° 10, 1985, pp. 1308-1326.

Postma, H., "Sediment Transport and Sedimentation in the Estuarine Environment," Estuaries, Amer. Assoc. Adv. Sci., Pub. N° 83, G. H. Lauff, ed., 1967, pp. 158-179.

Rattray, M., and Dworsky, J. G., "Comparison of Methods for Analysis of the Transverse and Vertical Circulation Contribution to the Longitudinal Advective Flux in Estuaries," Est. Coastal Mar. Sci., 11, 1980, pp. 515-536.

Ross, M. A., "Vertical Structure of Estuarine Fine Sediment Suspensions," Ph. D. Dissertation, University of Florida, Gainesville, Florida, 1988.

Schlichtling, H., Boundary-Layer Theory, 7^{th} ed., Mc Graw-Hill Book Company, New York, 1979.

Soulsby, R. L., Salkield, A. P., and Le Good, G. P., "Measurements of the Turbulence Characteristics of Sand Suspended by a Tidal Current," Cont. Shelf Res., 3, N° 4, 1984, pp. 439-454.

Su, J.L., Wang, K., and Li, Y., "A Plume Front in Hangzhou Bay and its Role in Suspended Sediment Transport," Second Institute of Oceanography, State Oceanic Administration, Report (in print), Hangzhou, Zhejiang, People's Republic of China, 1988.

Su, J. L., and Xu, W., "Modelling of the Deposition Patterns in Hangzhou Bay," Proc. XIX Int. Coastal Eng. Conference, ASCE, New York, 1984, pp. 2181-2191.

Teeter, A. M., "Vertical Transport in Fine-Grained Suspension and Newly-Deposited Sediment," Estuarine Cohesive Sediment Dynamics, A. J. Mehta, ed., Springer-Verlag, Berlin, 1986.

Tennekes, H., and Lumley, J. L., A First Course in Turbulence, M. I. T. Press, Cambridge, Massachusetts, 1972.

Uncles, R. J., Elliott, R. C. A., and Weston, S. A., "Lateral Distributions of Water, Salt and Sediment Transport in a Partly Mixed Estuary," Proc. XIX Int. Coastal Eng. Conf., ASCE, New York, 1984, pp. 3067-3077.

Uncles, R. J., Elliot, R. C. A., and Weston, S. A., "Observed Fluxes of Water, Salt and Suspended Sediment in a Partly Mixed Estuary," Est. Coastal Shelf Sci., 20, 1985a, pp. 147-167.

Uncles, R. J., Elliott, R. C. A., and Weston, S. A., "Dispersion of Salt and Suspended Sediment in a Partly Mixed Estuary," Estuaries, 8, 1985b, pp. 256-269.

van Leussen, W. and Winterwerp, J. C., "Laboratory Experiments in the Delft Tidal Flume on the Sedimentation of Fine-Grained Sediments,"

Conference on Physics of Shallow Estuaries and Bays, Pacific Grove, California, 1988.

Vanoni, V. A., "Sedimentation Engineering," Report of Engineering Practice, N° 54, American Society of Civil Engineers, New York, 1975.

Villaret, C., and Paulic, M., "Experiments on the Erosion of Deposited and Placed Cohesive Sediments in an Annular Flume and a Rocking Flume," UFL/COEL-86/007, Coastal and Oceanographic Engineering Department, University of Florida, Gainesville, Florida, 1986.

Wellershaus, S., "Tidal Dynamics and Mud Shoaling in the Weser Estuary," Arch. Hydrobiol., 92, 1981, pp. 161-198.

West, J. R., and Oduyemi, K. O. K., "Turbulence Measurements of Suspended Solids Concentration in Estuaries," J. Hyd. Eng., ASCE, 115, N^0 4, 1987, pp. 457-474.